UNIVERSITY OF CALIFORNIA
RIVERSIDE

Development of a Fischer-Tropsch Gasoline Process for the Steam Hydrogasification Technology

A Dissertation submitted in partial satisfaction
of the requirements for the degree of

Doctor of Philosophy

in

Chemical and Environmental Engineering

by

Yang Li

December 2013

Dissertation Committee:

Dr. Joseph Norbeck, Chairperson
Dr. Charles Wyman
Dr. Ian Wheeldon

The Dissertation of Yang Li is approved:

_____

_____

_____

Committee Chairperson

University of California, Riverside

ACKNOWLEDGMENTS

I would like to express my sincere gratitude to my advisor, Dr. Joseph M. Norbeck, for his insightful suggestions, warm encouragement and consistent support. I would also express my earnest appreciation to Dr. Chan S. Park, my co-advisor, who gave me important guidance to my research and encourage me to “learn everything”. I owe my sincere gratitude to my reading committee members, Dr. Charles Wyman, Dr. Ian Wheeldon, and my candidacy committee members, Dr. David Cocker and Dr. Yadong Yin, for their detailed and constructive comments. In addition, I would like to thank Dr. Yushan Yan for his support and advise on catalyst synthesis. Also, I warmly thank the Lab Manager Junior Castillo, and engineer Sean Franco, who offered great help on lab work. I am also grateful to my colleagues for their help and suggestion: Wei He, Xiaoming Lu, Qian Luo, Xin Fan, Zhongzhe Liu, Yoothana, and Amonrat. Finally I would like to give my special thanks to my parents and my wife. I would not have been able to complete my thesis without their love and support.

Yang Li

ABSTRACT OF THE DISSERTATION

Development of a Fischer-Tropsch Gasoline Process for the Steam Hydrogasification Technology

by

Yang Li

Doctor of Philosophy, Graduate Program in Chemical and Environmental Engineering
University of California, Riverside, December 2013
Dr. Joseph M. Norbeck, Chairperson

The CE-CERT Steam Hydrogasification Technology efficiently converts carbonaceous materials to high energetic synthesis gas. This thesis investigates the direct production of gasoline range liquid hydrocarbons with high iso-paraffin content from synthesis gas. The goal is to provide a process to efficiently produce renewable gasoline that can be used directly without modification of engine or infrastructure.

An H-ZSM-5 shell Co/Al_2O_3 Fischer-Tropsch catalyst is prepared using a secondary-growth hydrothermal synthesis method. The catalyst not only synthesizes long-chain

hydrocarbons from synthesis gas, but also cracks and isomerizes them into gasoline-range hydrocarbons with high iso-paraffin content. Characterization results show that the catalyst has good H-ZSM-5 shell coverage with no cracks or pinholes, with a shell thickness is around 4.29 μm. H-ZSM-5 shell composition is confirmed by EDX and XRD. In addition, the zeolite-shell catalyst has a 10% increase of surface area, compared to a conventional Fischer-Tropsch catalyst.

A high-temperature high-pressure lab-scale continuous Fischer-Tropsch reactor with LabVIEW automation system was designed and built. The reactor system has online gas and liquid sampling capabilities. It also has a PID controller with gain scheduling for precise heating control during Fischer-Tropsch synthesis test. Safety during reactor operation is ensured with alarms and automatic emergency response system.

Performance of a H-ZSM-5 shell Co/Al_2O_3 Fischer-Tropsch catalyst was investigated under various conditions. A maximum CO conversion of 97.1%, with a highest gasoline yield of 58% and iso-paraffin selectivity of 14.3%, was obtained. Sensitivity analysis shows that reaction temperature significantly affects CO conversion and iso-paraffin selectivity. Catalyst silicon to aluminum ratio also influences iso-paraffin selectivity, but

has no effect on CO conversion. In addition, H-ZSM-5 shell Co/Al_2O_3 Fischer-Tropsch catalyst has much less carbon deposition than conventional catalyst, which can help reduce catalyst deactivation rate.

Table of Contents

List of Tables

List of Figures

CHAPTER 1 Introduction

1.1 Background

Over 80% of the world's energy is provided by fossil fuels such as coal, petroleum and natural gas, and it is projected that energy consumption will rise by nearly 50% from 2009 through 2035 [1]. Two major issues have drawn more and more attention with the fast increase of fossil fuel consumption: concern of fossil fuel depletion in many places of the world [2, 3] and global warming caused by burning fossil fuels [4, 5]. Technologies have been developed to provide alternative energy sources [3, 6]. Biomass is the major source of renewable energy that is produced from the photosynthesis process [7, 8]. Biomass to fuels process is one of the viable ways because of abundant reserves in most places of the world and its environmental-friendly nature as a carbon sink [9-11]. The utilization of biomass helps reduce reliance on fossil fuels and global warming [12, 13]. There are mainly two ways to convert biomass to fuels: thermochemical processes such as combustion, pyrolysis, and gasification; and biological pathways such as enzymatic fermentation and trans-esterification [14-16].

1.2 Introduction of the CE-CERT Process

The College of Engineering Center for Environmental Research and Technology (CE-CERT) at the University of California, Riverside (UCR) is developing a multi-step thermal chemical process, which has been shown to convert carbonaceous materials such as wood waste, agriculture waste, and municipal waste, to syngas (a mixture of H_2 and CO) at high conversion efficiency [17-19]. This process has been evaluated by the National Energy Technology Laboratory (NETL), and it is reported that the CE-CERT process has the potential to have 12% higher efficiency and 18% lower capital cost than the most up-to-date conventional mainstream gasification technologies [20].

A diagram of the CE-CERT process is shown in figure 1.1. In the first step, carbonaceous feedstock, along with water and hydrogen, is fed into Steam Hydrogasification Reactor (SHR) in the form of slurry, where the feedstock is converted to gases including methane (CH_4), hydrogen (H_2), carbon monoxide (CO), and carbon dioxide (CO_2). The product gas will then be cleaned to remove the fine particles and sulfur species. After the cleanup reactor, the gases will pass through a Steam Methane Reformer (SMR), where CH_4 in the gases will be catalytically reformed to CO and H_2. This gas mixture is also called syngas.

In the final step, the syngas is fed into a Fischer-Tropsch Reactor (FTR), and converted to liquid fuel product.

The basic reactions that take place in the CE-CERT process are described as follows:

Steam hydrogasification:

$$C + H_2O + 2H_2 \rightarrow CH_4 + H_2O + others\ (CO, CO_2, etc \quad (1.1)$$

Steam methane reforming:

$$CH_4 + H_2O \rightarrow 3H_2 + CO \quad (1.2)$$

Fischer-Tropsch synthesis:

$$nCO + (2n + 1)H_2 \rightarrow C_nH_{2n+2} + H_2O \quad (1.3)$$

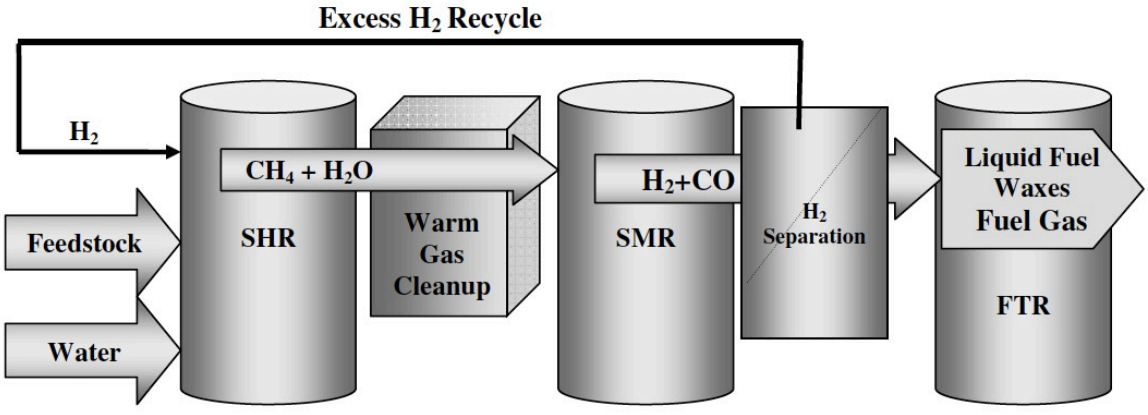

Figure 1.1 Diagram of the CE-CERT Process

The main advantages of the CE-CERT process are summarized as follows [17-19]:

1. Feedstock is fed in the form of slurry, which offers cost reduction of drying the feedstock and more efficient feedstock handling;
2. SHR is operated under reductive conditions. No requirements for external O_2 supply;
3. SHR is working under relatively lower temperature and pressure, compared with other gasification processes such as partial oxidation (POX), which reduces capital cost and offers versatility for both small and large scale applications;
4. Methane is produced from the SHR at a high rate, which could be used as synthetic natural gas directly if liquid fuel production is not desired;
5. An optimum H_2 to CO ratio can be achieved by controlling the input water to carbon ratio of the SHR.

1.3 Introduction of Fischer-Tropsch Synthesis

1.3.1 Fischer-Tropsch Synthesis Reactions and Product Distribution

Fischer-Tropsch (F-T) synthesis is a process that converts syngas (a mixture of CO and H_2) to hydrocarbon products. Chemical reactions taking place in F-T synthesis is complex but can be simplified in to the following reactions [21]:

Heavy hydrocarbons:

$$nCO + 2nH_2 \rightarrow (-CH_2-)_n + nH_2O \quad (1.4)$$

Methane:

$$CO + 3H_2 \rightarrow CH_4 + H_2O \quad (1.5)$$

Alcohols:

$$nCO + 2nH_2 \rightarrow C_nH_{2n+2}O + (n-1)H_2O \quad (1.6)$$

Water-gas shift (WGS):

$$CO + H_2O \leftrightarrow CO_2 + H_2 \quad (1.7)$$

F-T synthesis will also generate other oxygenates such as aldehyde, ketone, ester, etc. Reaction (4) is the predominating reaction. It can be seen that the optimum syngas ratio

(H_2/CO) is about 2. However, the ratio may vary significantly depending on types of catalysts and the extent of other reactions.

F-T synthesis produces a wide range of hydrocarbon products from C_1 to over C_{60}. In a commercial scale F-T facility, it is not likely to produce, on a carbon atom basis, more than 18% C_2, 16% C_3, 42% gasoline (C_5-C_{12}), and 20% diesel fuel (C_{12}-C_{20}) [21]. F-T product distribution follows Anderson-Schulz-Flory (ASF) distribution [22, 23]:

$$W_n/n = (1-\alpha)^2\alpha^{n-1} \quad (1.8)$$

Where

W_n: the mass fraction of the species with carbon number of n;

α: the probability of chain growth.

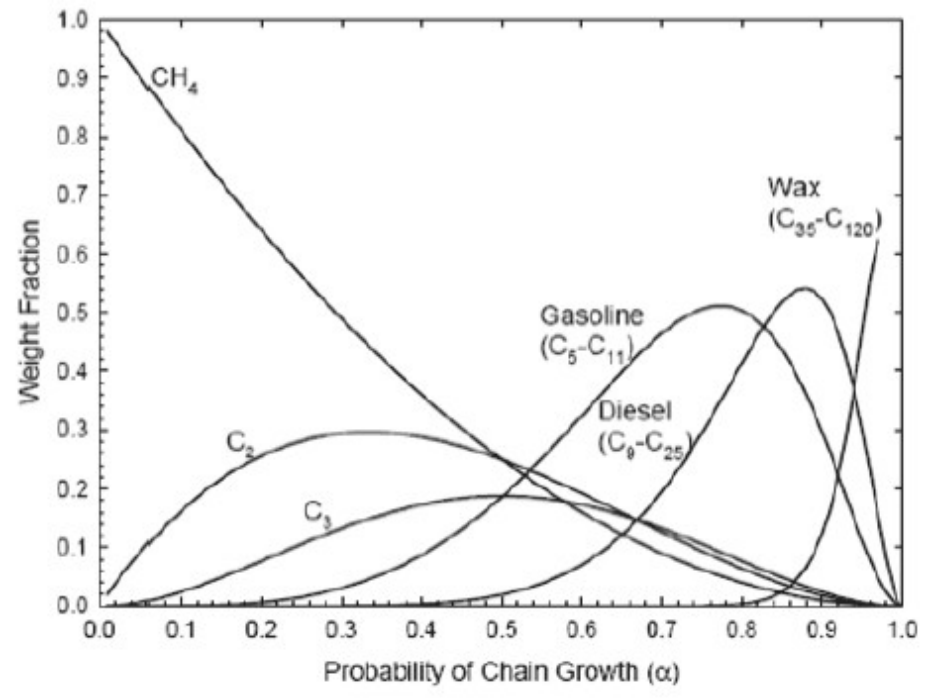

Figure 1.2 Product selectivity as a function of chain growth probability

The relation between product selectivity and α is shown in figure 1.2. It can be seen from the figure that product distribution will vary at different α. As an undesirable product, methane is always present in the products and its selectivity ranges from 1% to 100% (100% selectivity is obtained when using nickel catalyst and operating at high temperature). At the other end of the spectrum, the selectivity of hard wax (C_{20+}) could

range from 0 to 70%. As an indication of certain product distribution, α can be varied by changing operating temperature and pressure, catalysts, syngas ratio, and space velocity. Hamelinck et al [24] developed an empirical model for F-T synthesis product distribution, which can be expressed in equation 1.9:

$$S_{C_{5+}} = a_1 + a_2 \cdot T + a_3 \cdot \frac{[H_2]}{[CO]} + a_4 \cdot ([H_2] + [CO]) + a_5 \cdot p_{Total} \quad (1.9)$$

Where,

$S_{C_{5+}}$: mass fraction of C_{5+} in the total product;

a_i: the parameter depending on different catalyst and type of reactor;

T and p: temperature (K) and pressure (bar);

$[H_2]$ and [CO]: the concentrations expressed as fraction of the feed gas.

With the least sum of square fit of the model with experimental results on Co catalyst reported by Dry[25], equation 9 becomes:

$$S_{C_{5+}} = 1.7 - 0.0024T - 0.088\frac{[H_2]}{[CO]} + 0.18([H_2] + [CO]) + 0.0078p_{Total} \quad (1.10)$$

Then α can be approached by:

$$\alpha \approx 0.75 - 0.373\sqrt{-\log\left(S_{C_{5+}}\right)} + 0.25S_{C_{5+}} \qquad (1.11)$$

The computer model can be used to calculate W_n from ASF distribution expressed in equation 8.

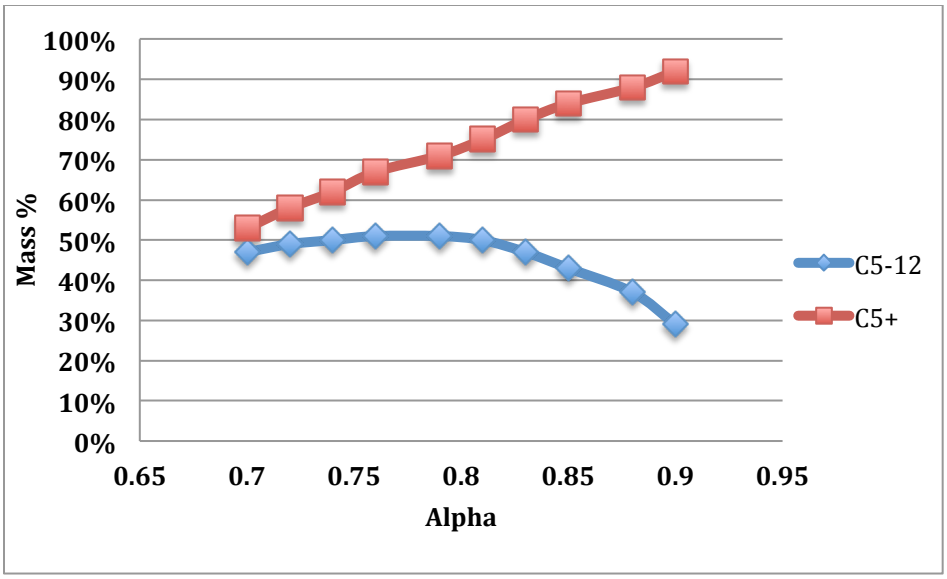

Figure 1.3 Relation of F-T selectivity and α

Control of the selectivity, to a large extent, is determined by the factors that affect α. Hence the relation of selectivity and α is firstly studied, as shown in figure 1.3. From the figure we can see that, the selectivity of liquid and solid products (C_{5+}) rises with

increasing α. When α increases from 0.7 to 0.9, there is a 40% growth of non-gas products selectivity. At the point where α is 0.9, only 8% of the total yield is gasous products. The relation of α and the selectivity of gasoline-range products (C_5-C_{12}) shows a different trend. The selectivity of gasoline-range products (C_5-C_{12}) increases with the increase of α in the beginning then reaches a peak value of 51% at α is from 0.75-0.8. In the range of α larger than 0.8, selectivity of gasoline-range products declines sharply with increasing α. The possible reason that causes this trend is when *the* α value is low most products are gases and light gasoline-range liquids. With the increase of α, the selectivity of gasoline-range products increases because of a drop of gaseous product selectivity. However, further increase of α causes a significant increment of C_{13+} products, which lower the selectivity of C_5-C_{12} products. F-T synthesis running at a high α value will suppress the selectivity of gaseous product and increase the efficiency of liquid fuel production.

The change of α with different temperature and pressure are shown in figure 1.4. In figure 1.4A, the reaction temperature is set to 220 °C, and H_2 to CO molar ratio is 2:1. While in figure 1.4B, the syngas pressure is 25 bar, and H_2:CO=2:1. It shows in figure 1.4A that, when operating temperature and syngas ratio remain constant, α rises with increasing

syngas total pressure. The reason may be that the increase in operating pressure favors the formation of products with less total pressure, i.e., more liquid and above product and less gas. This meets the operating condition with a high α. Hence α will go up with increasing syngas total pressure. A high pressure of 20-40 bar is often favorable in the F-T process. The relation of α and operation temperature at constant pressure and H_2: CO ratio is shown in figure 1.4B. A decrease of α with ascending temperature is observed. The mechanism of chain growth can be used to explain this phenomenon. Desorption of growing hydrocarbons from catalyst surface is one of the main chain termination steps. Since desorption is an endothermic process, higher temperature will increase the rate of desorption, which will then cause an increasing selectivity of light product. As a result, α will decrease.

The effect of H_2/CO ratio on α and gaseous products (C_1-C_4) selectivity is also modeled, the relation are shown in figure 1.5. In this comparison, operating temperature and pressure is 220 °C and 25 bar, respectively. From the figure it can be seen that, with increasing H_2/CO ratio, α keeps dropping while the gas selectivity has a significant increase. Increase of H_2/CO ratio indicates higher H_2 partial pressure and lower CO partial pressure, i.e., lower amount of CO monomer. As discussed in section 1.3.4, two

key steps leading to chain termination are olefin formation by desorption of the chains and paraffin formation by hydrogenation of the chains. On the one hand, the lower the CO monomer amounts, the lower the catalyst surface coverage by monomers, thus the higher probability of desorption (chain termination); on the other hand, the higher the partial pressure of H_2, the higher the probability of chain termination by hydrogenation. As a result, increasing H_2/CO ratio cause a higher probability of chain termination, hence promotes selectivity of gaseous products and lowers α.

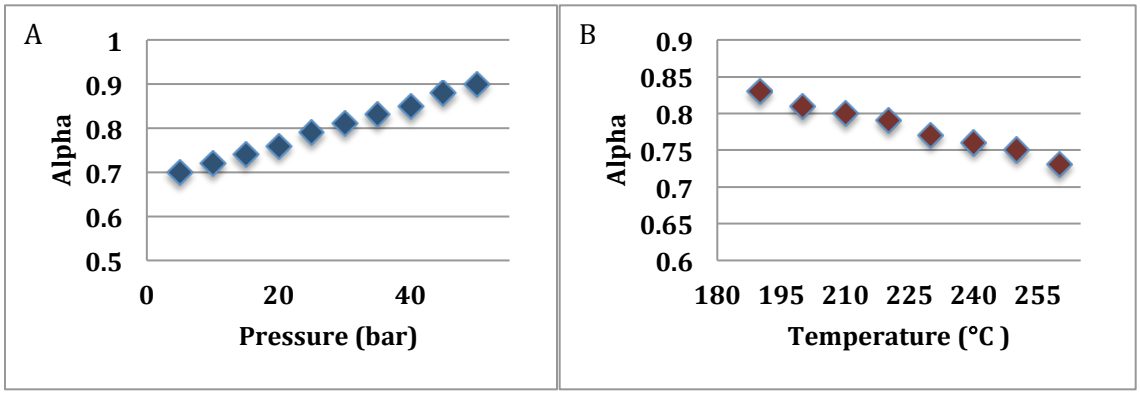

Figure 1.4 A: relation of α and pressure at T=220°C; B: relation of α and operation temperature at p_{Total}=25bar

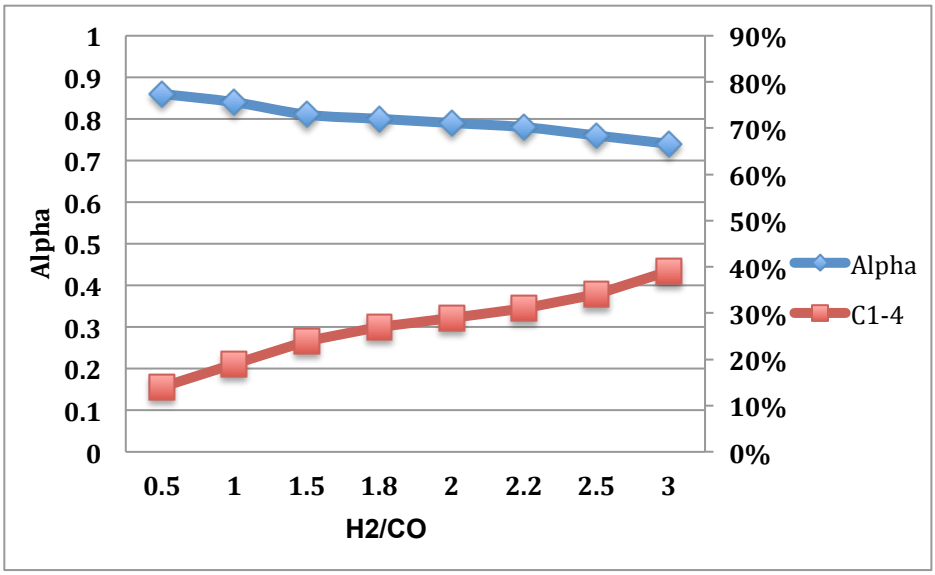

Figure 1.5 Change of α and gas selectivity with H_2/CO ratio

To sum up, selectivity is closely related with α. A high value of α is favorable in F-T liquid fuel production. α increases with decreasing temperature, increasing syngas total pressure, and decreasing H_2/CO ratio. The operating temperature for cobalt F-T synthesis is usually set at 220°C and no lower than 200°C to maintain high reaction rate. The total syngas pressure ranges from 20-40 bar, in consider of cost of syngas and high pressure vessels, and safety issues; H_2/CO ratio ranges from 2.06~2.16 [21] to ensure sufficient usage of syngas.

1.3.2 F-T Reactors

There are mainly three kinds of F-T reactors in commercial use: fixed bed reactor, fluidized bed reactor, and slurry phase reactor, as shown in figure 1.6 [26-28]. The fluidized bed reactors (figure 1.6B) operates in the temperature range of 320 °C to 350 °C, which is 100 °C higher than fixed bed reactor (figure 1.6A) and slurry phase reactor (figure 1.6C) of 220 °C to 250 °C. As a result, they are often described as high temperature Fischer-Tropsch (HTFT) and low temperature Fischer-Tropsch (LTFT), respectively.

Fluidized bed reactors operate with iron catalysts at about 340°C and 20-40 bar. This HTFT process mainly produces light olefins, light oxygenates, and gasoline. As shown in figure 1.3B, there are two types of fluidized bed reactors: circulating fluidized bed (CFB) and fixed fluidized bed (FFB). FFB reactors are more advanced than CFB reactors with about 40% lower cost, higher operating pressure, and better catalyst protection. Sasol Advanced Synthol (SAS) reactor is one of the FFB reactors that could achieve CO conversion up to 90% and yield of 20,000 barrel/day (850,000 tons per year) [21, 26, 27].

Slurry bed reactor is widely applied in F-T wax production, which has been extensively studied [27, 29-31]. During the operation, catalysts are suspended in hydrocarbon liquid,

and syngas is fed from the bottom in the form of bubbles. This allows the catalyst to have more chance to react with syngas, and increases the catalyst activity. Also, the liquid-phase reaction has better heat transfer, which allows the F-T synthesis operated at a high temperature [32]. A slurry bed reactor can work very efficiently, even better than a fixed bed reactor. However, it also has some disadvantages compared with fixed bed reactors such as difficulties in product separation, low sulfur tolerance [33], catalyst attrition, and difficulties in reactor design [34-36].

Fixed bed reactors are used in LTFT process, and hard wax is the main product target [37]. Fixed bed reactors are constructed in multi-tubular with the catalyst loaded inside the tube and cooling medium on the shell side. In order to transfer the heat generated in the reaction efficiently to the cooling medium, small tube diameters and high space velocity are preferred in fixed bed F-T synthesis. Besides, F-T catalysts are usually made small to obtain a large surface area and also high conversion [38, 39]. Fixed bed reactors have many advantages. They are easy to operate; product collection is easy since the liquid wax will trickle down the bed and is collected in a downstream trap; they have relatively higher sulfur tolerance than other types of reactors; and since the catalysts don't move during operation, it has much less chance of attrition when operating in fixed

bed reactors [40, 41]. However, the pressure drop in a fixed bed reactor is higher than other reactors, which result in higher cost for gas compression. In addition, catalyst loading and unloading is also troublesome in narrow tubes [21, 37].

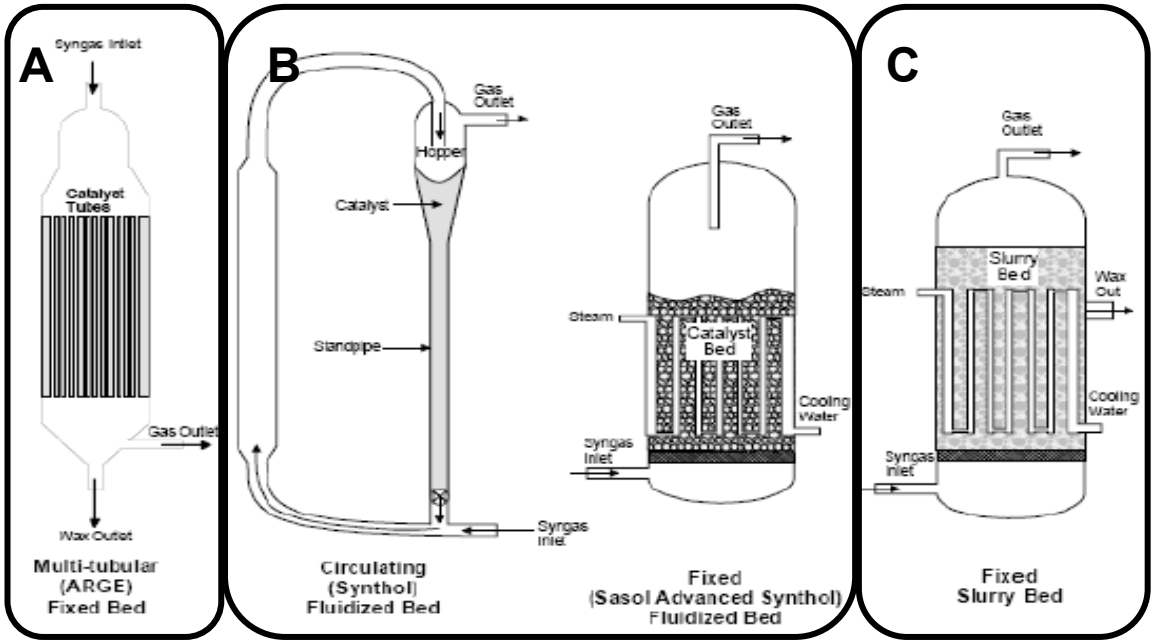

Figure 1.6 Fischer-Tropsch reactors. Fixed bed reactor: A; fluidized bed reactor: B; slurry bed reactor: C.

1.3.3 F-T Catalysts

There are four metals that have F-T synthesis activity: Co, Fe, Ni and Ru. Among all the metals, Ru is most active [42]. However, high cost and low availability prevent it from

large-scale application. Nickel is also very active, but it has a higher selectivity of methane than Co and Fe catalyst [21]. So current F-T plants such as Sasol and Shell's Malaysian plant only use Fe and Co catalyst. For the production of high value linear alkenes and oxygenates, Fe catalyst, as shown in figure 1.7A, is often used in fluidized bed reactor at high temperature [43, 44]. Besides, Fe catalyst is also applied to coal based F-T synthesis, due to its high water-gas shift activity (Equation 1.7) [45, 46]. Coal derived syngas has a H_2/CO ratio lower than 2, but Fe catalyst is able to convert certain amounts of CO to H_2. As a result, the optimum H_2/CO ratio for Fe catalyzed F-T synthesis is about 1.6/1 [21].

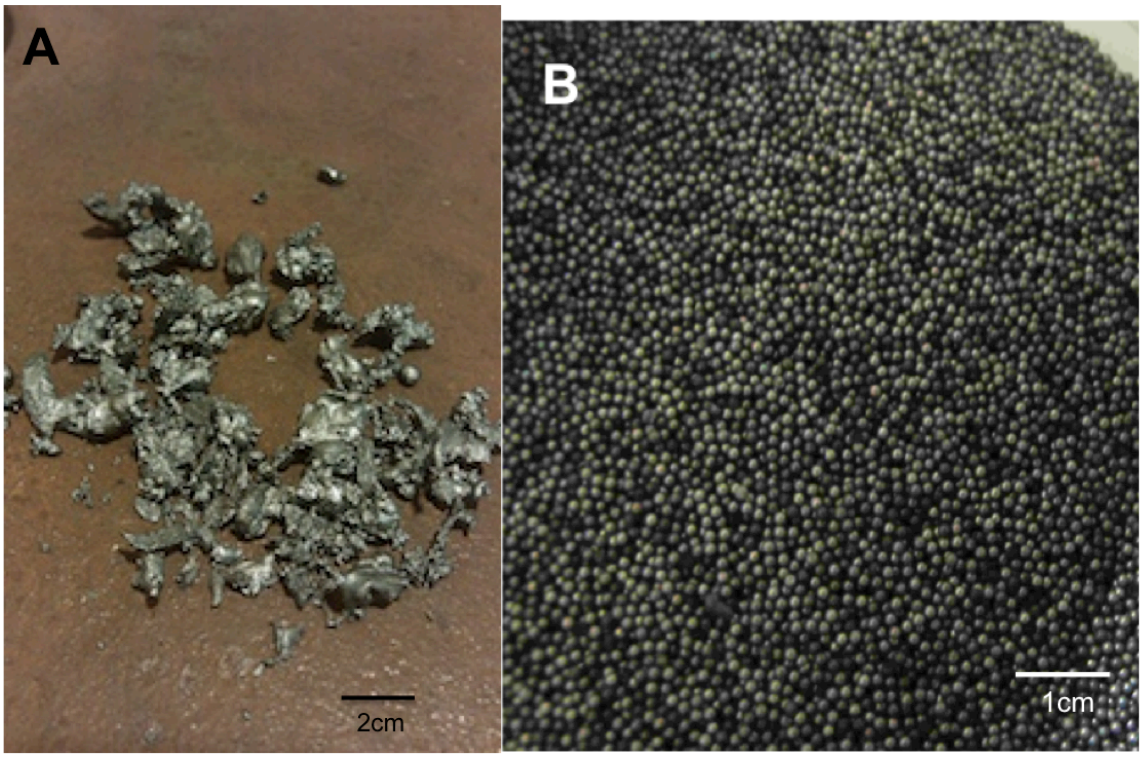

Figure 1.7 Fischer-Tropsch catalysts. Fe catalyst: A; Co catalyst: B

Co catalyst, as shown in figure 1.7B, is much more active than Fe, therefore F-T plants focusing on liquid fuel production mainly use Co-based catalyst. Co is 1000 times more expensive than Fe. Because of the high cost of cobalt, it is important to minimize the cobalt content while maintain a high cobalt metal surface area. A common method is incipient wetness impregnation, by which cobalt is supported on stable oxides that having large surface areas and required pore size distribution [47]. In addition, an important characteristic for Co catalyst is that it has very low water-gas shift activity, so the

optimum syngas ratio for Co catalyst is about 2.06-2.16 [48]. Due to the high cost of cobalt, minimizing the rate of activity decline in order to ensure a long lifetime is very desirable for Co catalyzed F-T process. Other than oxygen, sulfur compounds in the syngas will permanently poison Co catalyst. It is suggested that sulfur content should be lower than 0.5 ppm [49]. However, a fixed bed reactor will provide better sulfur tolerance, since sulfur will be absorbed by upper sections of the catalysts, leaving the lower sections unaffected. Another important factor in the deactivation of Co catalyst is water vapor. There are three aspects involved, sintering of the cobalt metal particles, oxidation of cobalt, and formation of F-T inactive compounds such as cobalt silicates and cobalt aluminates [50, 51]. It can be seen from Equation 1.4 that water is produced during F-T synthesis, so high syngas space velocity is recommended to help remove the water vapor.

1.3.4 Mechanism of F-T Synthesis

Product selectivity as a function of chain growth probability α is shown in figure 1.2. In order to explain this product selectivity, it is assumed that the basic building blocks

(monomers) of the F-T synthesis are the CH_2 units, which are chemisorbed on the catalyst surface. The reaction that may take place is shown in figure 1.8.

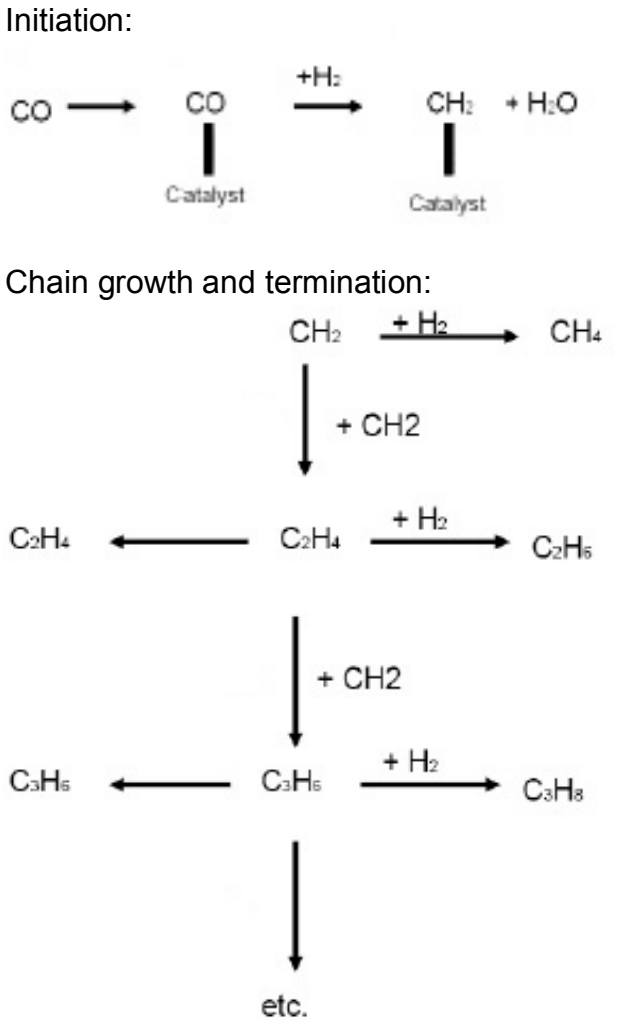

Figure 1.8 Fischer-Tropsch reaction sequences

A CH_2 unit can react with hydrogen to form methane, which will desorb from the surface; or it can link up with another CH_2 to form C_2H_4. C_2H_4 species have three choices: it can link up with another CH_2, or it can be hydrogenated to yield ethane, or it can desorb to form ethene. The first option is the probability of chain growth, which is referred as α; while the last two options are the probability of chain termination, (1- α). The reaction sequences can continue and thus the product hydrocarbons can range from methane to high molecular weight waxes. The higher the value of α, the longer the hydrocarbon chains are [23, 52]. Assume that the probability of chain growth is independent of chain length, then the weight fraction of any hydrocarbon produced could be described by α, as shown in Equation 1.8.

1.4 Introduction of ZSM-5 Catalyst

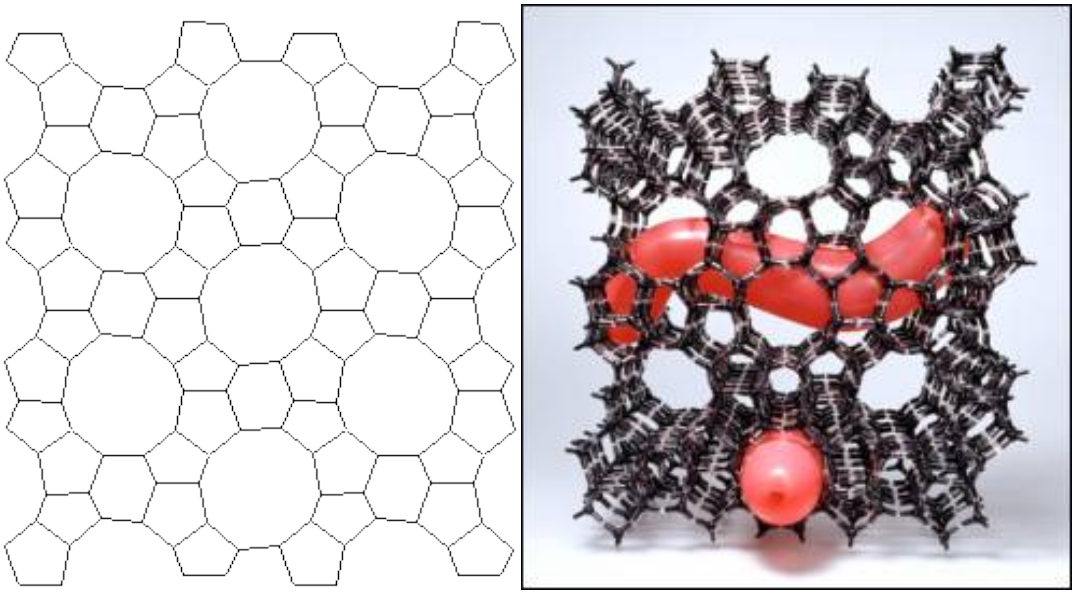

Figure 1.9 Structure of ZSM-5catalyst.

A zeolite is a three-dimensional crystalline aluminosilicate that is made by vertex-sharing of AlO_4 and SiO_4 tetrahedra. ZSM-5 is one kind of zeolite, which is composed of pentasil units linked together by oxygen bridges, as illustrated in figure 1.9. These units are linked to form pentasil chains, and the chains are interconnected by oxygen bridges to form corrugated sheets with 10-ring holes. The diameter of the 10-ring holes is about 0.51-0.55 nm, which would only allow molecules with smaller size to pass through [53].

In addition, when an Al^{3+} cation replaces a Si^{4+} cation in the structure, an additional positive charge is needed to keep a neutral charge. With proton (H^{+}) as the cation, the material can become very acidic [54]. As a result, ZSM-5 can be utilized for acid-catalyzed reactions such as hydrocracking, hydrocarbon isomerization and alkylation. ZSM-5 is now widely applied in refinery process, working as catalyst in fluid catalytic cracking (FCC) units [55, 56]. Researches have been done to investigate cracking properties for different catalyst including ZSM-5 [57-59]. Corma et al. [57] compared the cracking of n-alkanes of ZSM-5, USY, and zeolite beta, and it is found that ZSM-5 has the best hydrogen transfer selectivity, highest product olefin to paraffin ratio, and low selectivity to aromatics. Zhao et al. [60] also implied that, compared with H-mordenite zeolite, H-ZSM-5 has better acid strength and stability in performance test.

1.5 Combination of F-T catalyst and zeolite

In recent years, researches have been done on combining conventional F-T catalysts with zeolite or other acidic support to produce more iso-paraffin, and narrow product distribution, which is close to synthetic gasoline. Firstly, the combination was a physical

mixture of zeolite with conventional F-T catalyst [61]. Martínez et al.[62] prepared a hybrid catalyst by physically mixing K-Fe-Co F-T catalyst with ZSM-5 catalyst at 1:1 mass ratio. It is found that product distribution is shifted towards gasoline-range iso-paraffin and aromatics. In addition, another combination of F-T catalyst with zeolite support was also investigated [63-65]. Espinosa et al.[66] synthesized a bifunctional catalyst by impregnating Co in Beta zeolite. F-T synthesis experiment with this catalyst showed significant increase of iso-paraffin selectivity. However, the selectivity of C13-C17 range is about 20 wt%, which means that this catalyst cannot effectively break down heavy components. Recently, F-T catalyst with zeolite shell has been developed. The zeolite shell can effectively remove all heavy components larger than it's channel size, thus gasoline range product selectivity is significantly improved. Yang et al. [67] synthesized a zeolite-shell catalyst, which has a zeolite shell around conventional F-T catalyst. This core-shell structure has a very high selectivity towards gasoline-range iso-paraffin. However, the zeolite shell cause different diffusion rate of H_2 and CO, which results in a high selectivity of methane. Methane selectivity were reduced by using H-β/Co/Al2O3 core-shell catalyst, while maintaining high iso-paraffin selectivity [68]. Similarly, Huang et al.[69] prepared CoZr/H-ZSM-5 hybrid catalysts through

hydrothermal synthesis method. The combination of Fischer-Tropsch catalyst and acidic zeolites can improve gasoline-range hydrocarbon selectivity and isoparaffin selectivity. Street et al.[70] studied gasoline-range aromatics production from syngas. Mo/HZSM-5 catalyst had been synthesized, and Fischer-Tropsch synthesis was conducted with CO_2 containing syngas mixture. The product liquid is mostly gasoline-range aromatics. However, organic phase selectivity of the synthesis is only 0.8%. Chevron is also actively involved in F-T gasoline research. They have developed a zeolite-support Co hybrid F-T catalyst, which impregnate Co in ZSM-12 zeolite [71]. This catalyst is basically same with [66], except that they use different kind of zeolite support. Tsubaki et al [72, 73] developed a new catalyst by coating a zeolite membrane on the surface of the Co F-T catalyst. With this special core-shell structure, syngas could still pass through the zeolite shell and react on Co catalyst; and the heavy hydrocarbons formed must enter the zeolite channels to be hydrocracked and isomerized. The hydrocarbons produced from the new catalyst are of smaller size than zeolite channel, which range from C_1 to C_{10}. Thus gasoline could be produced by simply separating the gaseous components. This work shows a promising way to produce gasoline in one step from F-T reactor. However, it is reported that due to the difficulty of zeolite synthesis on Co catalyst, the H-ZSM-5

coating is not perfect [74]. In addition, methane selectivity of the F-T synthesis is 15%. According to figure 2, an α value of about 0.6 is obtained. This indicates that F-T synthesis is not operating in the optimum condition, and there is still potential of further improvements.

1.6 Thesis Objectives

The overall objective of the thesis is to develop an efficient, economical, and technically viable Fischer-Tropsch gasoline process for the steam hydrogasification technology. The detailed objectives is described as follows:

1. The first objective is to develop a hybrid Fischer-Tropsch catalyst with zeolite shell. The catalyst can not only produce long chain hydrocarbons from syngas, but also crack long chain hydrocarbons into short chains, and isomerize straight chain paraffin to iso-paraffin. The zeolite-shell F-T catalyst with different silicon to aluminum ratio will be prepared using secondary-growth hydrothermal synthesis method. Then the catalyst surface and cross section will be examined by SEM.

Zeolite shell composition will also be tested using EDX and XRD. Finally, catalyst surface area will be measured by BET test.

2. The second objective is to design and construct a lab-scale high-temperature high-pressure continuous Fischer-Tropsch synthesis reactor system. The reactor system will be equipped with safety features such as walk-in hood, CO monitor, auto shut-off valve, and pressure relief valve. Also, the reactor should be compatible with both conventional F-T catalyst and zeolite-shell F-T catalyst. In addition, the reactor system should have online gas and liquid sampling feature to improve test efficiency and reduce total experiment time. Finally, reactor automation system will be built using LabVIEW program. The automation program will be able to read and write all process variables and control reactor heating with built-in PID controller.
3. The third objective is to evaluate performance of F-T gasoline performance. F-T synthesis test will be conducted at various temperature and space velocity conditions, using zeolite-shell F-T catalyst with different silicon to aluminum ratio. CO conversion and methane selectivity will be measured to evaluate catalyst activity. Liquid product speciation will also be accomplished to evaluate

gasoline range hydrocarbon selectivity and composition. In addition, sensitivity analysis will be used to assess the significance of process variables on gasoline selectivity and quality. Finally, time on stream study and thermal gravimetric analysis will be done to evaluate catalyst life.

CHAPTER 2 Synthesis of H-ZSM-5 shell Co/Al_2O_3 Fischer-Tropsch Catalyst

In this chapter, development of a hybrid Fischer-Tropsch catalyst with zeolite shell will be discussed. The zeolite-shell F-T catalyst with different silicon to aluminum ratio will be prepared using secondary-growth hydrothermal synthesis method. Then the catalyst surface and cross section will be examined by SEM. Zeolite shell composition will also be tested using EDX and XRD. Finally, catalyst surface area will be measured by BET test.

2.1 Synthesis of Co/Al_2O_3 Fischer-Tropsch Catalyst

The conventional Co/Al_2O_3 Fischer-Tropsch catalyst was prepared by Dr. James Spivey at Louisiana State University using incipient wetness co-impregnation method [75, 76]. The nominal combination of the catalyst was 20 wt. % Co and 1 wt. % Ru supported on γ-alumina (Sasol 610110).

To start impregnation procedure, the precursors, $Co(NO_3)_2 \cdot 6$ H2O (Alfa Aesar 36418) and $Ru(NO)(NO_3)_3$ (Alfa Aesar 12175), were dissolved separately in de-ionized water and mixed together in proportions designed to give the target ratio of metals. Then γ-alumina with diameter of 1 mm was immersed in the precursor liquid. Because of the

limited pore volume and solubility of these precursors, four impregnations were required for the sample (pore volume = 0.46 cc/g). Between each impregnation, the samples were dried in air at 80 °C for 16 hr. When impregnation process completed, the catalyst were calcined in flowing air with a temperature ramp of 1°C/min to 300 °C and held at this temperature for 6 hours. The prepared catalyst is named LSU-1.

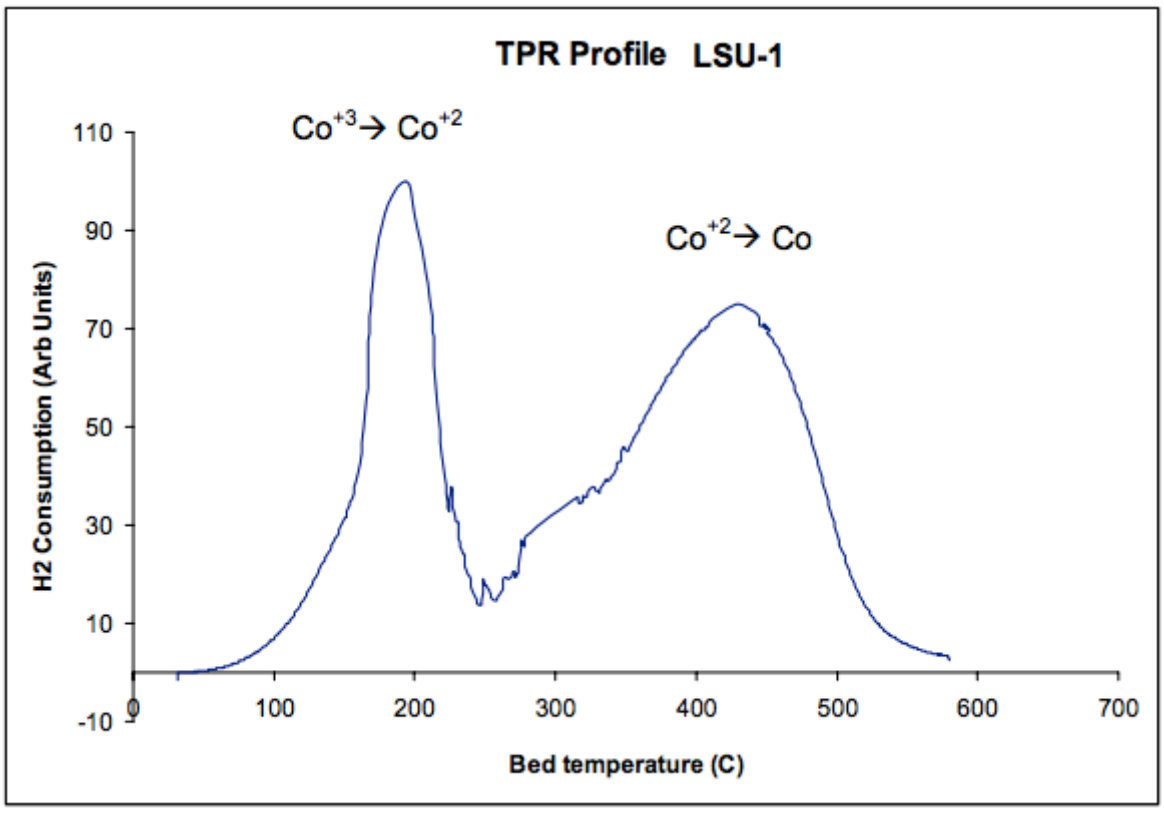

Figure 2.1 H_2-TPR profile of LSU-1 Co/Al_2O_3 Fischer-Tropsch Catalyst [77]

Temperature-programmed reduction is a technique for characterization of solid materials to find optimum reduction condition, which is often used in the field of heterogeneous catalysis [78-80]. The oxidized catalyst sample is reduced in flowing gas at programmed temperature ramp. The TPR profile given in Figure 2.1 was carried out on LSU-1 catalyst. A sample of this catalyst weighing 0.8g was pretreated with Argon at 100 cc/min while the temperature was ramped to 120 °C at 10 °C/min and held for 30 minutes. After cooling down, the flow was changed to a 10% H2/Ar mixture (the reducing gas) as the temperature was ramped to 600 °C at 5°C/min and held for 5 minutes. A TCD (Thermal Conductivity Detector) was used to qualitatively measure hydrogen consumption with temperature. There are two H_2 consumption peaks observed from the figure. The low temperature peak at around 200 °C is assigned to the reduction of Co^{+3} to Co^{+2}, and the high temperature peak to the reduction of Co^{+2} to Co. Thus, in order to ensure complete catalyst reduction, a minimum temperature of 300 °C is required. In this thesis, reduction condition is 350 °C for 6 hr.

2.2 Synthesis of H-ZSM-5 shell Co/Al_2O_3 Fischer-Tropsch Catalyst

2.2.1 Introduction of Zeolite Membrane Synthesis

There are mainly two methods of zeolite membrane synthesis: ex-situ synthesis and in-situ synthesis. For ex-situ synthesis, zeolite powder is first synthesized using hydrothermal synthesis method. Then the zeolite powder fills or deposits on non-porous substrates and form membrane [81-83]. As to in-situ membrane synthesis, zeolite membrane is directly hydrothermal synthesized on porous or non-porous substrates [84, 85], which is the most common method used.

In in-situ zeolite membrane synthesis, substrate is immersed in the synthesis gel in autoclave. At certain temperature, high pressure is created by saturated steam, and zeolite membrane is grown on the substrate surface. The factors that affect in-situ zeolite synthesis are composition of synthesis gel, crystallization temperature, and substrate pretreatment, where synthesis gel composition is the most influential factor. Wang et al. [86] studied ZSM-5 membrane formation with different synthesis gel composition, and found that ZSM-5 membrane with no defect can be synthesized at synthesis gel composition of 0.32TPAOH: TEOS: $165H_2O$. Yan et al. [87] also found the optimum synthesis gel composition of TPAOH: SIO_2: H_2O: NaOH: Al_2O_3= 1: 6: 571: 4: 0.005, and

synthesized ZSM-5 membrane with thickness of 10 μm. In addition, reaction temperature is also an important factor on zeolite membrane synthesis. Yan et al. [88] studied temperature effect on zeolite membrane formation at synthesis gel composition of 0.32TPAOH: TEOS: 165H_2O. It is found that ZSM-5 membrane could be synthesized at temperature higher than 165 °C. With increasing synthesis temperature, zeolite crystal size also increases, but membrane thickness is unchanged. In situ zeolite membrane synthesis is relatively easy and low cost. However, without multiple hydrothermal syntheses, the synthesized membrane is often discontinuous and defective.

In order to achieve better zeolite membrane quality, secondary growth method is developed for synthesis of MFI (mainly ZSM-5 and Silicalite-1) zeolite [89-92]. In secondary growth method, substrate is first immersed in Silicalite-1 seed gel, and form precursor membrane. It is then put in autoclave contained zeolite synthesis gel for secondary growth of zeolite membrane. Tsapatsis et al. [93] successfully synthesized Silicalite-1 zeolite membrane on macroporous α-alumina ceramic tube and porous stainless steel tube using secondary-growth method. The membrane thickness is from 15 to 20 μm. Richter et al. [94] studied secondary-growth of ZSM-5 on ceramic tube or capillary tube, and observed that decreasing seed particle size reduced thickness of

zeolite membrane. Wang et al. [95] also pointed out the advantage of secondary-growth method compared with in-situ membrane synthesis, and synthesized Silicalite-1 zeolite membrane with thickness of only 200-800 nm.

2.2.2 Zeolite-shell F-T Catalyst Synthesis Preparation

The list of experimental reagents is shown in table 2.1. Tetrapropylammonium hydroxide (TPAOH) is used as synthesis template; Tetraethyl orthosilicate (TEOS) is used as silicon source; Aluminum nitrate ($Al(NO_3)_3$) is used as aluminum source; Potassium hydroxide (KOH) is used to pretreat Co F-T catalyst; Hydrogen chloride (HCl) is used to neutralize KOH solution; and ethanol is used as solvent.

Reagents	Remarks	Specs	Manufacturers
TPAOH	Light yellow liquid	1.0 M in H_2O	Sigma-Aldrich
TEOS	Colorless liquid	98%	Sigma-Aldrich
$Al(NO_3)_3$	White powder	≥98%	Sigma-Aldrich
HCl	Colorless liquid	1.0 M in CH_3COOH	Sigma-Aldrich
KOH	White flakes	90%	Sigma-Aldrich
EtOH	Colorless liquid	≥99.5%	Sigma-Aldrich

Table 2.1 List of experimental reagents

Besides, experiment tools are also prepared, including weighing balance, stir plate, sample tubes, beakers, and pipettes, as shown in figure 2.2.

Figure 2.2 Photo of experimental tools in the hood

In addition, a furnace is used for catalyst calcination, and an oven is used for catalyst synthesis, as shown in figure 2.3 and 2.4, respectively. Both the oven and furnace are connected to FieldPoint modules and controlled by LabVIEW program. Thus data acquisition and recording can be done automatically, and temperature ramp of the oven and furnace can be controlled precisely. The LabVIEW program also provides auto shut-off function in case of emergency.

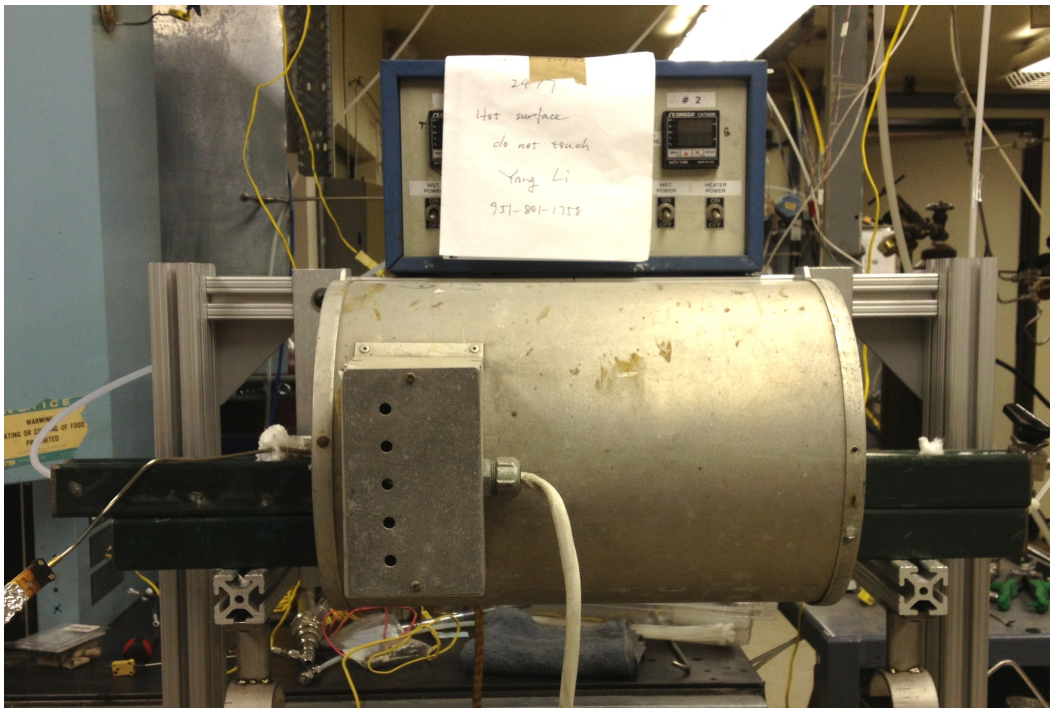

Figure 2.3 Photo of furnace

Figure 2.4 Photo of oven for zeolite synthesis with autoclave rotator

The oven for catalyst synthesis also equipped with a tailor-made autoclave rotator (figure 2.4). The autoclaves are placed on two rebar. One of the rebar can rotate freely while the other one is connected to a gear motor placed outside the oven. Once the rebar is rotating with the motor, autoclaves will rotate with the rebar. Since the driving force for

autoclaves is friction, a small motor is needed, which saves equipment cost and power consumption.

The reason why autoclaves need to be rotating during catalyst synthesis is to make sure all catalyst has equal chance to contact with synthesis gel, so synthesized catalyst can have better and more uniformed shell coverage. If autoclave is not rotating during synthesis or rotation speed is too low, there will be catalyst chunks observed (figure 2.5A), and catalyst surface is not completely covered by zeolite (figure 2.5B).

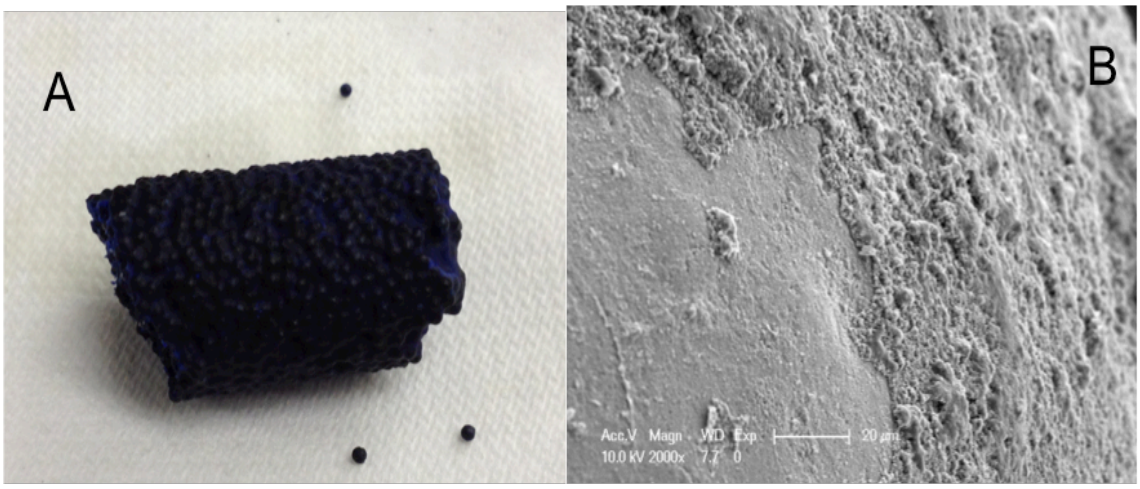

Figure 2.5 Zeolite shell F-T catalysts without autoclave rotation. Photo of catalyst chunk: A; SEM image of zeolite surface: B

2.2.3 H-ZSM-5 shell Co/Al_2O_3 Fischer-Tropsch Catalyst Synthesis Procedure

The schematic illustration of the membrane synthesis process is shown in figure 2.6. There are mainly four steps.

1. The first step is synthesizing Silicalite-1 seed gel. It is prepared by mixing TPAOH, EtOH and water, and then TEOS is added dropwise. The precursor gel is then agitated for 24 hours, and then put into autoclaves for crystallization at 98 °C for 24 hours [96].
2. The second step is catalyst seeding. Conventional Co F-T catalyst pellets were cleaned with 2M KOH solution. Then the pellets were neutralized by concentrated HCl and distilled water. Afterwards, the catalyst pellets were immersed in the Silicalite-1 seed sol with ultrasound treatment for 2 min, then washed with deionized water, dried in room temperature and calcined in air at 450 °C for 3hr. with temperature of 1 °C/min.
3. The third step is preparation of secondary-growth gel. It is prepared by dissolving $Al(NO_3)_3$ in TPAOH and distilled water, followed by dropwise addition of TEOS. The recipe for zeolite synthesis with different silicon to aluminum ratio is shown in table 2.2.

4. The last step is secondary-growth of ZSM-5 shell. 5g of the seeded catalysts were immersed in 25mL of the secondary growth solution, and put in autoclave at 185 °C for 48h. After the synthesis, the ZSM-5 coated catalysts were washed with deionized water, dried in room temperature and then calcined at 450 °C for 3 hr. with temperature of 1 °C/min, in order to remove the template in the zeolite pores.

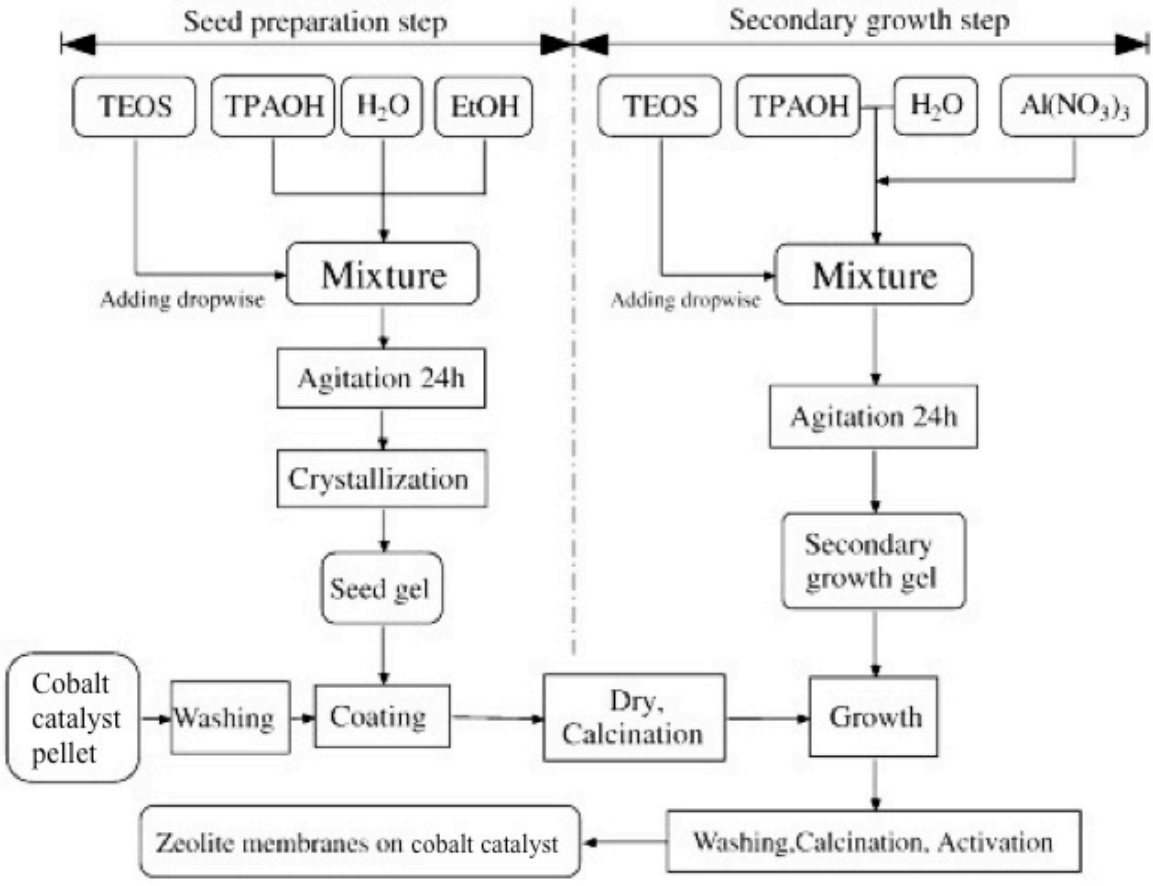

Figure 2.6 Schematic diagram of the zeolite shell synthesis by secondary growth method [97]

Reagents	TPAOH (g)	$Al(NO_3)_3$ (g)	TEOS (g)	H_2O (g)
SAR 50	9.126	0.425	11.925	103.585
SAR 80	9.138	0.266	11.940	103.784
SAR 110	9.143	0.194	11.947	103.875
SAR 150	9.147	0.142	11.952	103.939
SAR 200	9.149	0.107	11.955	103.984
SAR 250	9.151	0.085	11.957	104.010

Table 2.2 Composition and amount of chemicals of 125g Secondary-growth gel for ZSM-5 with different silicon to aluminum ratio (SAR)

2.3 Catalyst Characterization

2.3.1 Introduction

There are five methods used for catalyst characterization: scanning electron microscopy (SEM), energy-dispersive X-ray spectroscopy (EDX), X-ray diffraction (XRD), BET surface area, and thermogravimetric analysis (TGA).

Scanning electron microscopy (SEM) is an electron microscope that images the sample surface by scanning it with a high-energy beam of electrons. Compared with conventional light microscopes that use a series of glass lenses to bend light and create magnified images, SEM creates images by using electron beams instead of light waves. Since the size of focused electron beams is much smaller than light wavelength, images from SEM have much higher magnification. Due to the high resolution of SEM, it is widely used in surface characterization of catalyst [98-100].

Energy dispersive X-ray analysis (EDX) is a technique to analyze near surface elements, estimate element proportion at different position, and give an overall mapping of a sample. EDX is used in conjunction with SEM. During SEM test, an electron beam strikes the surface of sample, and creates X-rays with different energy depend on the material. EDX is often used in catalyst characterization for elemental analysis [101, 102].

X-ray diffraction (XRD) analysis is used to determine crystal structure of molecules and atoms. It can provide information about crystallinity, crystallite size, orientation of the crystallites, and phase composition in crystalline materials. The basic principle of XRD is: when an X-ray beam is created and encountered a crystal lattice of the sample, scattering occurs and a peak is shown. With different rotation angle of sample, different peaks will shown at different rotation angle, and a unique pattern is created for specific crystal. XRD is often used to identify zeolites [103, 104].

BET surface area analysis is used to measure the surface area of a sample. This is done by physical adsorption of gas on the surface of the solid and then calculating the amount of gas adsorbed. The physical adsorption results from Van Der Waals force between the gas molecules and adsorbent surface. BET test is carried out at the temperature of liquid nitrogen, and sample needs to be degased before test. BET analysis is widely used in zeolite characterization [105, 106].

Thermogravimetric analysis (TGA) is performed by gradually increasing the sample temperature in a furnace and measuring the remaining weight on an analytical balance, then weight change of the sample as a function of temperature can be obtained. It is mainly used to measure material thermal stability, moisture and solvent content, and the

percentage of different components in a compound [107, 108]. In this thesis, TGA is used to measure catalyst moisture content and amount of carbon deposition.

2.3.2 SEM and EDX Results

Surface SEM images of H-ZSM-5 shell Co/Al_2O_3 Fischer-Tropsch catalyst is shown in figure 2.7. It can be seen that the catalyst has smooth surface (figure 2.7 A), no cracks and pinholes can be observed even with further magnification (figure 2.7 B).

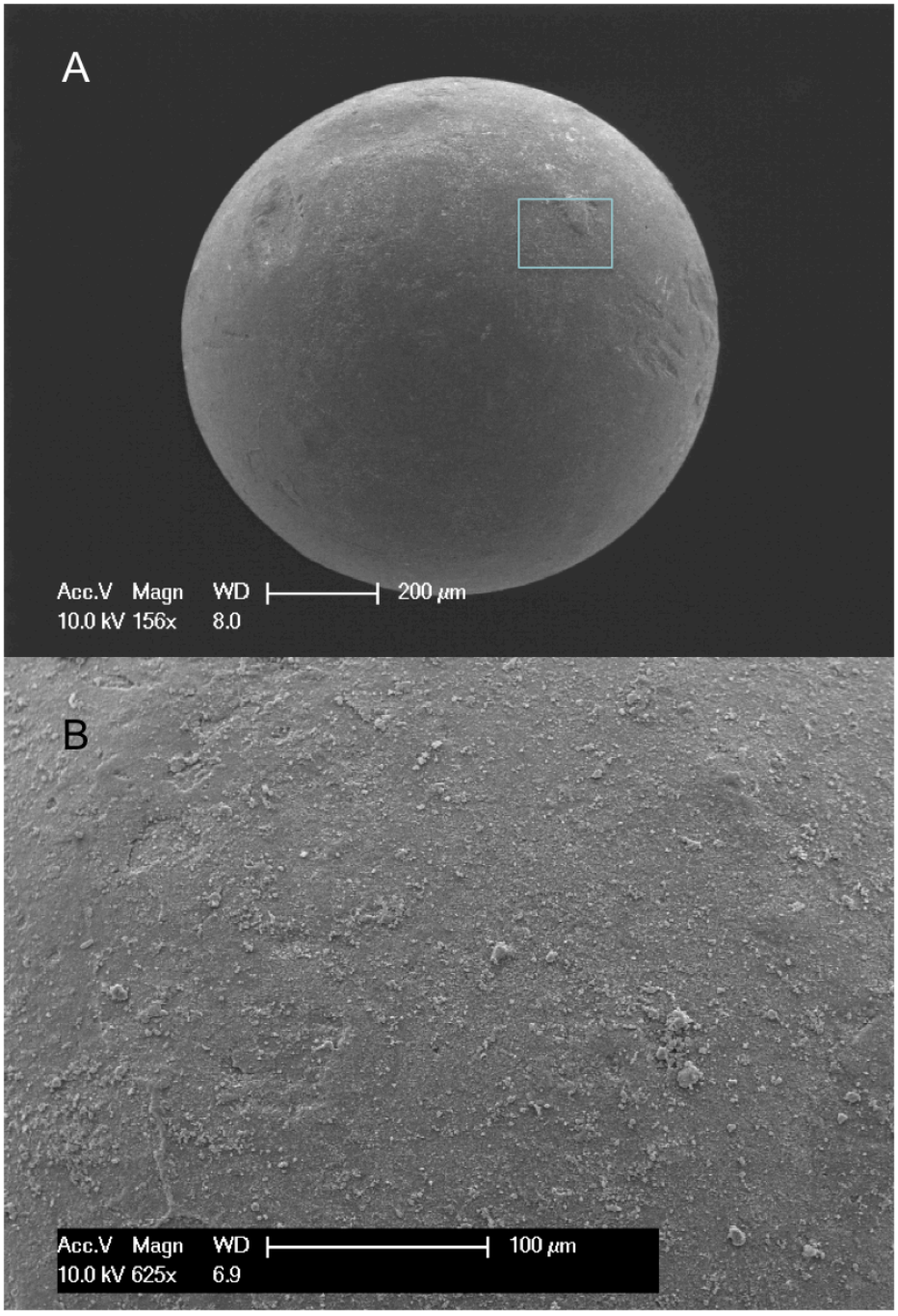

Figure 2.7 SEM images of H-ZSM-5 shell Co/Al_2O_3 Fischer-Tropsch Catalyst. A: Catalyst pellet; B: Image of rectangular area in A

In addition, SEM images with higher resolution are shown in figure 2.8. Figure 2.8A shows the rough surface of Co/Al_2O_3 Fischer-Tropsch catalyst. SEM image of Catalyst surface after seed coating is shown in figure 2.8B. It can be observed from the figure that Silicalite-1 seeds with diameter of 0.2-0.4 μm is coated on the Co F-T catalyst surface. Similar result has been obtained from Gouzinis et al. [89]. Surface SEM image of catalyst after secondary-growth coating is shown in figure 2.8C. It can be seen from the figure that H-ZSM-5 crystal has grown on catalyst surface with good coverage. The surface morphology is very similar to H-ZSM-5 surface SEM image from other researchers [90].

In order to verify the existence of H-ZSM-5 coating, the zeolite-shell F-T catalyst is cut in half, and a cross-sectional image is obtained, as shown in figure 2.8D. We can observe a clear coating with thickness of around 4.29 μm.

In order to exclude the possibility that the coating observed is not a crack of Co F-T catalyst, two EDX analyses have been performed on catalyst core and shell, respectively, and the result is shown in figure 2.9. In EDX images, each peak represents a specific chemical element, and the amount of element if proportional to the peak area. For EDX result of catalyst core, we could find a high aluminum content, and no silicon element is shown, which indicate the Al_2O_3 support of Co F-T catalyst. For EDX result of catalyst

shell, however, there is high silicon content but lower aluminum content. The ratio of silicon to aluminum is similar to silicon to aluminum ratio of zeolite, thus it is confirmed that the shell formation results from secondary growth.

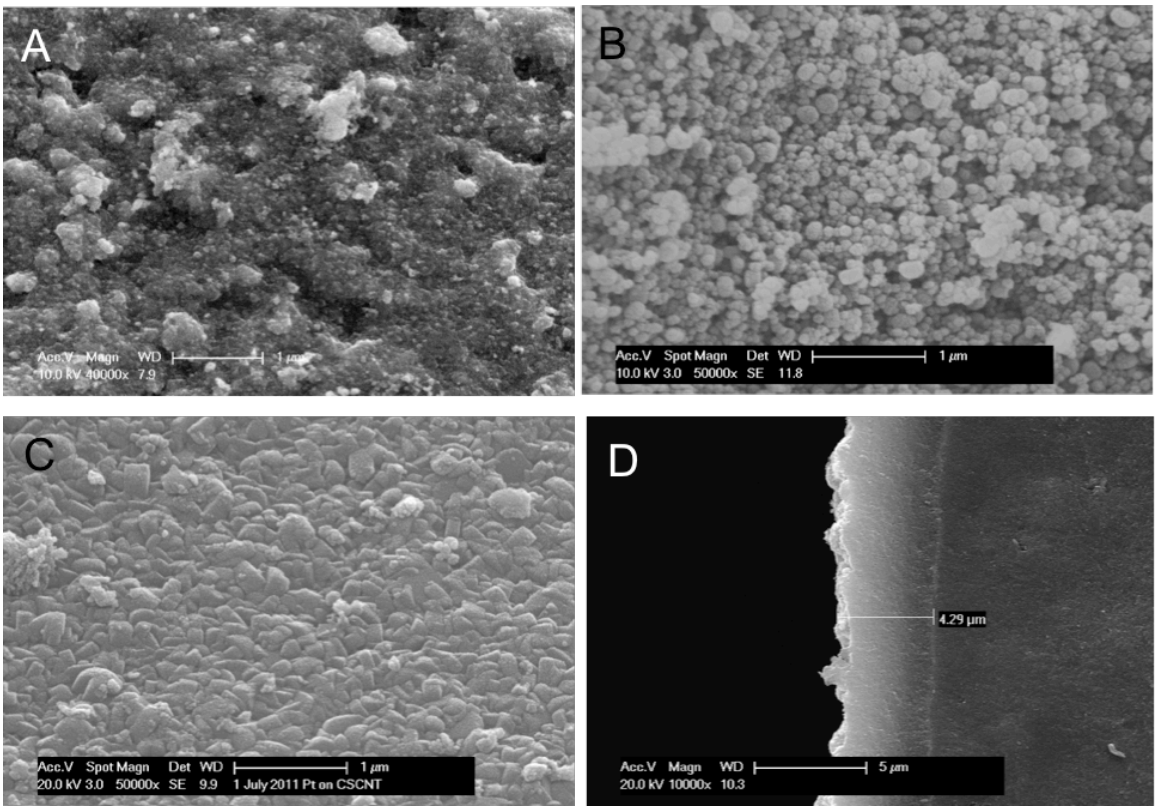

Figure 2.8 SEM images of H-ZSM-5 shell Co/Al_2O_3 Fischer-Tropsch Catalyst. A: surface of Co F-T catalyst; B: surface after seed coating; C: surface after secondary-growth coating; D: cross-sectional image

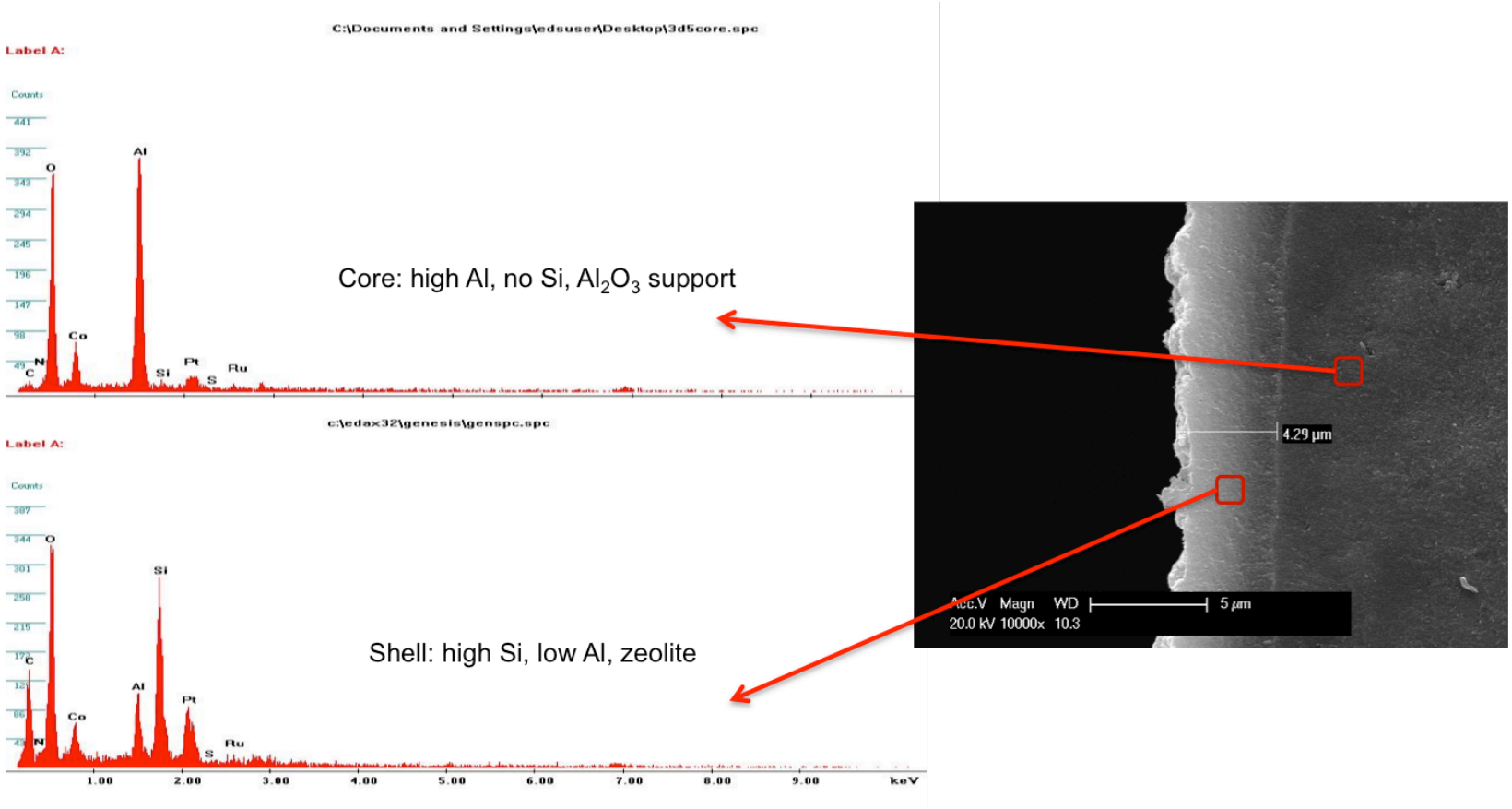

Figure 2.9 EDX analysis result for catalyst core and shell

2.3.3 XRD Result and Discussion

XRD result of H-ZSM-5 synthesis is shown in figure 2.10. H-ZSM-5 synthesis is studied solely without any catalyst addition, and synthesis time is from 1 day, 2 days and 3 days, respectively. Also, zeolite synthesis precursor solution has the same composition with that of secondary-growth gel. From the figure we can observe the characteristic peaks of H-ZSM-5 for all the samples, which means that H-ZSM-5 can be synthesized in 1-day synthesis and the composition remains stable through 3-day synthesis. The time selection for secondary growth is 2 days, which is within the suitable duration for H-ZSM-5 synthesis.

In order to confirm the composition of catalyst shell, XRD test for zeolite-shell catalyst is carried out. Also, conventional Co F-T catalyst and H-ZSM-5 are also tested for comparison. The test result is shown in figure 2.11. The characteristic peaks of H-ZSM-5 are marked with stars [109] and that of γ-Al_2O_3 are marked with circle [110]. It is observed from the figure that zeolite-shell F-T catalyst has the characteristic peaks of both H-ZSM-5 and γ-Al_2O_3. Thus we can confirm that H-ZSM-5 is successfully coated on Co Fischer-Tropsch catalyst.

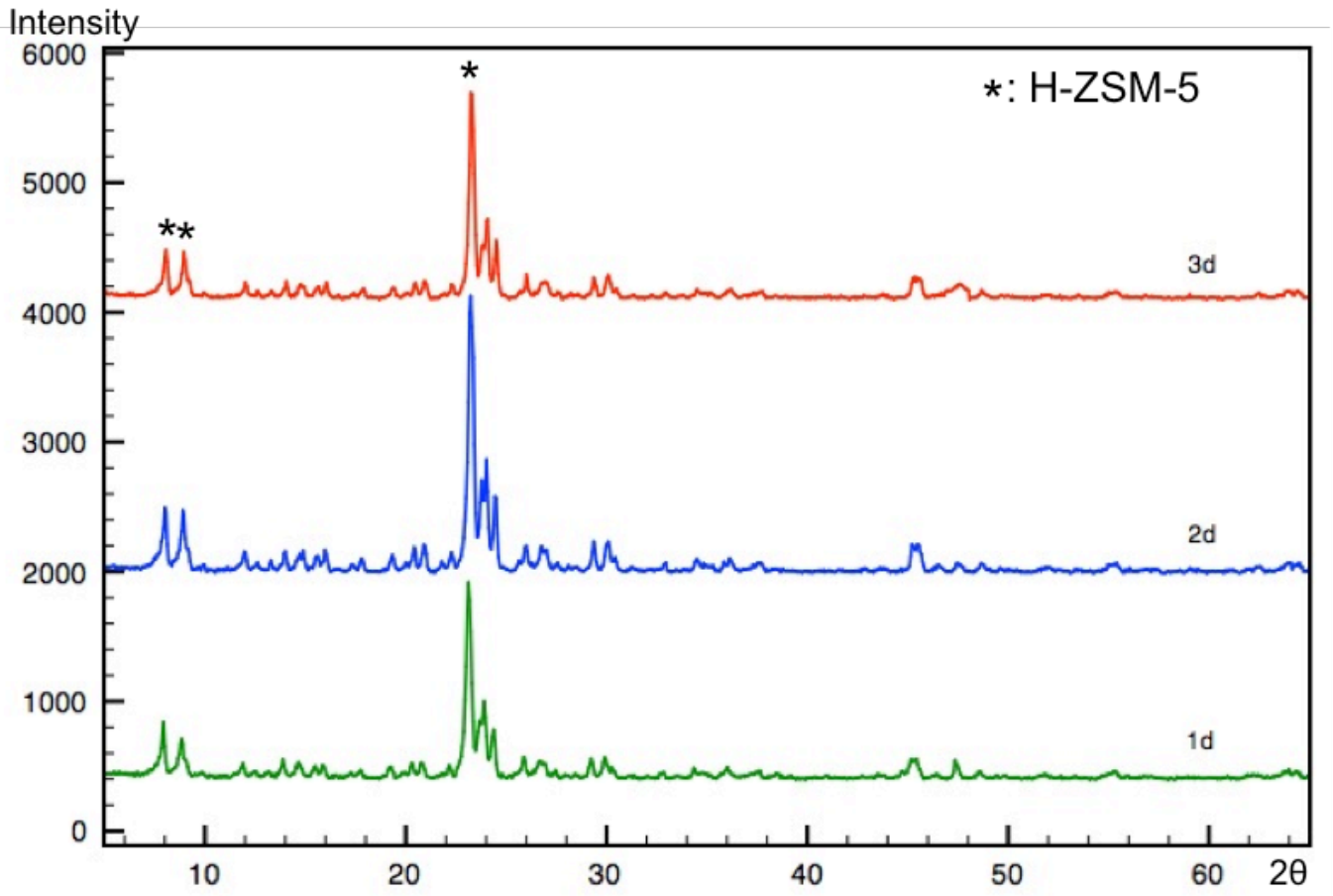

Figure 2.10 XRD results of H-ZSM-5 synthesis time study

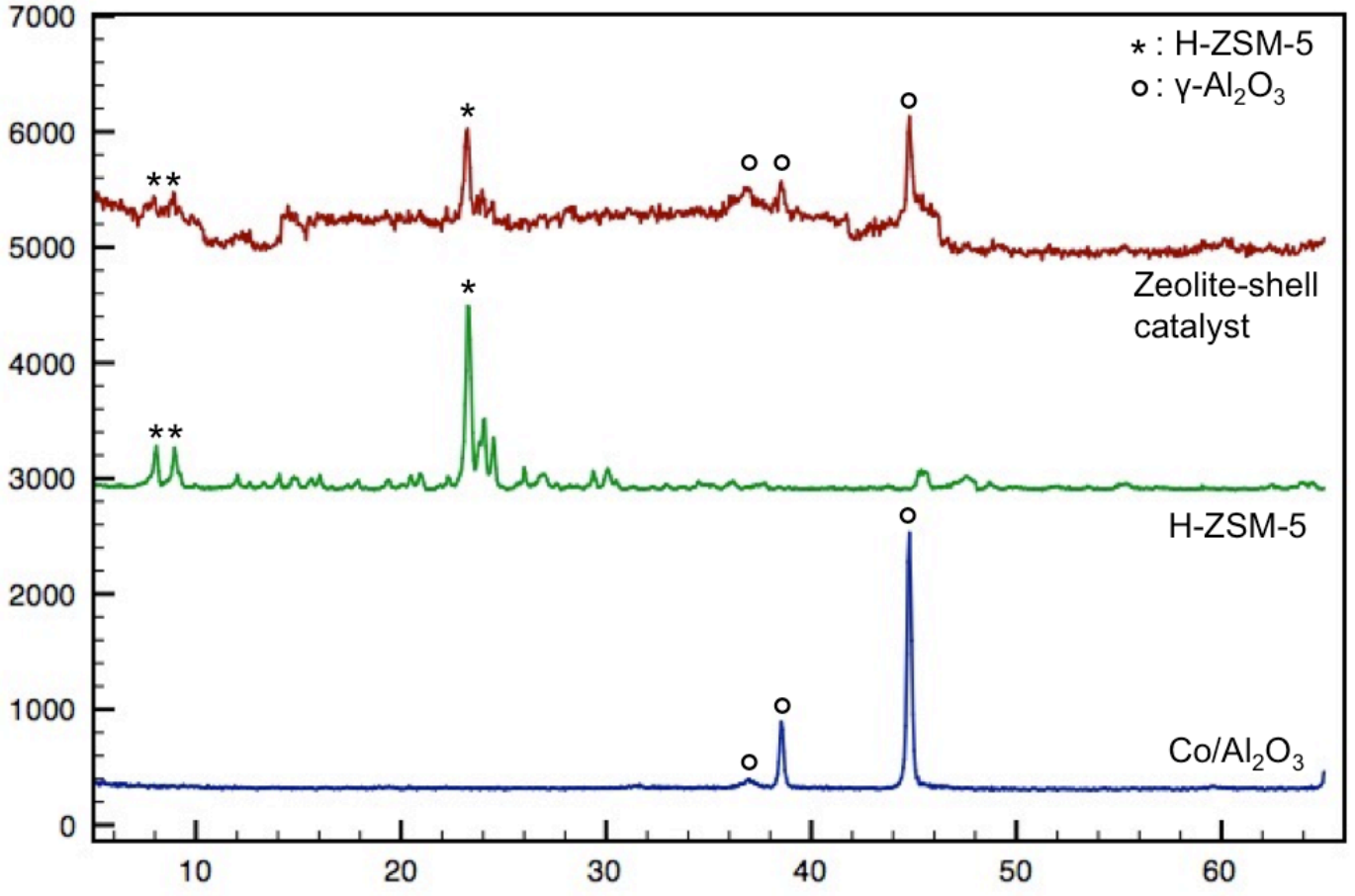

Figure 2.11 XRD powder patterns for Co/Al_2O_3 F-T catalyst, H-ZSM-5, and zeolite-shell F-T catalyst

2.3.4 BET Surface Area Results and Discussion

BET surface area results are shown in figure 2.12. It can be observed from the figure that BET surface area for conventional F-T catalyst is around 103 m^2/g, while BET surface area of all the zeolite-shell F-T catalyst is higher by at least 10%. This is because ZSM-5 coating has a BET surface area of 300-400 m^2/g [111, 112], which improves the total surface area. This result also confirms successful H-ZSM-5 coating.

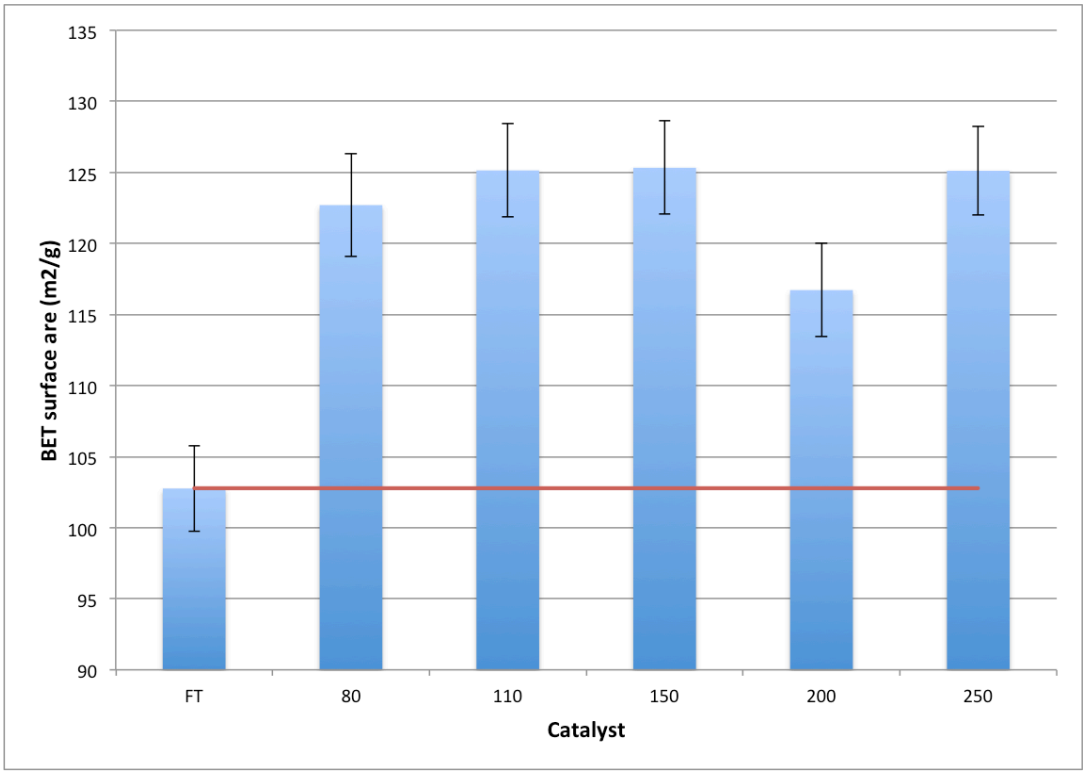

Figure 2.12 BET surface area of different catalysts

2.3.5 TGA Result and Discussion

TGA result of fresh Co/Al_2O_3 Fischer-Tropsch catalyst is shown in figure 2.13. It can be seen from the figure that catalyst weight gradually decreases with increasing temperature. At temperature of 500 °C, catalyst weight loss is around 6%, which is due to evaporation of water in the catalyst pores. This result gives a baseline of catalyst weight loss, and will be used to compare with the TGA results of catalysts after F-T synthesis.

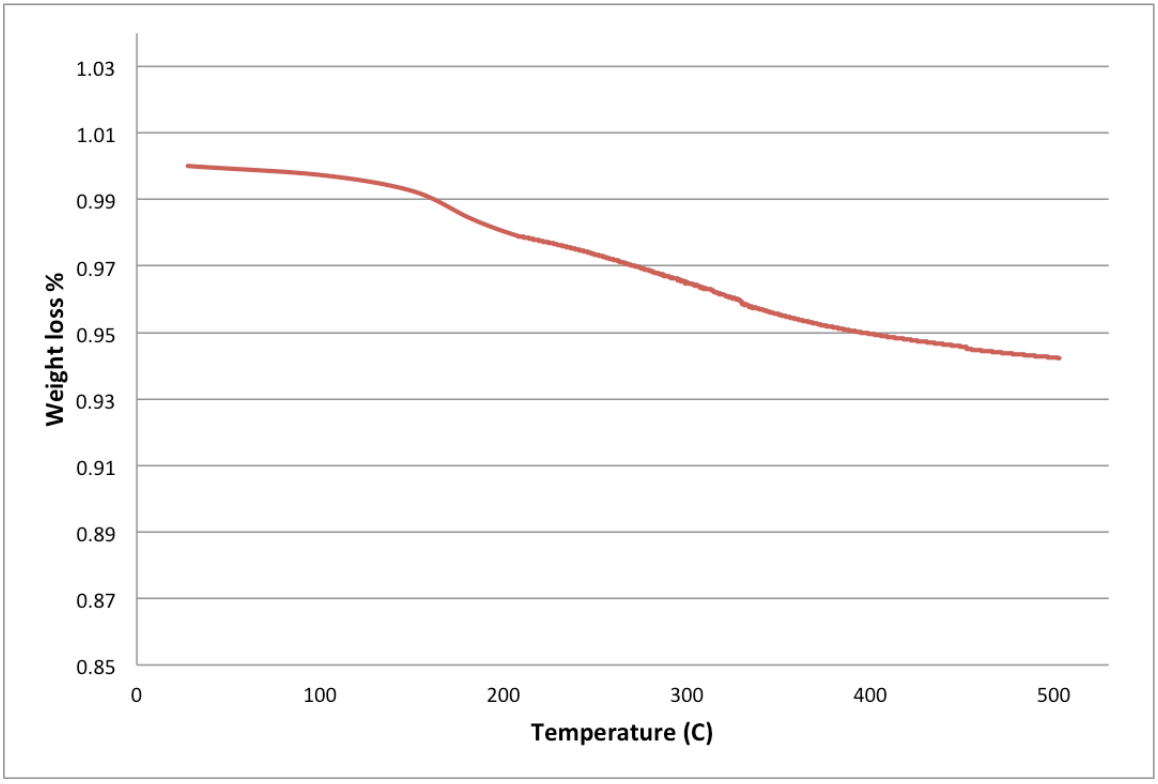

Figure 2.13 TGA result of fresh Co Fischer-Tropsch catalyst

2.4 Conclusion

Synthesis of H-ZSM-5 shell Co/Al_2O_3 Fischer-Tropsch catalyst is carried out, and various characterizations are performed. The conclusions are summarized as follows.

1) H-ZSM-5 shell Co/Al_2O_3 Fischer-Tropsch catalyst with different silicon to aluminum ratio is prepared using secondary-growth hydrothermal synthesis method.
2) SEM surface image result shows that the zeolite shell F-T catalyst has smooth surface with no cracks or pinholes; SEM cross-sectional image shows a clear coating with thickness of 4.29 μm. EDX results show that the elemental composition of catalyst shell is similar to that of secondary-growth gel.
3) XRD analysis and confirms that H-ZSM-5 is successfully coated on Co F-T catalyst surface. Zeolite-shell F-T catalyst has higher surface area than conventional F-T catalyst, which indicate better reaction activity.

CHAPTER 3 Design and Construction of Fischer-Tropsch Reactor System

This chapter focuses on design and construction of a lab-scale Fischer-Tropsch (F-T) reactor system. Compared with commercialized F-T reactors, lab-scale reactors have similar design criteria such as structure, temperature and pressure rating. Besides, additional consideration is needed in lab-scale reactor design, such as gas supply, reactor heating, product sampling, and experiment efficiency. In this chapter, two versions of Fischer-Tropsch reactors are introduced for F-T synthesis study. The design criteria, features, operation and control of the reactors are presented in detail.

3.1 First Generation Lab-scale Fischer-Tropsch Reactor System

3.1.1 Design Criteria

The structure of a lab-scale Fischer-Tropsch reactor is similar to a conventional continuous reactor system, which consists of gas inlet, inlet gas flow controller, reactor, product collector, back pressure regulator, outlet gas flow meter, and gas sampler. The flow diagram of a universal reactor is shown in Figure 3.1.

Figure 3.1 Flow diagram of a universal reactor system

In addition to reactor structure, other design criteria are considered for building lab-scale F-T reactors.

1) Safety. Safety is the primary consideration for any reactor design. The operating temperature of F-T synthesis can go up to 350 ºC, and pressure is up to 300 psi. As a result, Swagelok tubing and fittings are used in constructing reactors and all flow systems. The flow system has temperature rating of up to 800 ºC, and pressure rating of up to 400 psi. Besides, the feedstock for F-T synthesis is the mixture of CO and H_2, which is toxic and flammable. And two CO monitors are installed close to gas inlet and gas outlet, respectively. Monitor alarm will sound in case of a CO leak, so measures can be taken in time to prevent serious accidents. A portable CO alarm is also used to better protect the test operator.

2) Catalyst compatibility. In this thesis, F-T synthesis with both conventional F-T catalyst and zeolite-shell F-T catalyst will be conducted. Thus, the designed F-T reactor should be suitable to test both catalysts. The difference between the two is that the new

catalyst has a core-shell structure. The zeolite shell should be well protected from collision with other catalysts, or it will be cracked and lose its function. Compared with other types of reactors, catalyst in fixed bed reactors can be better protected because it will not collide with other catalyst or reactor. In addition, product collection operation for a fixed bed reactor is more convenient than other reactors, since liquid product can trickle down the reactor and collected by gravity. Finally, catalyst in fixed bed reactors has better sulfur tolerance, since sulfur in syngas will first poison the top layer of catalyst, and catalyst at bottom layer can be well protected. Because of these considerations, a fixed bed reactor will be used for the system.

3) Temperature control. Due to strong exothermic property of F-T synthesis, temperature control is critical. Poor temperature control will significantly affect reaction stability, result precision, and catalyst performance. Also, ceramic fiber heater has slow heating response because of the air layer between heater and reactor, which make temperature control more challenging. In order to ensure precise temperature control and minimum fluctuation, a LabVIEW program with a PID controller is utilized, which will be introduced in detail in section 3.3.1. Also, gas inlet, gas outlet as well as reactor are

covered with insulation. And inlet preheater is also equipped to further reduce temperature fluctuation.

4) Online sampling. Starting a F-T synthesis test can take 36-72 hrs. In order to improve test efficiency and reduce total test time, online sampling function for both gas and liquid samples is added to the system. Gas collection port can be installed after back-pressure regulator, which has ambient pressure. However, liquid sampling is more complicated because it's in the middle of the system and has pressure of about 180 psi. Thus, two-stage collectors with a valve in between are used to collect liquid product online while maintain system pressure. The online liquid sampling system will be introduced in detail in section 3.1.2.

3.1.2 Reactor System Description

First generation lab-scale F-T reactor system is built, and the schematic diagram and photo of the reactor are shown in figure 3.2 and figure 3.3, respectively. The reactor system can be divided into three parts: gas inlet & preheat, reactor, and product collectors. In the first part, syngas is pretreated to meet the reaction requirements. There are three kinds of gases used in the experiment. Besides the reactants CO and H_2, N_2 is also needed to dilute the reactants, maintain total pressure and protect the catalyst in case

of an emergency. The flow rate of the gases is controlled by mass flow controllers (MFCs), which will be introduced in section 3.2.2. A check valve is put following each MFC to prevent the gas from flowing backward. After that, all the gases are converged to a single line, and two needle valves and a union T fitting are placed in case we need to replace gas cylinders during operation without introducing any O_2. Then, all the gases will enter the first oven, which is set to a temperature of 220°C. A coil pipe is used to enhance the efficiency of preheat. Besides, a trap filled with Fe powder is followed to eliminate O2. The trap can also function as a mixing chamber.

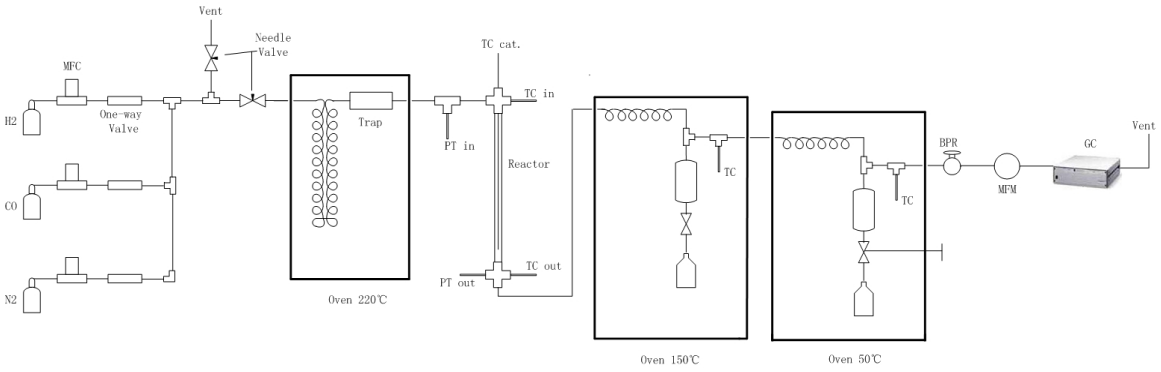

Figure 3.2 Schematic diagram of first generation F-T reactor

Part two is the core of the system, where the reactor is located and all the reactions take place. The reactor is a 316 stainless steel tube with the outside diameter (OD) of 0.5 in.

and length of 15 in. Reaction heat is provided by a ceramic fiber heater. Since F-T synthesis is very sensitive to temperature and pressure fluctuation, four thermocouples (TCs) and two pressure transducers (PTs) are used to ensure an accurate temperature and pressure measurement. In addition to the temperature and pressure detection at both the inlet and the outlet of the reactor, another TC attached on the outside wall of the reactor is used as the signal source for heater control. Besides, one more TC with a 1/8 in. tube shell is inserted into the reactor to monitor the catalyst temperature during reaction. Note that this TC is movable inside the tube shell, so it can also be used to detect the axial temperature gradient of the catalyst bed.

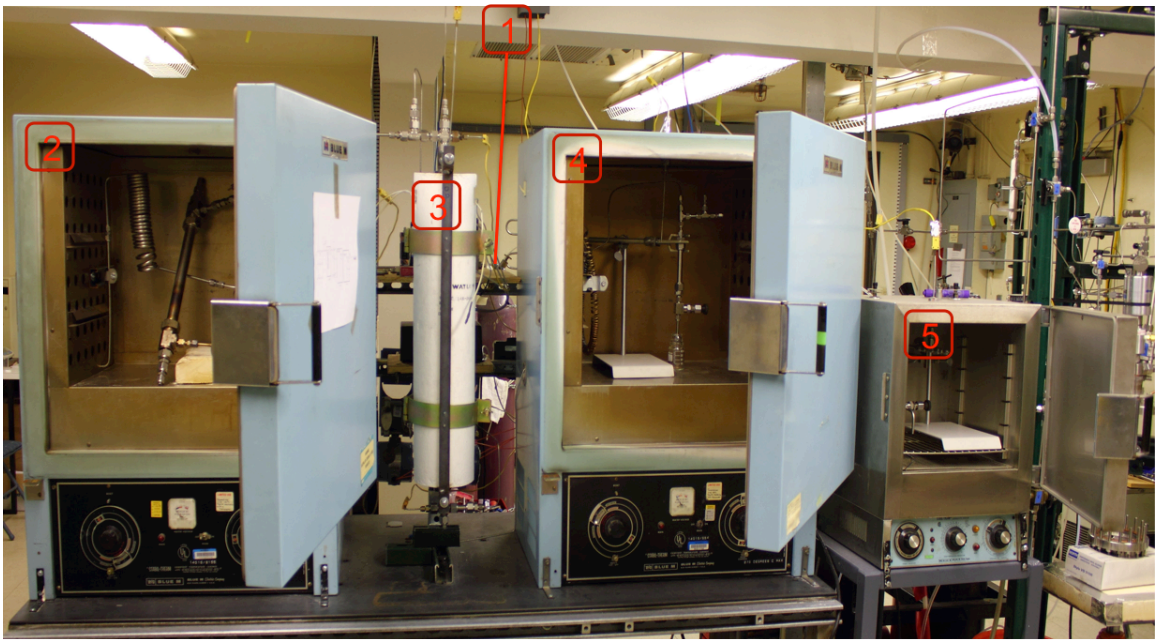

1. Gas inlet and mass flow controller
2. Oven with preheating coil and trap
3. Reactor
4. Oven with wax trap
5. Oven with liquid trap

Figure 3.3 Photo of first generation F-T reactor

After reactor, product gas will pass through two traps located in two ovens. The oven for the first trap is set to 150°C, where wax with a relatively high boiling point could be collected. The oven for the second trap is set to 50°C. The product in this trap is liquid hydrocarbons and water. In order to collect the product without shutting off the experiment, a high temperature valve is connected to the bottom of the trap, with the other end linked to a collection bottle. The handle of the valve is extended to the outside the oven, so sample collection can be done without opening the oven. This design ensures

that sample collection could be frequently done without affecting operating pressure. After the traps, a back pressure regulator (BPR) is used to maintain the system pressure. The gases will then pass a mass flow meter (MFM), and be analyzed by gas chromatography (GC) and residual gas analyzer (RGA).

3.2 Second Generation Lab-scale Fischer-Tropsch Reactor System

3.2.1 Design Criteria

F-T synthesis with first generation is successful. The reaction is under control, and online sampling feature also functions well. However, there are also some disadvantages of the first generation F-T reactor. First, the reactor system is exposed to the lab environment. To ensure a safe working environment even there is CO leak, the ventilation fan in the lab should be kept on during test, which is very loud and waste energy. Besides, the total length of the pipeline is too long, which cause a high delay in product collection. Finally, the control system needs to be optimized to realize more intelligent control. In order to solve those problems, and further improve experiment safety, stability and efficiency, the

second-generation lab-scale Fischer-Tropsch reactor system is designed and constructed. There are several design criteria considered for upgrades.

1) Safety. In addition to safety features in the first generation reactor, the second generation reactor will be built in a walk-in hood. This will isolate the reactor with the environment, and people in the lab can be well protected even CO leak happens. In addition, a solenoid valve is also added to the gas inlet. It can be controlled by LabVIEW program and works as an auto shut-off valve. In case of emergency, the valve can shut the gas flow automatically, and chemical reaction in the reactor can be stopped. This function can further improve operation safety, since it has faster response and people don't need to stay in the hood to stop reaction.

2) System simplification. Heating coils and ovens are widely used in the first generation reactor to meet test stability requirements. However, total pipeline length is also significantly increased, which cause a high liquid collection delay. With more experiment experiences and more intelligent process automation, heating coil in ovens is not necessary any more, so they can be removed from the system to minimize reactor system size, and reduce product collection delay. In addition, the new zeolite-shell F-T catalyst can limit product distribution to C15, which means that solid wax is not produced

from the reactor. As a result, wax trap can also be removed to further simplify the system, and improve system reliability.

3) Mixture gas. In the first generation reactor, syngas was made from separate CO and H_2 gas cylinders. The disadvantage for this setup is pressures for both of the cylinders should be exactly the same, or flow rate accuracy will be affected. Also, gas supply with mixing two gases requires two mass flow controllers, which adds additional cost to the system. Since H_2 to CO ratio doesn't need to change during tests, cylinders of mixture gas with desired syngas ratio are used. Only one mass flow controller is needed for the new setup, and syngas ratio can also be well maintained.

3.2.2 Reactor System Description

The schematic diagram and photo of the second generation lab-scale F-T reactor system is shown in figure 3.4 and 3.5, respectively.

1) Gas inlet

For the new reactor, syngas is supplied by one cylinder with mixture of H_2 and CO. In addition, a H_2 cylinder is used for catalyst activation, and a N_2 cylinder is used for leak test and gas dilution in emergency condition. Since H_2 and N_2 gas are not used at the same time, the two cylinders share the same inlet. A 3-way valve is installed with one end

connect to syngas, and the other connected to inlet of N_2 and H_2. The 3-way valve is used to switch between different operating conditions such as catalyst activation, reaction, or gas dilution. Note that H_2 and N_2 cylinders are placed outside the walk-in hood, and not shown in the photo.

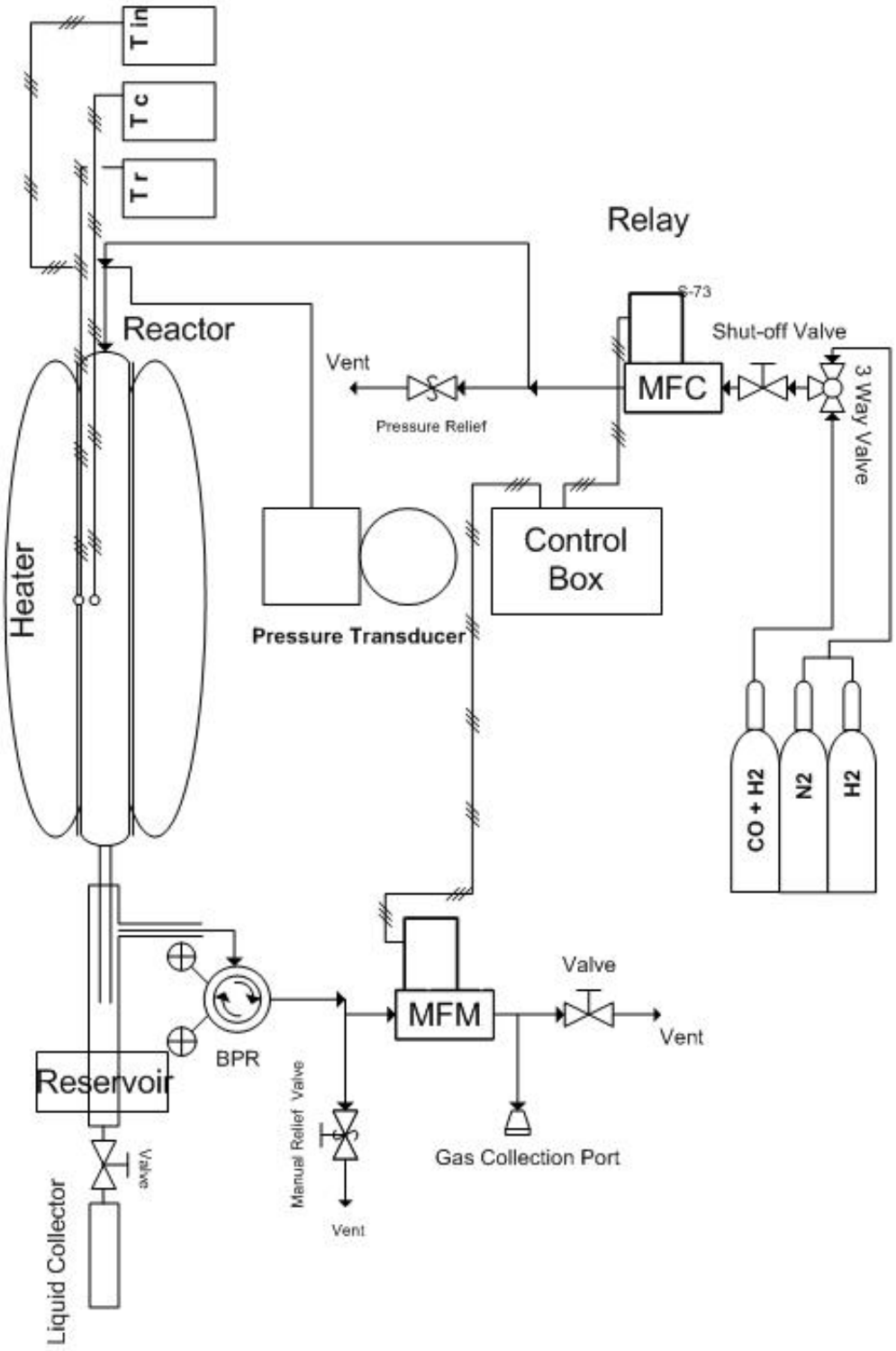

Figure 3.4 Schematic diagram of second generation F-T reactor

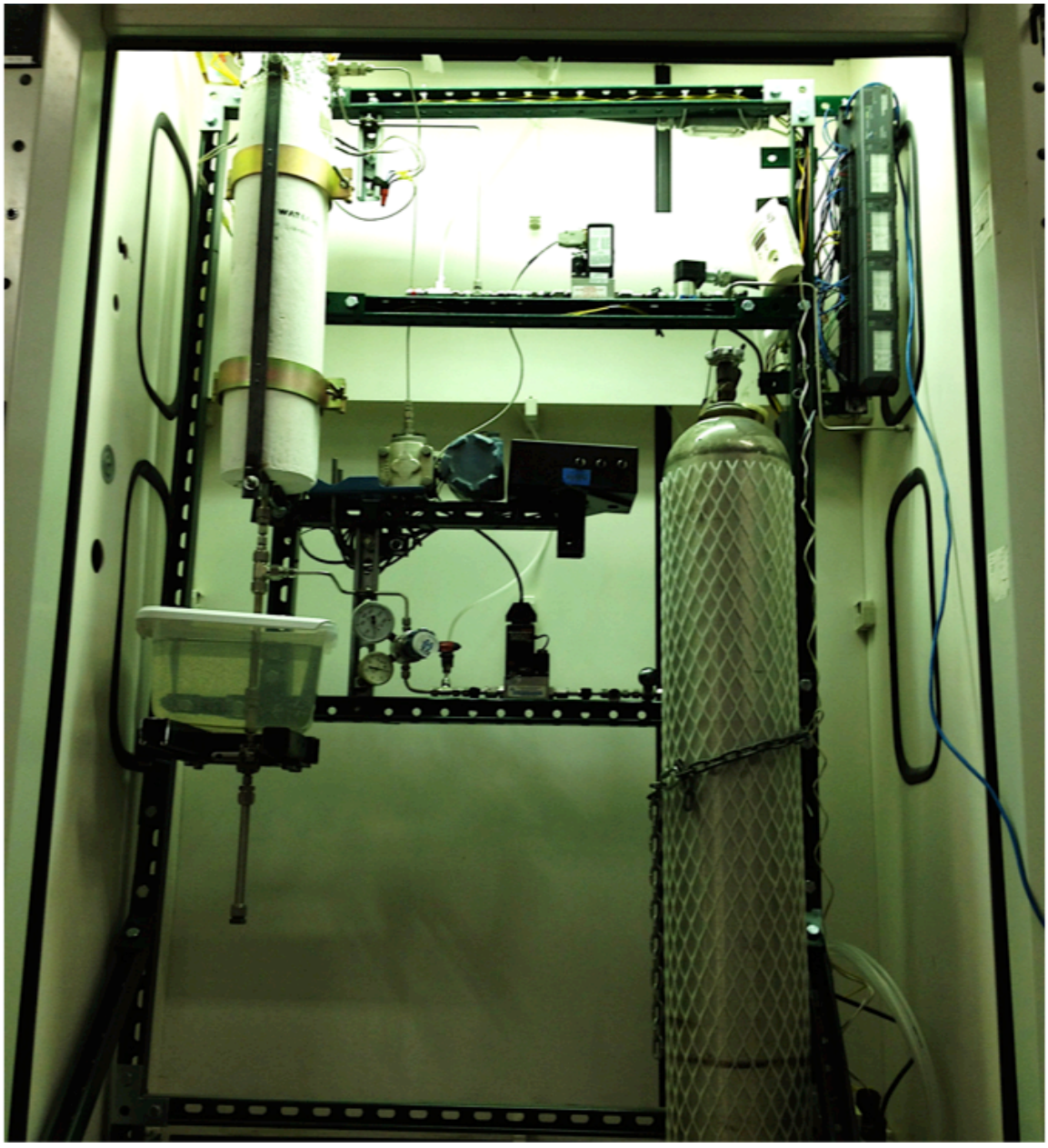

Figure 3.5 photo of second generation F-T reactor

2) Emergency shut-off valve

After 3-way valve, a solenoid valve is newly added to the flow pipeline. A solenoid valve is an electromechanically operated valve. The photo and operation principle is shown in figure 3.6. The valve is controlled by electric currents through a solenoid. When no power source is connected, diaphragm B is closed to stop any flow, as shown in the figure in upper right corner. When connected to a power source, the solenoid converts electricity into mechanical force, and pull the valve open, as shown in the figure at lower right corner. As a result, the mechanical opening and closing of a valve can be controlled by connecting or disconnecting to electrical power, and power connection can be controlled by computer program like LabVIEW. When detecting abnormal operating conditions like temperature run-away or pressure built-up, LabVIEW program can cut-off power supply of solenoid valve, and realize auto shut-off in case of emergency. In addition, since the solenoid valve has a normally closed design, which means that it will remain closed when no electric power is connected, the valve can also shut off reactions automatically in case of a power outage.

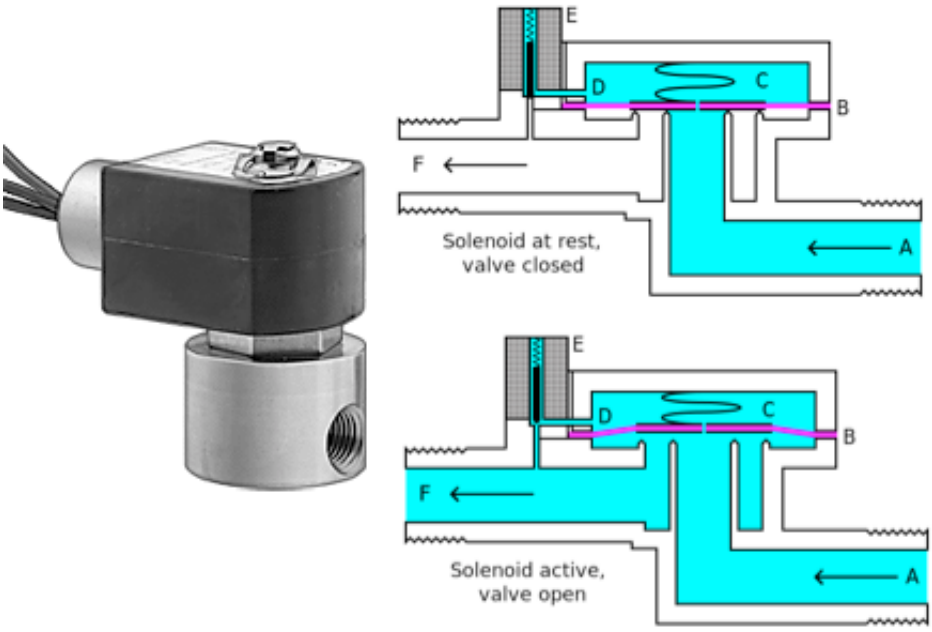

Figure 3.6 Photo and operation principle of a solenoid valve

3) Inlet mass flow controller

After shut-off valve, gases will go through a mass flow controller (MFC). A MFC can be calibrated to control a specific flow rate of gases. Two MFCs are used for the reactor; the models are both Brooks 5850e. One MFC has a D-connector, which is used as inlet flow controller; the other one, which is used as outlet mass flow meter, has a card edge connector. Photos of the MFCs and pin arrangement for each connector are shown in figure 3.6. From figure 3.6a, a MFC has two gas connectors for inlet and outlet, and the

arrow on the body shows the direction of flow. The cylindrical part is the valve, which is used to control specific flow rate. Thought the two MFCs have different connection type, the operation principles are the same.

a

Model 5850E
Mass Flow Controller
with Card Edge Connector

Model 5850E
Mass Flow Controller
with D-Connector

b

Chassis GND	1	A	Command input
0-5 V signal common	2	B	Command common
0-5 V signal output	3	C	Power common
+15 V	4	D	
	5	E	
	6	F	-15 V
	8	H	
	9	I	
	10	J	

PIN NO.	*FUNCTION*	*COLOR CODE*
1	Command Common (Potentiometer Pin "CCW")	*Black*
2	0-5 Volt Signal Output	White
3	Not Used	Red
4	Valve Off	Green
5	+15 Vdc Supply	Orange
6	-15 Vdc Supply	Blue
7	Valve Test Point	Wht/Blk
8	Command Input (Potentiometer Pin "S")	Red/Blk
9	Supply Voltage Common	Grn/Blk
10	0-5 Volt Signal Common	Org/Blk
11	+5 Volt Reference Output (Potentiometer Pin "CW")	Blu/Blk
12	Valve Override	Blk/Wht
13	Not Used	Red/Wht
14	Chassis Ground	Grn/Wht
15	Remote Transducer Input*	Blu/Wht

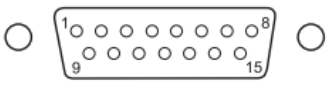

Notes:

1. Cable shield tied to chassis ground in meter connector. Make no connection on customer end.
2. All power leads must be connected to power supply.

c

Figure 3.7 a: picture of mass flow controllers with card edge connector and D-connector; b: pin arrangement of card edge connector; c: pin arrangement of D-connector

Several connections are needed to make sure an MFC can work properly. As shown in figure 3.7b and 3.7c, despite of different connector types and pin arrangements, they both share following connections. First of all, +15 V, -15 V, and power common ports are used to provide power for MFC. Second, command input and command common ports are used to provide command signal for specific flow rate. Command signal can range from 0-5 V DC, which has a linear relationship with zero to full scale of real flow rate. However, calibration of MFC is always required for accurate flow rate control and measurement. Third, 0-5 V signal common and 0-5 V signal output ports provide feedback of real flow rate through MFC. At last, chassis GND is connected to the ground to remove any charge and protect MFC.

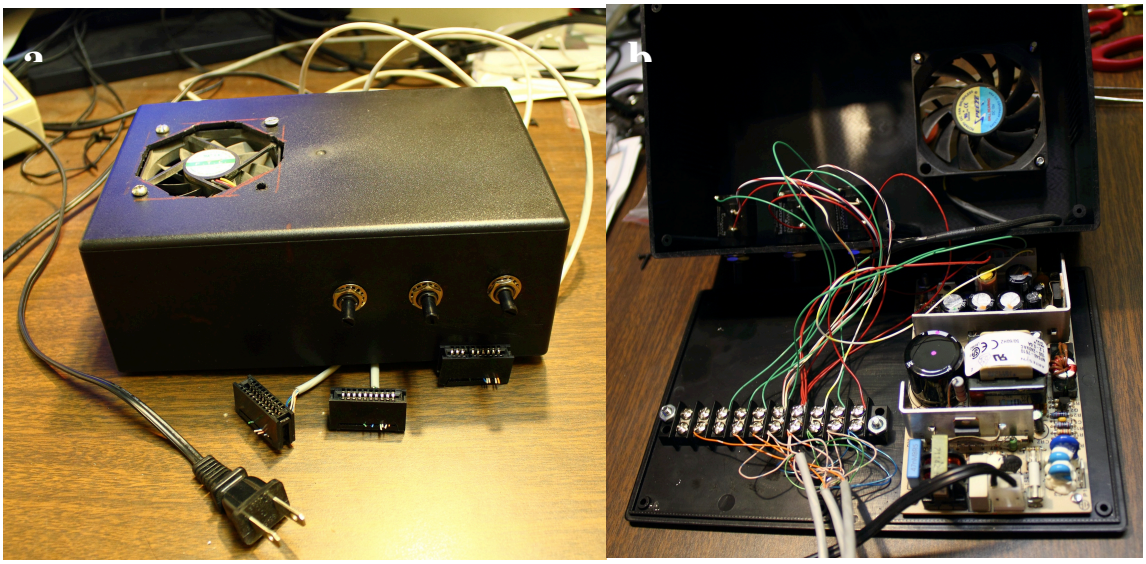

Figure 3.8 a: Exterior view of control box; b: interior view of control box

4) Control box for mass flow controllers

In order to control MFCs to provide specific flow rate, a control box is designed and built. The photo of the control box is shown in figure3.8. The circuit board in figure 3.8b is AC to DC converter; and a 80mm cooling fan is installed to remove heat generated from the board. The converter has one input of 120V AC, and has four DC output including +15V, -15V, +5V and common. +15V and -15V output are used to power the MFC, and three potentiometers (Bourns 3500S-2-104) are connected to 5V port, so they can provide a 0-5V DC output by tuning the knob. Instead of direct

connection, cables and all internal wires are connected to a hub to make clean and clear connection.

5) Pressure relief valve

Before entering the reactor, a pressure relief valve (Swagelok SS-4R3A) is used to avoid excessive pressure in case of a clog in the reactor. Relief pressure of the valve is preset before test. When pressure built-up happens in the reactor, the valve will open and vent excess gas, until system pressure is lower than relief pressure.

6) Reactor

The reactor of the new system is similar to that of the previous system. It's 316 stainless steel tubing with outside diameter of 0.5in. and length of 15in.. Reaction heat is provided by ceramic fiber heater (Watlow VC401A12A). There are four thermocouples (TC) used for temperature measurement and control. Two of them are installed at reactor inlet and outlet, respectively. Another TC is placed on the reactor outside wall. It is used to provide feedback for reactor temperature control. Since F-T synthesis is strongly exothermic, temperature inside the reactor is always higher than reactor outside wall. As a result, the last TC is inserted inside the reactor and placed at the catalyst bed to provide accurate catalyst temperature data. Besides, the temperature difference between catalyst bed and

reactor can also indicate catalyst reactivity. A high temperature difference indicates good catalyst activity. In addition to TCs, a pressure transducer is also utilized to measure system operating pressure.

7) Liquid product collector

After reaction, liquid product will trickle down by gravity and it is collected in liquid collector under the reactor. The liquid product collector is made of 1/2 in 316 stainless steel tubing. It has two parts, connected by a ball valve. The ball valve remains closed during test, and liquid product is collected in the top part. The top part is immersed in a reservoir filled with coolant to maintain temperature at around 20ºC to prevent product evaporation. When performing liquid sampling, ball valve opens and liquid product is pushed through the valve and collected at the bottom part. Then the valve is closed, and bottom part can be removed for collection. During the process, liquid sample is transferred outside the reactor, while other reactants and products are still isolated from the environment and system pressure remains stable.

8) Back pressure regulator

While liquid is trapped in the liquid collector, gaseous products pass along pipeline and go through a back pressure regulator (BPR). BPR is used to sustain system pressure, and

it can also adjust pressure with the tuning knob. System pressure increases when turning knob clockwise and decreases when turning counter-clockwise. While pressure of inlet is the same with system pressure, BPR outlet has ambient pressure.

9) Gas product collector

After back pressure regulator, there is a mass flow meter to measure gas flow rate, followed by a port connector. Tail gas is collected by a collection bag through a port connector, it is then transferred to GC or residual gas analyzer for composition analysis. The tail gas pipeline can also be connected to residual gas analyzer or non-dispersive infrared analyzer (NDIR) for online composition analysis.

3.3 Process Automation

3.3.1 Introduction

1) Automation

Automation is the use of control systems for controlling equipments. Automation is widely used in the thesis, including the control of Fischer-Tropsch synthesis reactors,

thermogravimetric analysis (TGA), oven for catalyst synthesis and furnace for catalyst calcination. There are three advantages for using automation.

High efficiency. The best benefit of automation system is high efficiency. Data acquisition in automation system can read and record process data automatically, and manual data recording is no longer needed. In addition, most of the mechanical controller can be replaced with electronic controller and controlled by automation system. And change of process variables can be processed in the program instead of manual adjustment, which also saves a lot of labor.

High control accuracy. Automation has better control accuracy than manual control. In some complex control system such as temperature ramp or control of a non-linear system, accurate manual control is difficult. However, with strong computing power of a PC, automation system can analyze process data and perform real time control operation, which ensures accurate process control.

Safety. Fischer-Tropsch synthesis is a very unstable process. It is strong exothermic, and reaction rate has non-linear relationship with operating temperature. The most common hazardous situation happens during F-T synthesis is temperature run-away. When a temperature run-away happens, temperature and pressure of the system will rise

dramatically and experiments will fail. The cause of temperature run-away is sudden change of process values such as temperature, pressure and flow rate. As a result, process automation with accurate control is necessary for F-T synthesis operation. In addition, with automation system, most of the operation can be done in front of a computer, such as change of temperature, pressure, and flow rate, open or close of valves, and data acquisition. Thus, operation close to the high temperature high pressure reactor can be minimized. At last, automation system has instant emergency response, which also improves test safety.

2) LabVIEW

LabVIEW is short for Laboratory Virtual Instrument Engineering Workbench. It is a design platform and development environment for a visual programming language developed by National Instruments. The programming language used in LabVIEW is called G language, which is a dataflow programming language. The name of LabVIEW program is called virtual instruments (VIs). A VI is composed of a front panel and a back panel with block diagrams. A screenshot of a sample VI is shown in figure 3.9. The front panel is built with controls and indicators. Controls are inputs, where users can provide information to the program; Indicators are outputs, they indicate process value or output

control result. The back panel contains source code for all the controls and indicators in the front panel. In addition, it also includes structures and functions, which can perform their functions and output results to indicators. Collectively, controls, indicators, structures and functions are called nodes. Logically related nodes are connected with wires to realize certain function. The graphical approach of LabVIEW programming allows non-programmers to built program by dragging and dropping virtual lab instruments, which they are already familiar with, and achieve the control and data acquisition functions.

3) PID control

PID control is short for proportional-integral-derivative control. PID controller has a control loop feedback mechanism. It measures difference between process variable and setpoint, and then adjusts process control inputs to minimize the difference. PID controller calculation algorism is shown in figure 3.10. PID controller algorism includes three parameters: the proportional (P), the integral (I) and the derivative (D). During control process, P,I and D value are summed to calculate the output of PID controller. The form of PID control algorism can be described as:

$$u(t) = K_p e(t) + K_i \int_0^t e(\tau)d\tau + K_d \frac{d}{dt} e(t) \qquad (3.1)$$

where

K_p: Proportional gain

K_i: Integral gain

K_d: Derivative gain

e: Error = setpoint-process variable

t: Time or instantaneous time (the present)

τ: Variable of integration; takes on values from time 0 to the present t.

The proportional term is given by:

$$P_{out} = K_p e(t) \qquad (3.2)$$

The value of proportional term is proportional to the current error value. If the proportional gain is too high, there is a large change of output for given input, and can make the system unstable. In contrast, a small gain will have small change of output for given change, and will reduce the sensitivity of controller.

The integral term is given by:

$$I_{out} = K_i \int_0^t e(\tau) d\tau \qquad (3.3)$$

The effect of integral term is related to magnitude and duration of error. The integral term sums instantaneous error during time and gives the accumulative offset. The offset is then

multiplied by the integral gain (Ki) and added to the overall output. The integral term can eliminate steady-state error. However, it can also cause current operating value to overshoot because it responses to accumulated error from the past.

The derivative term is given by:

$$D_{out} = K_d \frac{d}{dt} e(t) \qquad (3.4)$$

In the derivative term, the slope of error over time is calculated and then multiplied by the derivative gain (K_d). Derivative action detects the change of process variable, predict system behavior, and reduce system settling time. However, derivative is also sensitive to measurement noise. A severe system noise can cause erratic derivative response and degrade control performance.

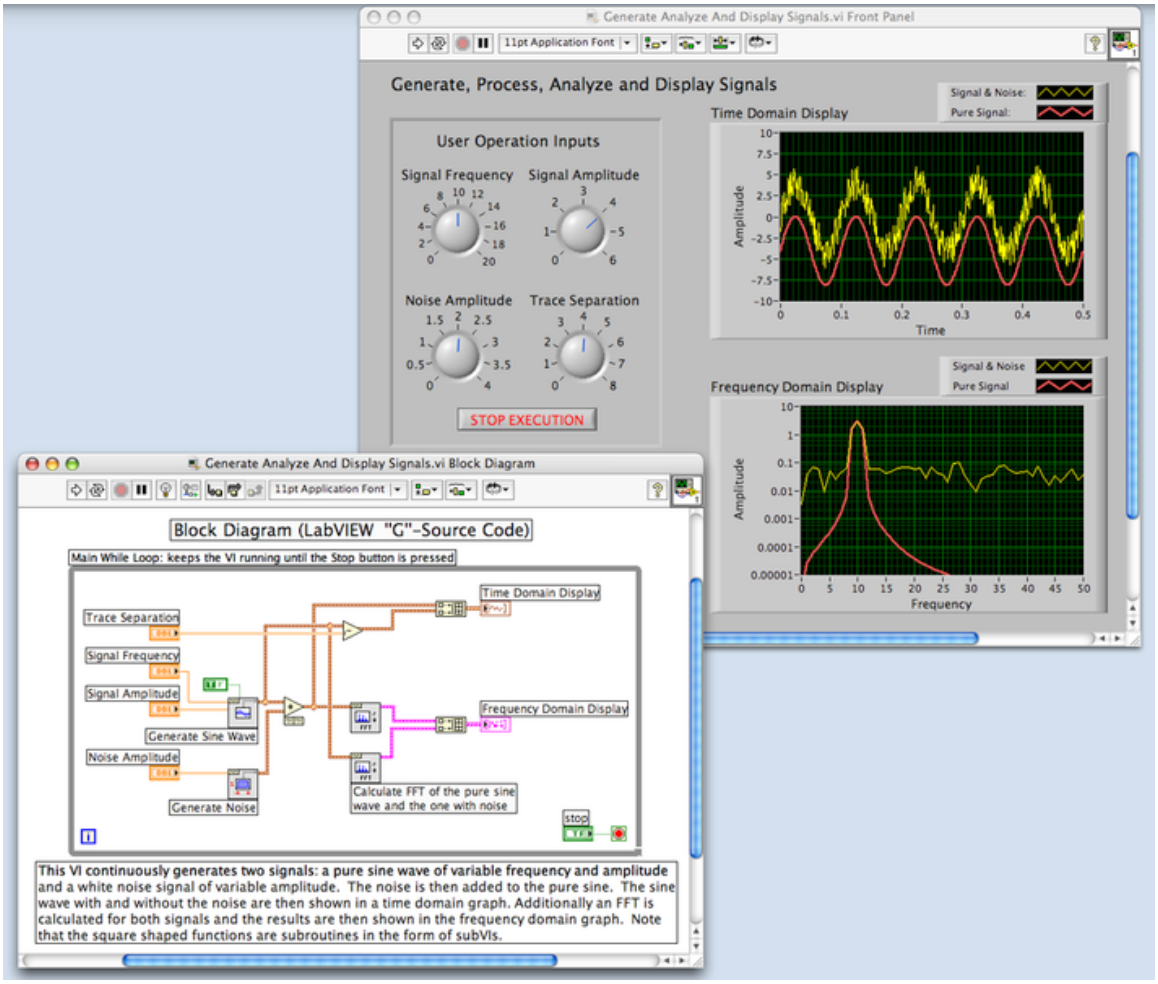

Figure 3.9 Screen shot of a sample VI

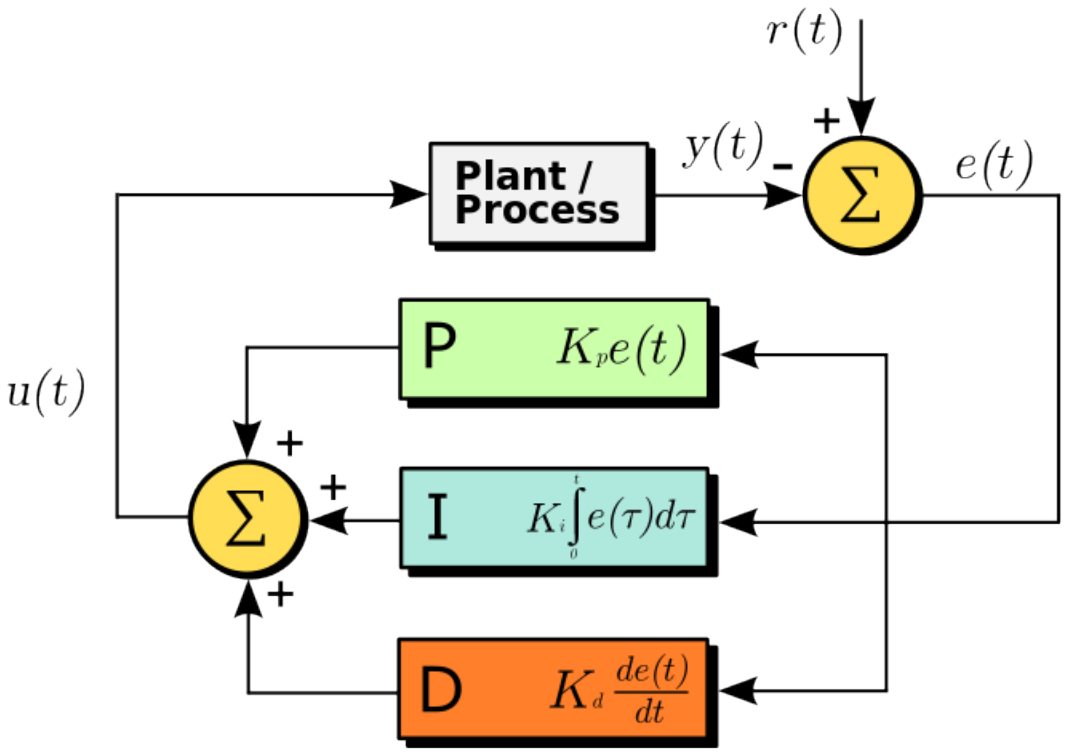

Figure 3.10 Block diagram of PID controller algorism

3.3.2 Automation system for F-T Synthesis reactor

1) Hardware connections

The schematic diagram of second-generation F-T reactor with automation system is shown in figure 3.11. In this figure, part 1 is the reactor system, and part 4 is a PC with automation program. Data acquisition and control commands between reactor and program are processed through a device called FieldPoint, as shown in part 3 of figure 3.11. A FieldPoint device is composed of a network module (FP-1601) and several I/O

modules. The selection of I/O modules depends on specific control and data acquisition needs. For the F-T reactor, there are three kind of modules used: thermocouple module (FP-TC-120), voltage and current analog input module (FP-AI-110), and pulse width modulation output module (FP-PWM-520). The thermocouple module is used to receive temperature signals of reactor temperature, reactor inlet temperature and catalyst temperature. Then, the signals are output to PC in part 4 through an ethernet cable, and then displayed on the indicators of automation program. The analog input module is used to measure voltage or current output signals from pressure transducers and mass flow controllers. The signals will also be sent to automation program, where they are converted to digital readings of pressure and flow rate. The pulse width modulation output module (PWM module) is used to control the power of heaters indirectly through relays (shown in part 2). A relay acts like a switch. When it is connected in the heater circuit loop, it can control heater power output by switching on and off at various time intervals. Thus, when PWM module receives power output command from automation program, it will send out on and off control signals to the relays, then signals cause different heating interval of heaters, and finally result in different power output of the heater. Similarly, the PWM module is also used in control of auto shut-off valve. In case

of emergency condition, automation program will send out command signal to PWM module to cut off power of relay and create an open circuit. As a result, the shut-off valve loses power and closes to stop gas flow.

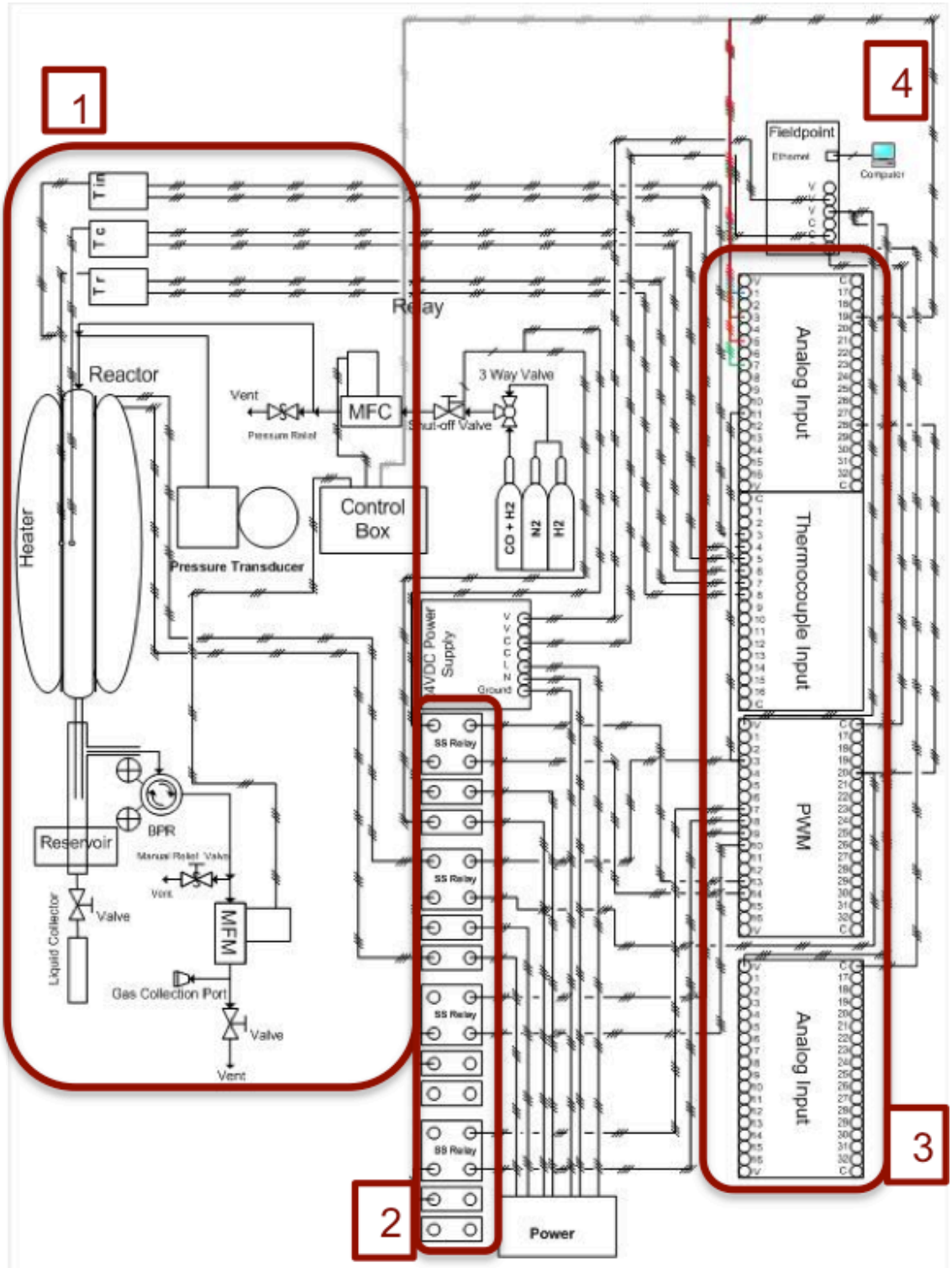

Figure 3.11 Diagram of F-T reactor with automation system

2) Front panel

The front panel of Fischer-Tropsch synthesis automation system is shown in figure 3.12. The panel can be divided into 4 parts. Part 1 is the main window. All process variables are shown in the left column, including reactor inlet temperature, reactor surface temperature, catalyst temperature, reactor pressure, inlet and outlet flow rate, gas composition and reactor power output. Two red lights under the column are temperature alarm and pressure alarm, respectively. In case of pressure built-up or temperature run-away, alarm lights will turn on, and operators will be noticed to conduct emergency response. The window on the right hand side of part 1 is a display of real-time system variables. All process variables in the left column will be plotted on the window, and any changes of process value can be easily noticed. In the plot window, x-axis is reaction time and values of different process variables are shown on the y-axis. In addition, line weight and color can also be customized to distinguish between different process variables.

Reactor control module is shown in part 2 of figure 3.12. In this part, operation commands can be input into the blanks on top, including setpoint, reactor temperature ramp, maximum PID output, and setpoint upper and lower limit. In addition, there are

four sets of PID gains shown at the bottom of part 2. The first set of PID gains is manual control. In case there is a sudden change of process value, and automation system cannot adjust system fluctuation very well, manual control can be turned on by pressing the button above manual PID block. At this time, K_p, K_i and K_d value can be changed manually to stabilize process values. When system is back under control, manual control can be switched off by click the button for one more time, and process control will be taken over by automation system.

The other 3 sets of PID gains are all automatic control. Each set of gains has unique PID gains, and it is used under specific operating conditions, which is called gain scheduling. The first set of gains is used under steady-state operating condition. At this condition, K_d is set at a relatively low value of 0.05, which is to make sure that control will not over-respond to small fluctuation. Beside, K_i is set at 1 to eliminate steady-state error. The first set of gains has good control performance at steady-state operation. However, when there is a fluctuation of process variable, it has slow response to changes and cause control difficulties. As a result, when high system fluctuation is detected, the second set of gains will take over the control. Since it is not a steady-state condition, term K_i is set to 0. In addition, K_d is increased to a higher value of 1, so system can have faster response to

stabilize fluctuation. If the second set of gains cannot work effectively and system stability is getting worse, the last gain set will be triggered. In this set of gains, K_i is set to 0 to avoid overshoot; K_p and K_d are set to high values of 100 and 10, respectively, to compensate fluctuation. If system fluctuation gets under control, control PID will switch to the second then the first set of gains; If fluctuation is getting worse and system is out of control, alarm will be triggered, heater power will be lower down to zero, and shut-off valve will close to stop gas flow.

Part 3 and 4 are both real time plots similar to the main plotting window in part 1. However, part 3 only shows readings of pressure and flow rate, and window in part 4 only displays the values of temperature variables.

3) Back panel

The back panel of Fischer-Tropsch synthesis automation system is shown in figure 3.13. The back panel, which is a block diagram, can be divided into 4 parts. Part 1 is data recording block. It reads all the process values every second, and then record the data in an excel file. Part 2 is data acquisition and indicator block. In this block, the program reads process variables such as temperature, pressure, flow rate and heater output in specific channels, then these variables are displayed in the front plotting window. In part

3, PID gain scheduling is programmed. Temperature logic is also included in this part. The function in part 4 is control of all heaters and electrical valve. Note that there are two spare channels added in case gas preheat and post heat is needed for experiments.

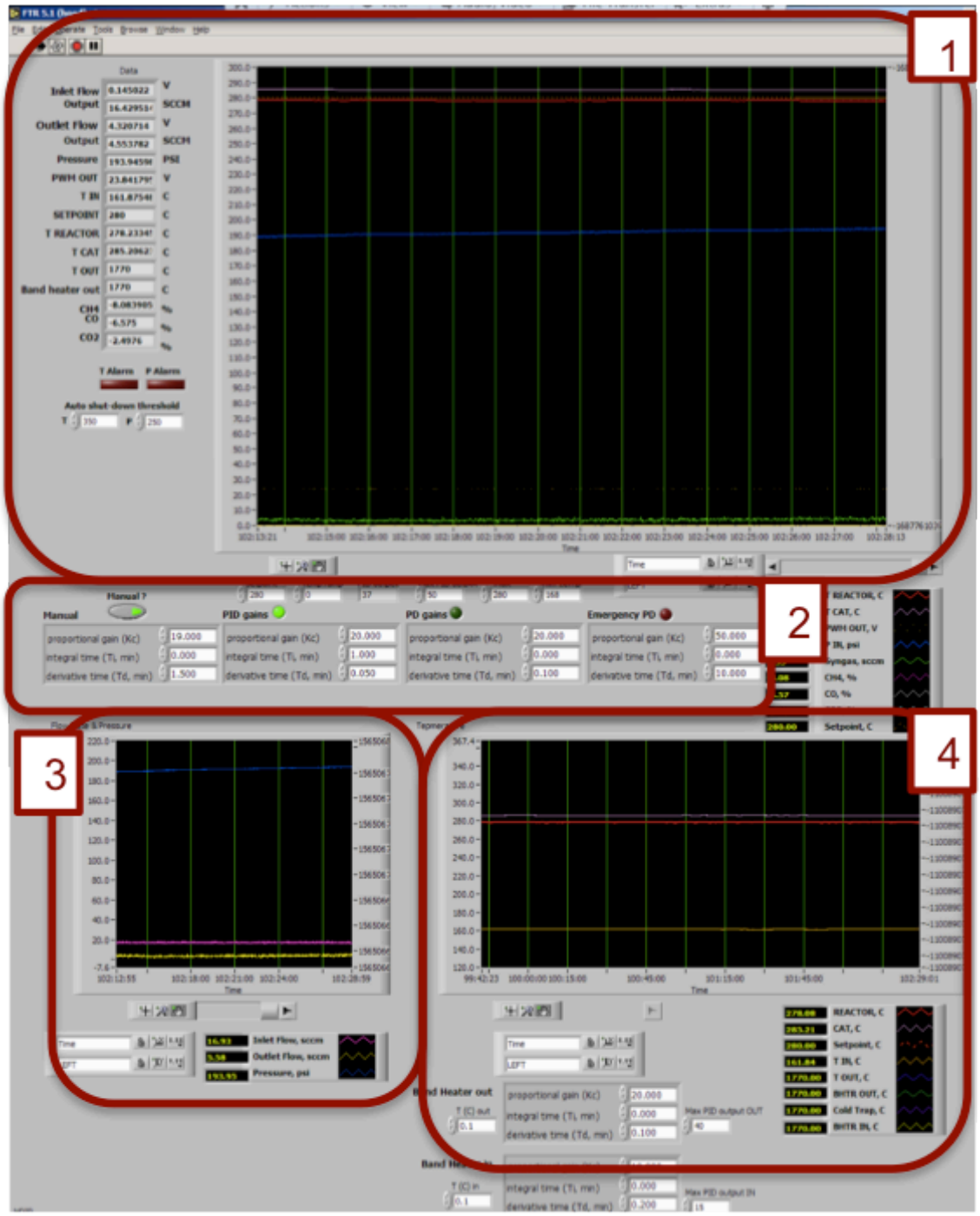

Figure 3.12 Front panel screen shot of F-T synthesis automation system

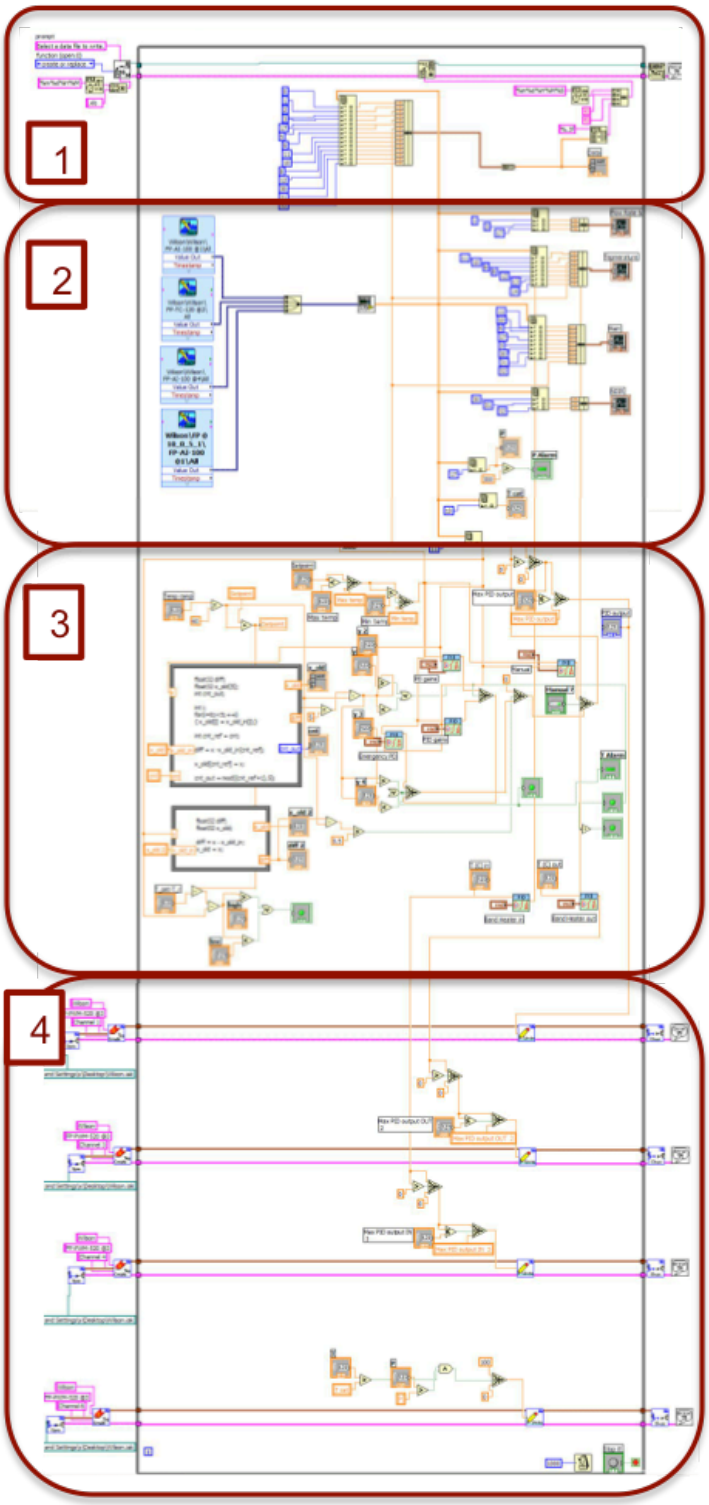

Figure 3.13 Back panel screen shot of F-T synthesis automation system

3.4 Conclusion

In this chapter, two versions of lab-scale Fischer-Tropsch reactor system are designed and constructed. In addition, an automation system is also programmed for system control and data acquisition. The conclusions are summarized as follows:

1) First generation lab-scale Fischer-Tropsch reactor system is designed and built. It is a high temperature high pressure continuous reactor system, which composed of gas supply, mass flow controller, reactor, liquid product collector, back pressure regulator, gas flow meter, and gas sampler. This reactor is compatible with both conventional F-T catalyst and new zeolite-shell F-T catalyst. Two CO alarms are equipped to ensure operation safety. It also has online gas and liquid sampling features to improve test efficiency and reduce total experiment time.
2) Second generation lab-scale Fischer-Tropsch reactor system is designed and built with several upgrades. It is built in a walk-in hood to improve operation safety. There are other safety features added to the system such as emergency auto shut-off valve and pressure relief valve. In addition, the reactor structure is also simplified to save energy and enhance system reliability. Total pipeline length for the new reactor is also shortened to reduce product collection delay.

3) Automation system is created using LabVIEW program to control F-T synthesis experiments. The automation program can read operation variables such as temperature, pressure, and flow rate, and plot all data in the front panel at real time. Selective data can also be saved to excel files automatically for post processing. In addition, PID controllers with gain scheduling are used for heating control to achieve minimum temperature fluctuation. Finally, built-in alarm system can notice operator with any abnormal condition, and shut inlet gas flow automatically in case of emergency.

CHAPTER 4 One Step Gasoline-range Isoparaffin Production from Syngas

This chapter focuses on gasoline-range Isoparaffin production with zeolite-shell F-T catalyst. In F-T synthesis tests, CO conversion, CH_4 selectivity and CO_2 selectivity is evaluated under various operation condition. Also, gasoline range product selectivity and product speciation is assessed. In addition, sensitivity analysis is conducted to evaluate the effect of process variables on catalyst performance, such as catalyst SAR, space velocity, operating temperature and pressure. Finally, time on stream study and thermal gravimetric analysis is done to evaluate catalyst deactivation during operation.

4.1 One Step Gasoline-range Isoparaffin Synthesis Experiment

4.1.1 Experiment Procedure

1) Start-up procedue

temperature high pressure continuous fixed-bed reactor system as described in chapter 3. 2g of catalyst is loaded based on Co/Al_2O_3, which means that 2g of conventional F-T catalyst and the weight of zeolite-shell catalyst is 2g plus the additional weight of zeolite shell in the weight test. The test temperature ramp schedule is shown in figure 4.1. The catalysts are in oxidized state, and have to be reduced in-situ before they are active for Fischer-Tropsch synthesis. To begin with, catalyst is activated with H_2 flow from ambient to 350ºC at a ramp of 1ºC/min, and hold for 6 hrs. After activation, reactor temperature is cooled down to 170ºC at a ramp of 1ºC/min. Then syngas with a H_2 to CO ratio of 2.1 is introduced to the system at space velocity of 2 NL/g-cat./hr and pressure of 180 psi.

System temperature is ramped at 0.05 ºC/min to 220 ºC or other operating temperature. At this time, significant catalyst activity is observed, and it is set as test start point. The activation process and temperature ramp take around 34 hours before test, so one test is usually last 7-10 days to ensure test efficiency.

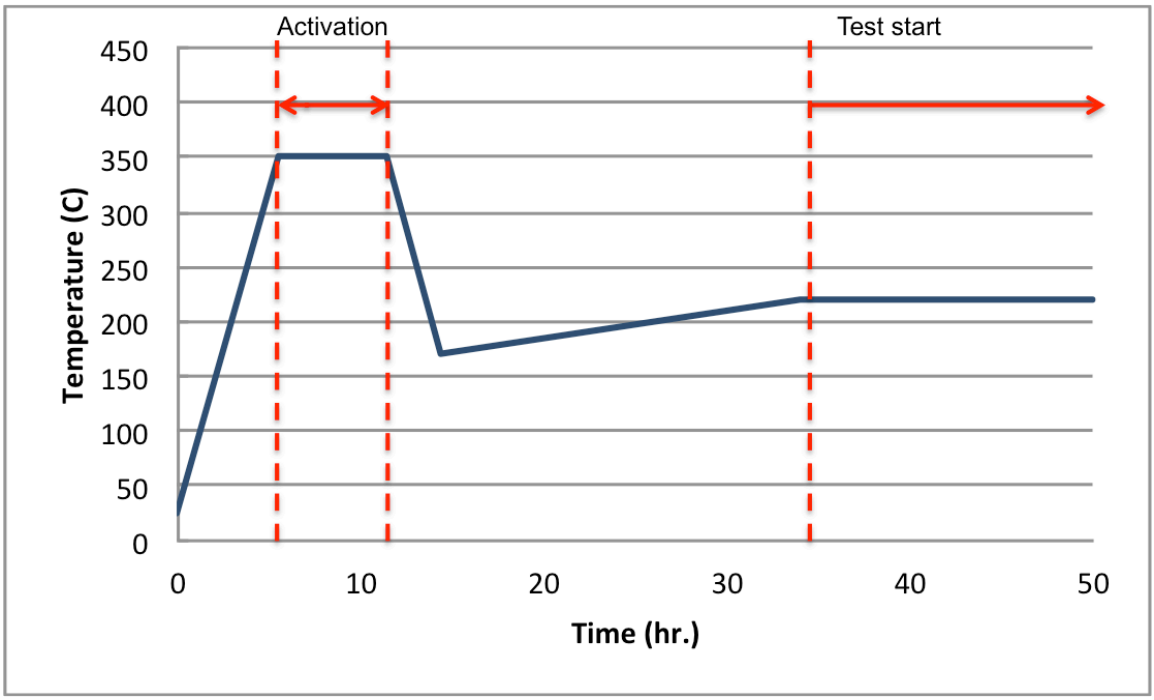

Figure 4.1 F-T test temperature ramp schedules

2) Gas and liquid sampling

Gas sampling has two options: online and offline. For online sampling, gas outlet is connected to the inlet of non-dispersive infrared (NDIR) or residual gas analyzer (RGA) directly, and sampling result can be analyzed automatically by the program; For offline gas sampling, product gases are collected by a gas sampling bag (Supel 30221-U)

through a port connector located at the gas outlet. Then the bag is connected to analyzers like RGA for composition analysis.

Liquid sampling is conducted every 24 hours. To begin with, the valve between two collectors is switched open, and liquid product at upper collector is pushed to the bottom collector because of pressure difference. Then valve is closed and bottom collector is loosened slowly to release pressure then disconnected. Afterwards, liquid products are transferred to sample vials and stored in refrigerator for at least 12 hours for hydrocarbon-water separation. During gas chromatography (GC) analysis, 15 μL of samples are injected to test vial and diluted by 200 μL of CS_2 (Sigma-Aldrich 335266-1L), and then the test vial is loaded on to GC auto sampler for composition analysis.

3) Shutdown procedure

When test is finished, heater is turned off by setting heater output to zero in automation program. In addition, turn back pressure regulator counter-clockwise to reduce system pressure to ambient. Then switch gas flow from syngas to N_2, and increase gas flow rate to expel syngas and help cool down the reactor. Maintain N_2 gas flow for 12 hrs. to make sure all syngas is expelled and then shut off gas flow and turn off electric power.

4.1.2 Analytical Apparatus

1) Residual gas analyzer

Residual gas analyzer (RGA) (MKS Instruments, Inc.) is used for gaseous product analysis, and the picture is shown in figure 4.2. RGA gas analysis is based on quadruple mass spectrometer, and there are several advantages of using RGA for gas analysis. First of all, RGA is able to analyze multiple components in mixture gas at the same time,

which provides fast online analysis results. Second, RGA is able to analyze gas composition over a wide dynamic range from percentage to ppb levels. At last, due to its bench-top configuration, the operation and maintenance of RGA is convenient.

Figure 4.2 Picture of Cirrus Atmospheric Pressure Residual Gas Analyzer

The RGA provides near real-time analysis of gaseous products by continuous scanning of mass spectra with an interval of 3-4 seconds. The sensitivity of RGA to a particular gas species is expressed as the peak intensity per unit measure in equation 4.1, which is assumed to be relatively unaffected in a wide range of RGA background.

$$S_C = \frac{I_C}{P_C} \qquad (4.1)$$

Where

Sc: RGA sensitivity to a gas species

Ic (torr): major intensity of a gas species in mass spectra

Pc (torr): partial pressure of a gas species in mixture gases.

The RGA records the mass spectra data in intensity with units of torr. The major products analyzed with RGA are CH_4, H_2, CO, and CO_2. The relative concentration of a gas

species in product gas is proportional to the intensity of this gas species. The sensitivity of a gas species in mixture gas can be obtained by calibration using certified calibration gas. And calibration is required before each analysis.

2) Non-dispersive infrared analysis

Non-dispersive infrared (NDIR) analysis is used for online gas analysis of CO, CO_2 and H_2. It is named non-dispersive because the gas wavelength that passes through the sampling chamber is not pre-filtered, while other infrared sensors have filters used before the detector. The main components of the NDIR are an infrared lamp, a sample chamber, and a wavelength sample chamber. The infrared light is directed through the sample chamber towards the detector, and gas concentration is measured electro-optically by its absorption of a specific wavelength in the infrared light. Also, there is another chamber in parallel, which enclosed reference gas, typically nitrogen. The detector has an optical filter, which eliminates all light except the wavelength that the selected gas can absorb. And gas concentration is calculated by the amount of light reaching the detector compared with that in reference gas chamber.

3) Gas chromatography

The collected liquid product is analyzed by gas chromatography (GC, Agilent 7890A). GC is widely used in analytical chemistry for separating and analyzing compounds that can be vaporized without decomposition, in this thesis, liquid hydrocarbons.

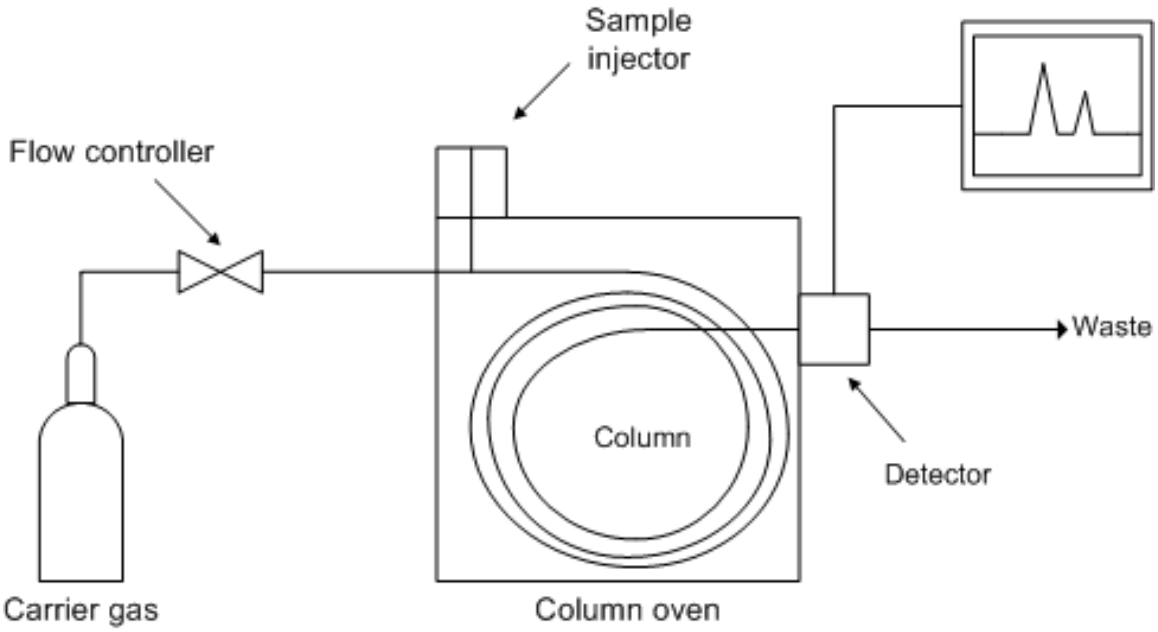

Figure 4.3 Diagram of a gas chromatograph

The GC is composed of four parts: auto sampler, inlet, column, and detector. Auto sampler provides means to introduce sample automatically into the inlets. The use of auto sampler can ensure clean and accurate sample loading to improve sample analysis repeatability. The inlet provides means to introduce sample to the column. When liquid sample is introduced through inlet, it is heated in a small chamber to vaporize, and mixed with carrier gas. Since the sample/carrier gas mixture has high sample concentration, the mixture is split and only a portion is swept into the column. The column is used to separate different species in the mixture based on different adsorption-desorption rate. In this thesis, and HP-5 column is equipped for liquid separation, which has a length of 30m, ID of 0.32 mm and a stationary phase of (5%-Phenyl)-methylpolysiloxane. After column separation, all gases approaches to the end of column at different retention time,

and they are analyzed by a flame ionization detector (FID). The detector has a flame fueled by H_2 / air, which pyrolyzes hydrocarbons and form cations and electrons. The cations and electrons are collected by detector electrodes and generate electric currents. Then the current is translated and appears as a peak in a chromatogram. Calibration is carried out before sample analysis. It is conducted by analyzing hydrocarbon samples with known species and concentration. Then the species and concentration of an unknown sample can be obtained by comparing retention time and peak intensity.

4.2 Gas Product Results and Discussion

4.2.1 CO Conversion

CO conversion shows the F-T activity of the catalyst. It is calculated by equation 4.1.

$$CO\ conversion = \frac{CO_{in} - CO_{out}}{CO_{in}} \times 100\% \qquad (4.1)$$

CO conversion of zeolite-shell F-T catalyst with SAR=250 is calculated, and results is shown in figure 4.4. During the test, space velocity varies between 0.5 to 1.5 NL/g-cat./hr, and temperature is 220 – 280 ºC. It is observed from the figure that at same operating temperature, CO conversion increases with decreasing space velocity. At T=280 ºC, CO conversion is 83.5% at space velocity of 1.5 NL/g-cat./hr. However, it is increased to 94.33% at space velocity of 0.5 NL/g-cat./hr. The reason is with decreasing space velocity, contact time between syngas and catalyst active site increases, and CO

conversion is promoted. In addition, with same space velocity, CO conversion increases with temperature. At space velocity of 1 NL/g-cat./hr, CO conversion 59% at 220 ºC, but 30% conversion increase is observed when temperature is increased to 280 ºC.

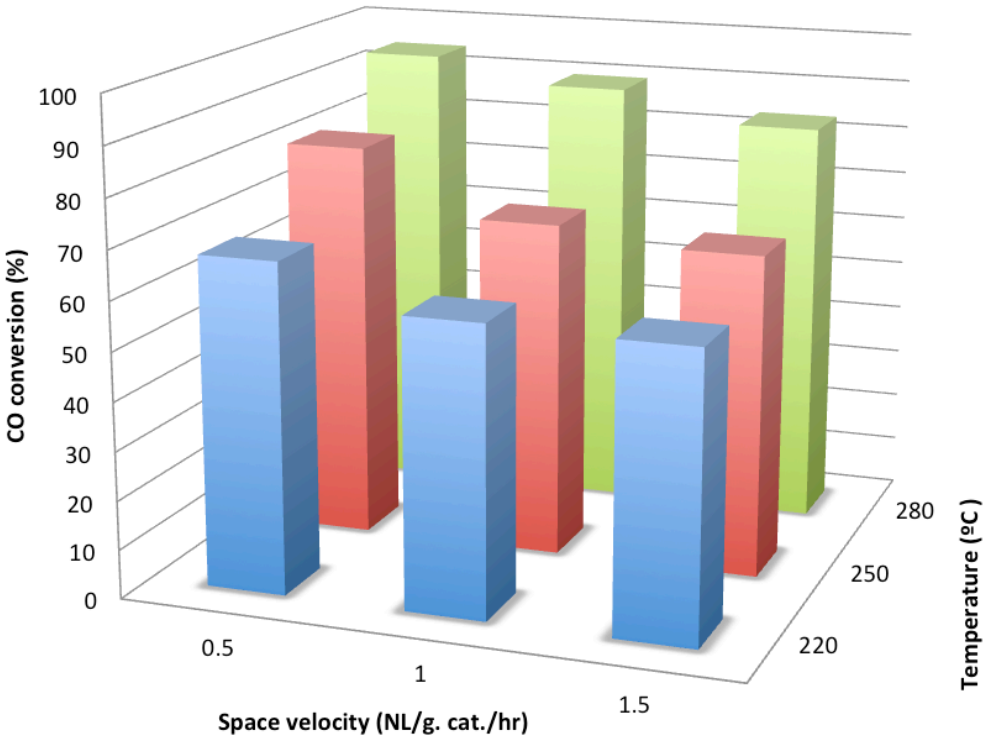

	0.5	1	1.5
220	67.4	59	58.3
250	81.6	68.8	65.9
280	94.33	89.46	83.5

Figure 4.4 Effect of reaction temperature and space velocity on CO conversion of zeolite-shell catalyst with SAR=250

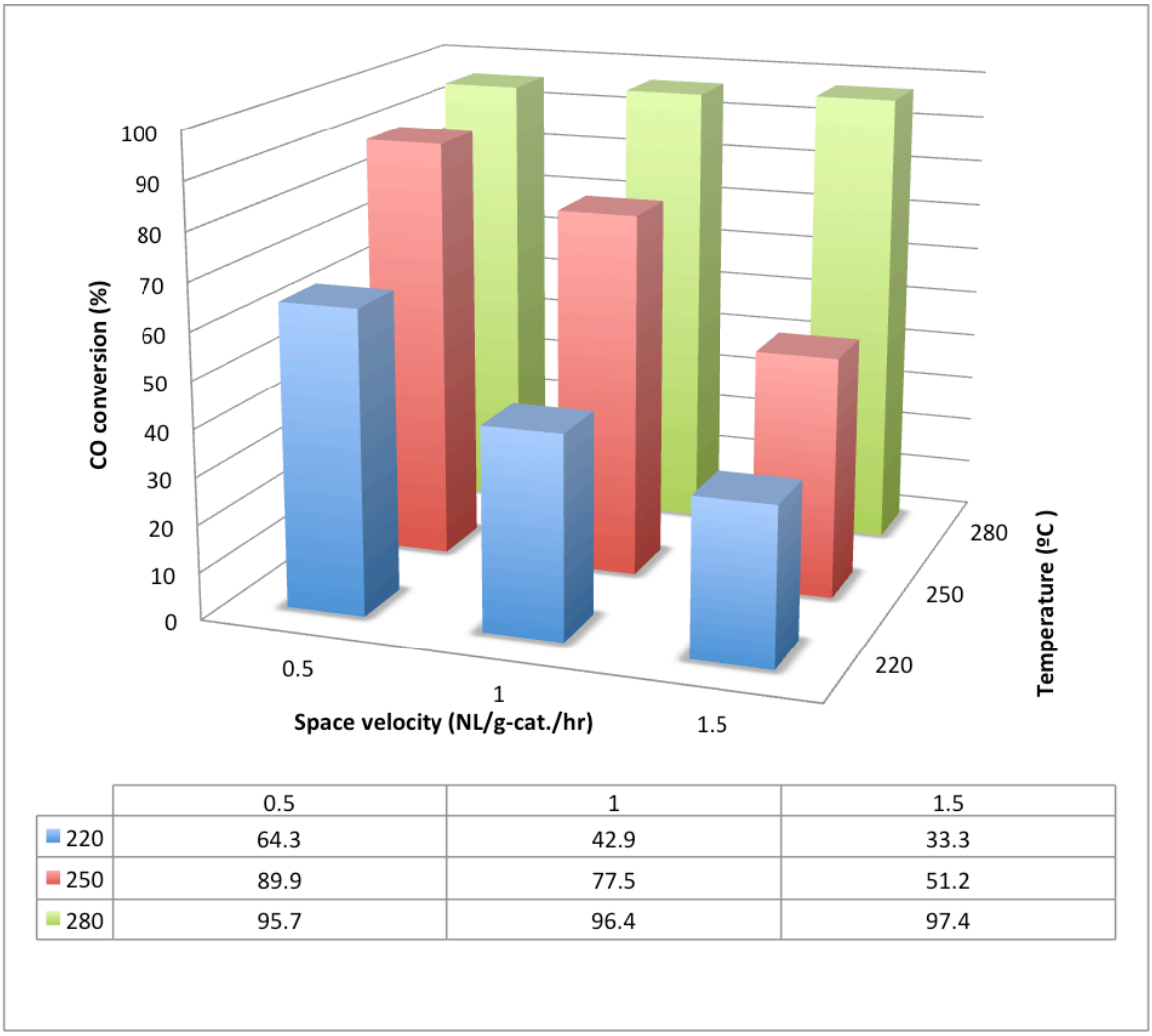

	0.5	1	1.5
220	64.3	42.9	33.3
250	89.9	77.5	51.2
280	95.7	96.4	97.4

Figure 4.5 Effect of reaction temperature and space velocity on CO conversion of zeolite-shell catalyst with SAR=150

The effect of reaction temperature and space velocity on CO conversion for zeolite-shell catalyst with SAR=150 is shown in figure 4.5. It is observed from the figure that CO increases with operating temperature at same space velocity. At space velocity of 1.5 NL/g-cat./hr and temperature is 220 ºC, CO conversion is 33.3%. However, this number is increased to 97.4% when temperature is at 280 ºC. When temperature is fixed at 220 ºC, CO conversion decreases with increasing space velocity. And same phenomenon is observed at temperature of 250 ºC. When temperature is at 280 ºC, however, CO conversion does not have significant change with space velocity, but maintained at 95% - 97%. This indicates that CO conversion reaches to maximum, due to high catalytic activity at 280 ºC.

The result of CO conversion of zeolite-shell F-T catalyst with SAR 80 is shown in figure 4.6. Space velocity varies between 0.5 to 1.5 NL/g-cat./hr, and temperature is between 220ºC and 280 ºC. The effect of space velocity and temperature on CO conversion of SAR 80 catalyst is similar to that of SAR 150 catalyst. At same space velocity, CO conversion increases with temperature. When temperature changes from 220 ºC to 280 ºC, a CO conversion increase of 31.4% and 64.1% is obtained at space velocity of 0.5 and 1.5 NL/g-cat./hr, respectively. In addition, when system is maintained at temperature of 220 ºC and 250 ºC, CO conversion is enhanced with decreasing space velocity. However, at 280 ºC, with changing space velocity from 0.5 to 1.5 NL/g-cat./hr, CO conversion is not significantly affected. Above results indicate that catalyst activity is promoted by increasing temperature. At high temperature of 280 ºC, maximum CO conversion is obtained even at relatively high space velocity.

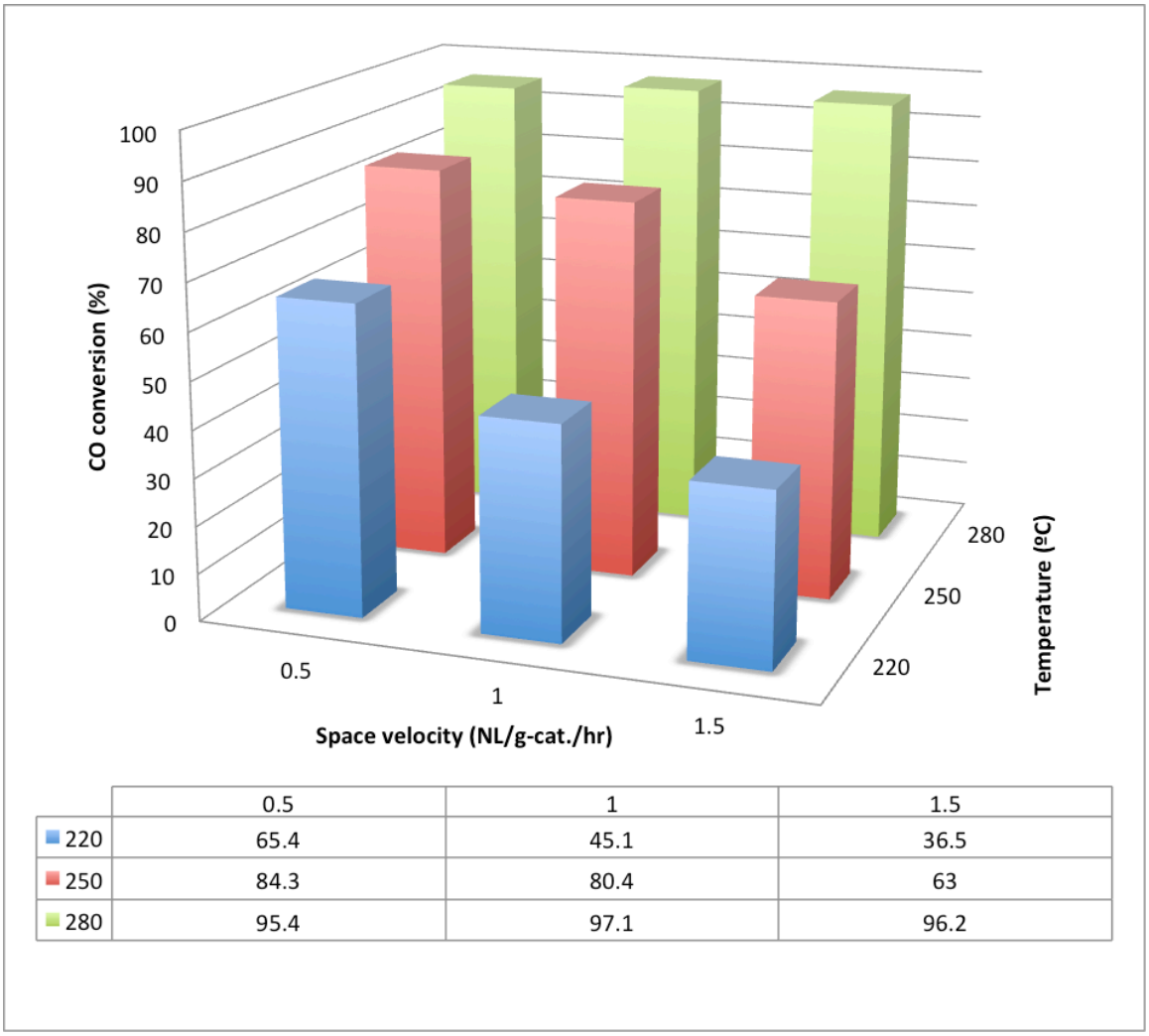

	0.5	1	1.5
220	65.4	45.1	36.5
250	84.3	80.4	63
280	95.4	97.1	96.2

Figure 4.6 Effect of reaction temperature and space velocity on CO conversion of zeolite-shell catalyst with SAR=80

4.2.2 CH_4 Selectivity

Methane selectivity is an indication of product distribution. High methane selectivity means low heavy product selectivity. As a result, low methane selectivity is favorable in F-T gasoline production. Methane selectivity is calculated in equation 4.2.

$$methane\ selectivity = \frac{moles\ methane\ produced}{total\ moles\ of\ carbon\ converted} \times 100\% \qquad (4.2)$$

The effect of temperature and space velocity on methane selectivity for SAR 250 zeolite-shell F-T catalyst is shown in figure 4.7. When space velocity is at 1 and 1.5 NL/g-cat./hr, methane selectivity increases with reaction temperature. When space velocity is lowered to 0.5, methane selectivity has 6% increase with temperature rise from 220 ºC to 250 ºC. With further temperature increase to 280 ºC, methane selectivity shows 2% decrease. At certain system temperature, methane conversion does not have clear trend with change of space velocity. At 220 ºC, space velocity does not have significant impact on methane selectivity. At 250 ºC, methane selectivity first increases when space velocity changes from 1.5 to 1 NL/g-cat./hr. However, with further increase of space velocity from 1 to 0.5 NL/g-cat./hr, methane selectivity slightly decreased from 9.7% to 8.6%. When temperature is at 280 ºC, methane selectivity increases with space velocity. At space velocity of 0.5 NL/g-cat./hr, methane selectivity is 6.6%. At space velocity of 1.5 NL/g-cat./hr, however, methane selectivity has over 10% increase to 17.3%.

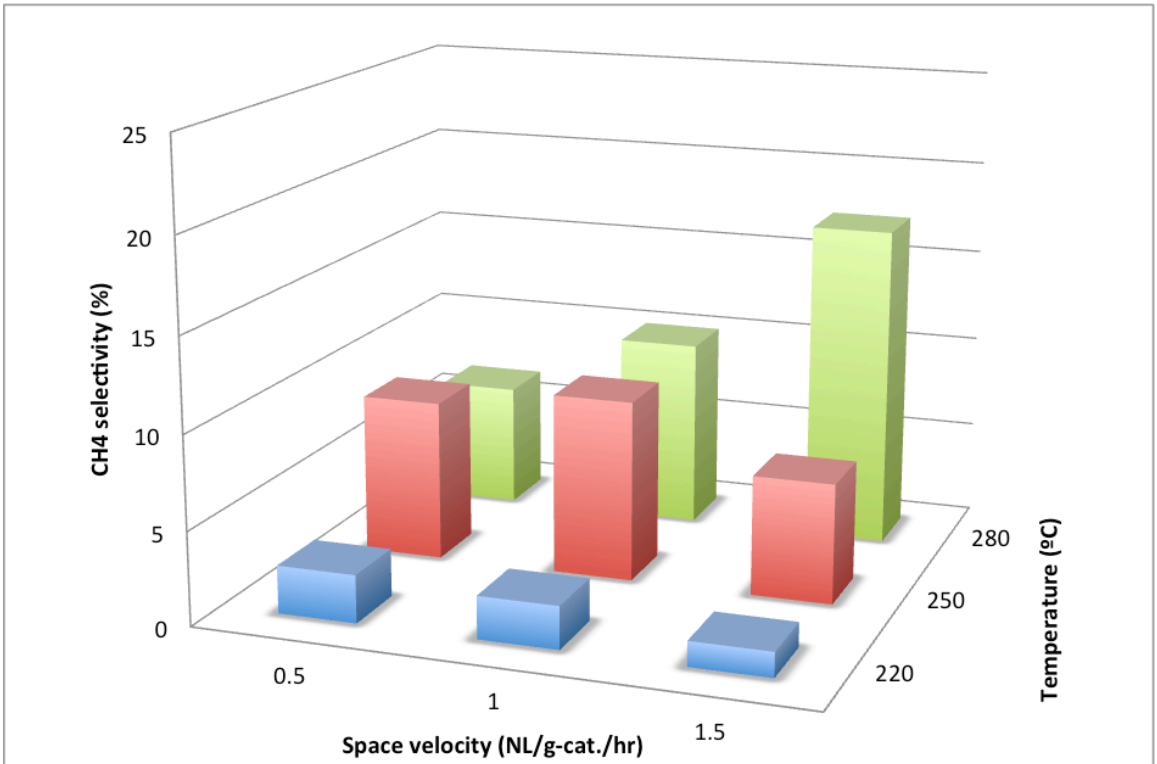

	0.5	1	1.5
220	2.56	2.28	1.33
250	8.6	9.7	6.43
280	6.6	10.1	17.3

Figure 4.7 Effect of reaction temperature and space velocity on CH_4 selectivity of zeolite-shell catalyst with SAR=250

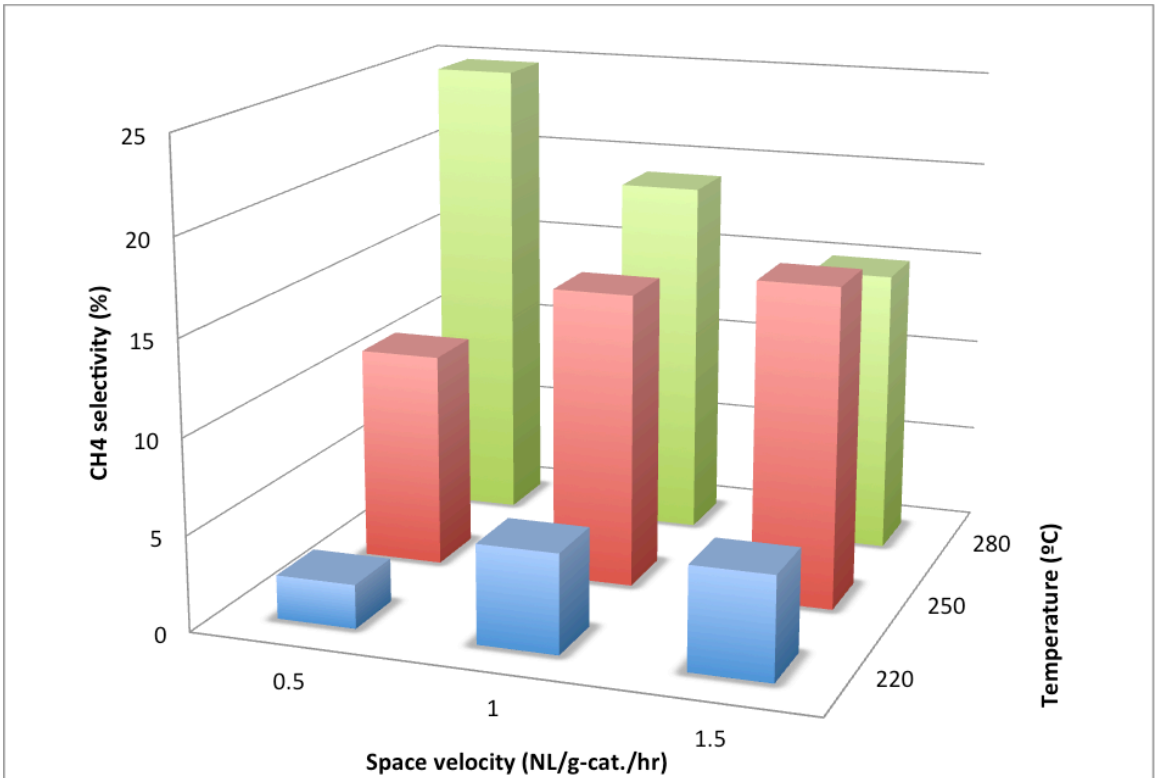

	0.5	1	1.5
220	2.3	5.2	5.4
250	11.3	15.5	16.8
280	24.8	19	15

Figure 4.8 Effect of reaction temperature and space velocity on CH_4 selectivity of zeolite-shell catalyst with SAR=150

The effect of temperature and space velocity on methane selectivity for SAR 150 zeolite-shell F-T catalyst is shown in figure 4.8. It is found from the figure that at space velocity of 0.5 NL/g-cat./hr, methane selectivity is promoted with increasing temperature. Similar effect can also be observed at space velocity of 1 NL/g-cat./hr. At space velocity of 1.5 NL/g-cat./hr, with temperature increase from 220 ºC to 250 ºC, methane selectivity increases from 5.4% to 16.8%. With further temperature increase from 250 ºC to 280 ºC, methane selectivity has slight decrease from 16.8% to 15%. At fixed system temperature, methane conversion does not have obvious trend with change of space velocity. At 220 ºC, methane selectivity increases with space velocity. At temperature of 250 ºC, same trend can be observed, though the absolute value of methane selectivity is much higher than that at 220 ºC. When temperature is at 280 ºC, methane selectivity shows a 10% decrease when space velocity increases from 0.5 to 1.5 NL/g-cat./hr.

Methane selectivity of SAR 80 catalyst is calculated, and effect of temperature and space velocity is shown in figure 4.9. From the figure it is found that methane selectivity increases with space velocity at reaction temperature of 220 ºC and 250 ºC. At 280 ºC, methane selectivity does not have significant increase with space velocity change from 0.5 to 1 NL/g-cat./hr. However, methane selectivity decreases from 18.7% to 12.8% when space velocity is further increased to 1.5 NL/g-cat./hr. When space velocity is 0.5 NL/g-cat./hr, methane selectivity increases significantly with temperature, which is 1.5% at 220 ºC, 11.6% at 250 ºC, and 18.3 at 280 ºC. Similar trend can also be observed at space velocity of 1 NL/g-cat./hr. From 220 ºC to 280 ºC, methane selectivity has over 15% increase from 2.8% to 18.7%. At space velocity of 1.5 NL/g-cat./hr, methane

selectivity first increases significantly from 220 ºC to 250 ºC, and then has 6% decrease from 250 ºC to 280 ºC.

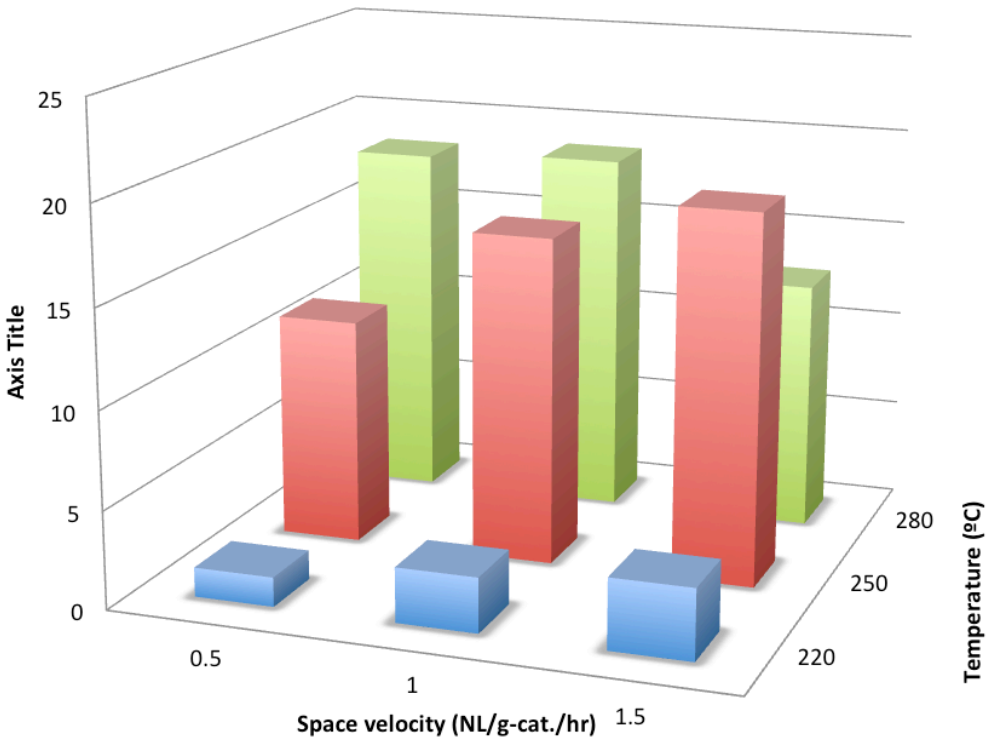

	0.5	1	1.5
220	1.5	2.8	3.6
250	11.6	16.8	18.9
280	18.3	18.7	12.8

Figure 4.9 Effect of reaction temperature and space velocity on CH_4 selectivity of zeolite-shell catalyst with SAR=80

4.2.3 CO_2 Selectivity

CO_2 is an undesirable product from F-T synthesis. It is produced from side reactions such as water-gas shift reaction. CO_2 selectivity is calculated in equation 4.3.

$$CO_2\ selectivity = \frac{moles\ CO_2\ produced}{total\ moles\ of\ carbon\ converted} \times 100\% \qquad (4.3)$$

The effect of temperature and space velocity on CO_2 selectivity for SAR 250 zeolite-shell F-T catalyst is shown in figure 4.10. It is observed from the figure that at 220 ºC, CO_2 selectivity is undetectable. At 250 ºC, CO_2 selectivity still maintained at a low value, which is less than 1%. And it does not have significant change with changing space velocity. When temperature is fixed at 280 ºC, CO_2 selectivity has 1.7% increase when space velocity changes from 0.5 to 1 NL/g-cat./hr. With further increase of space velocity to 1.5 NL/g-cat./hr, CO_2 selectivity dropped from 3.82% to 1.7%. When space velocity is fixed at 0.5 NL/g-cat./hr, CO_2 selectivity increases with temperature from negligible value at 220 ºC to 2.1% at 280 ºC. Similar trend is also observed when space velocity is maintained at 1 and 1.5 NL/g-cat./hr, respectively. When temperature increases from 220 ºC to 280 ºC, CO_2 selectivity has 3.82% increase when space velocity at 1 NL/g-cat./hr, and 1.7% increase when space velocity is at 1.5 NL/g-cat./hr.

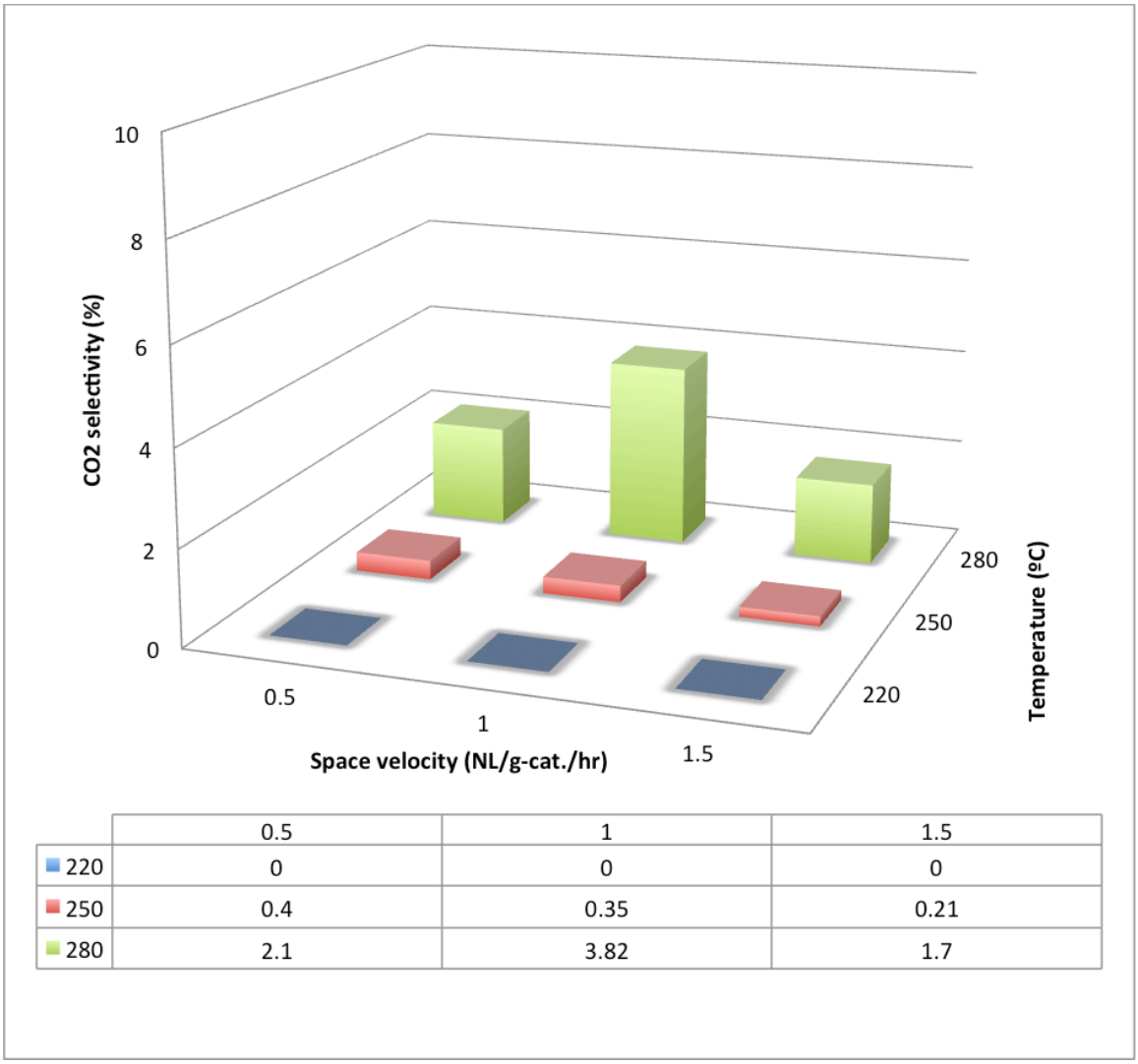

	0.5	1	1.5
220	0	0	0
250	0.4	0.35	0.21
280	2.1	3.82	1.7

Figure 4.10 Effect of reaction temperature and space velocity on CO_2 selectivity of zeolite-shell catalyst with SAR=250

The effect of temperature and space velocity on CO_2 selectivity for SAR 150 zeolite-shell F-T catalyst is shown in figure 4.11. It is observed from the figure that CO_2 selectivity is undetectable at 220 ºC. At 250 ºC, CO_2 selectivity is enhanced with increasing space velocity, which is 2.8% at 0.5 NL/g-cat./hr, 6.8% at 1 NL/g-cat./hr, and 7.7% at 1.5 NL/g-cat./hr. When temperature is at 280 ºC, CO_2 selectivity is reduced by increasing space velocity. A 5% CO_2 selectivity reduction is observed when space velocity changes from 0.5 to 1.5 NL/g-cat./hr. When space velocity is maintained at 0.5 NL/g-cat./hr, CO_2 selectivity increases with elevating temperature from 220 ºC to 280 ºC. At space velocity of 1 NL/g-cat./hr, CO_2 selectivity has 6.8% increase from 220 ºC to 250 ºC, and then stabilizes with further temperature increase to 280 ºC. When space velocity is set at 1.5 NL/g-cat./hr, CO_2 selectivity increases from 0 to 7.7% when temperature is elevated from 220 ºC to 250 ºC. Then CO_2 selectivity is slightly reduced from 7.7% to 6.5% with further temperature increase to 280 ºC.

CO_2 selectivity of SAR 80 catalyst is calculated, and effect of temperature and space velocity is shown in figure 4.12. From the figure it is found that CO_2 selectivity is undetectable when temperature is at 220 ºC. When temperature is at 250 ºC, CO_2 selectivity first increases from space velocity of 0.5 to 1 NL/g-cat./hr, then slightly decreases with further space velocity increase to 1.5 NL/g-cat./hr. At 280 ºC, CO_2 selectivity is reduced with increasing space velocity. At fixed space velocity of 0.5 NL/g-cat./hr, CO_2 selectivity increases with increased temperature from 220 ºC to 280 ºC. When space velocity is at 1 and 1.5 NL/g-cat./hr, Space velocity first increases with temperature from 220 ºC to 250ºC, then decreases from 250 ºC to 280 ºC.

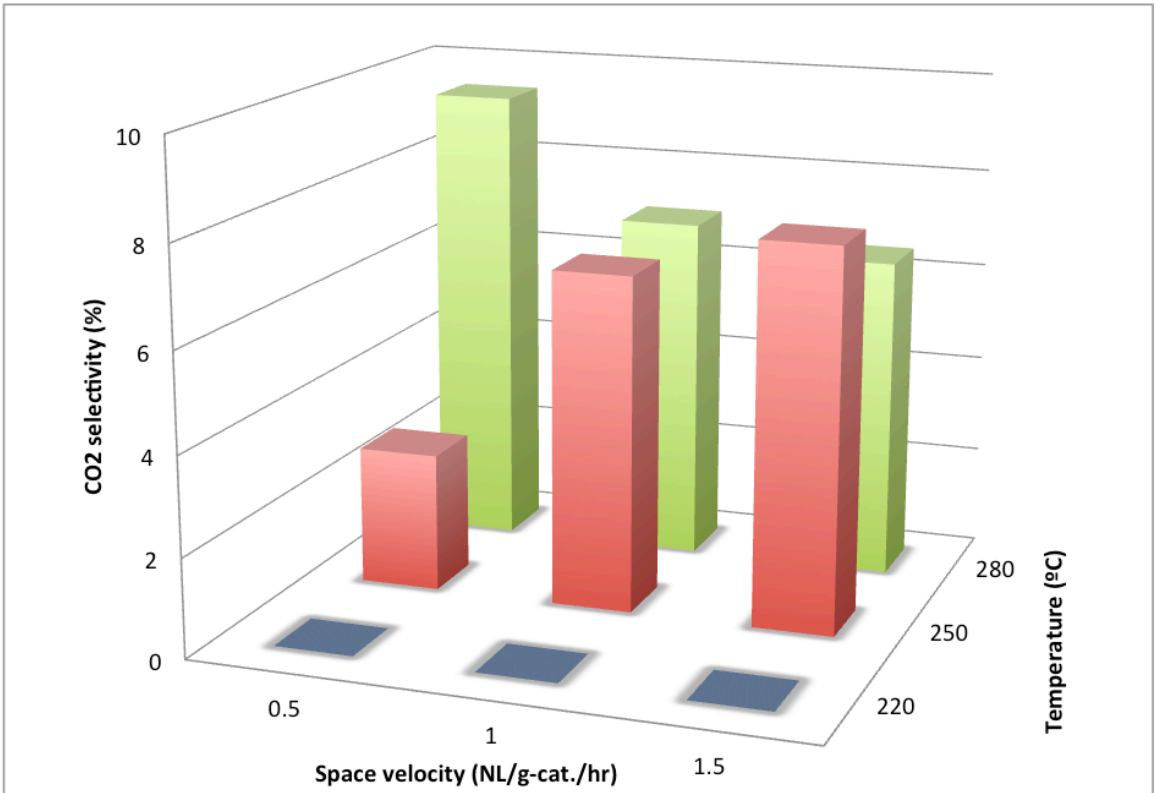

	0.5	1	1.5
220	0	0	0
250	2.8	6.8	7.7
280	9.4	7	6.5

Figure 4.11 Effect of reaction temperature and space velocity on CO_2 selectivity of zeolite-shell catalyst with SAR=150

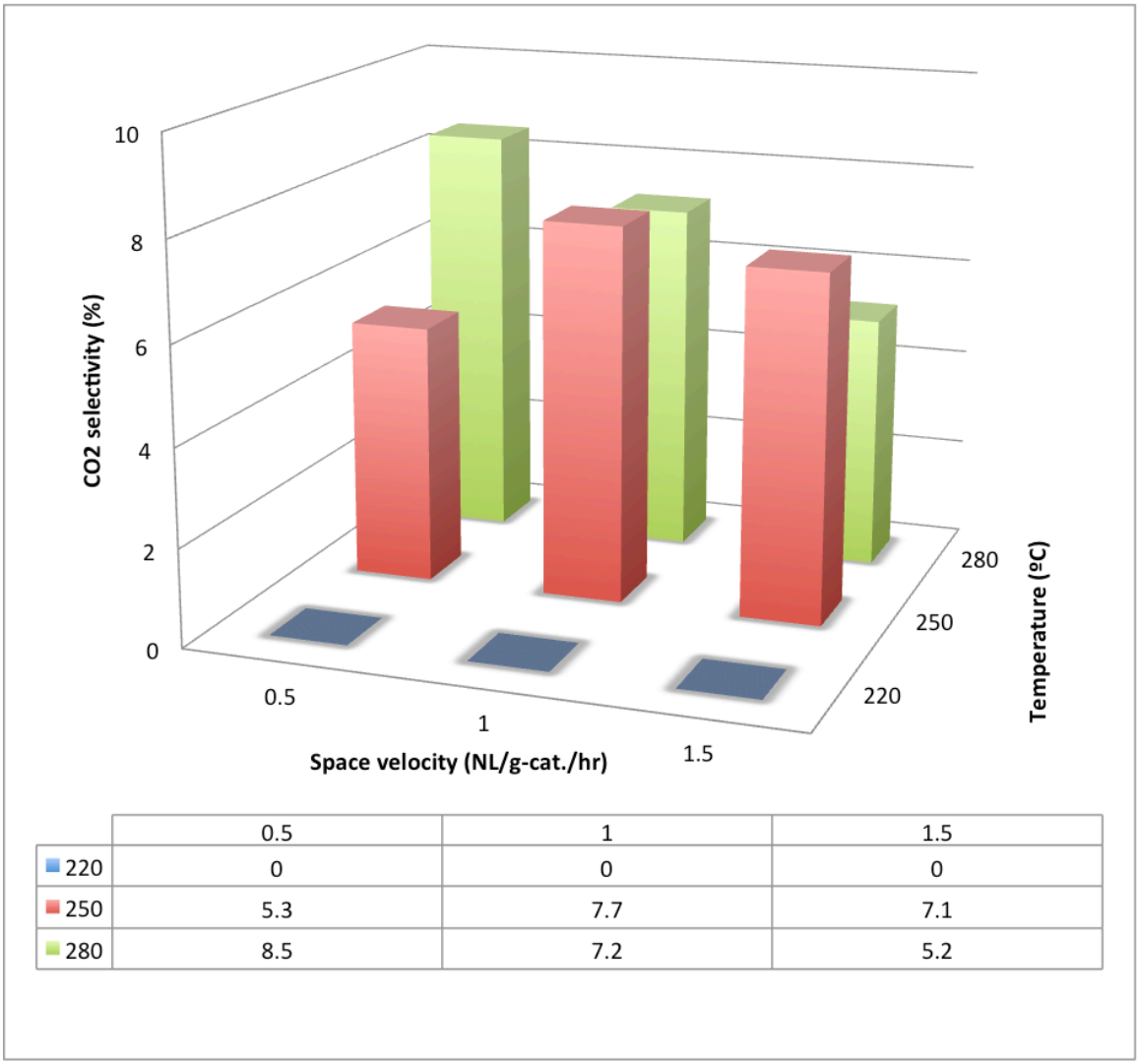

	0.5	1	1.5
220	0	0	0
250	5.3	7.7	7.1
280	8.5	7.2	5.2

Figure 4.12 Effect of reaction temperature and space velocity on CO_2 selectivity of zeolite-shell catalyst with SAR=80

4.2.4 Sensitivity Analysis

The result of CO conversion, CH_4 selectivity, and CO_2 selectivity with various temperature and space velocity is modeled using least square fitting, and sensitivity analysis result is shown in figure 4.13 to 4.15. In the sensitivity analysis, the baseline is set at temperature of 250 ºC, space velocity of 1 NL/g-cat./hr, and SAR of 160. The effect of changes is made by varying the input values with ±10% of baseline.

Sensitivity analysis result of CO conversion is shown in figure 4.13. It is observed from the figure that reaction temperature has the most significant effect on CO conversion. 10% increase of temperature will enhance CO conversion by 24%. It is reported that increasing reaction temperature can raise CO conversion rate [113], hence higher CO conversion is observed at higher temperature with same space velocity. It is also found from the figure that lowering space velocity improves CO conversion. The reason is, at lower space velocity, CO molecules have longer residence time on catalyst active site, which enhances CO conversion [114]. Finally, SAR shows no effect on CO conversion, because zeolite cannot catalyze F-T synthesis reaction.

Sensitivity analysis result of CH_4 selectivity is shown in figure 4.14. From the figure it is found that CH_4 selectivity is significantly promoted by reaction temperature [115]. With 10% increase of temperature, CH_4 selectivity increases 51%. In addition, 10% increase of space velocity slightly promotes CH_4 selectivity of 2%, which coincide with results reported elsewhere [116]. Finally, CH_4 selectivity is enhanced with reduced SAR. Low catalyst SAR indicates higher zeolite activity. High zeolite activity promotes hydrocracking performance, and cause high CH_4 selectivity [117].

Sensitivity analysis results of CO_2 selectivity are shown in figure 4.15. It can be seen from the figure that CO_2 selectivity has ±72% change with ±10% change of reaction temperature. It is because higher temperature promotes water-gas shift reaction rate to produce more CO_2 [118]. Hydrocracking reactions are also enhanced and contribute to CO_2 formation [117]. In addition, it is found that space velocity does not have significant effect on CO_2 selectivity. However, 10% decrease of catalyst SAR causes 11% CO_2 selectivity increase. This is also because of hydrocracking rate improvements by higher zeolite activity [117].

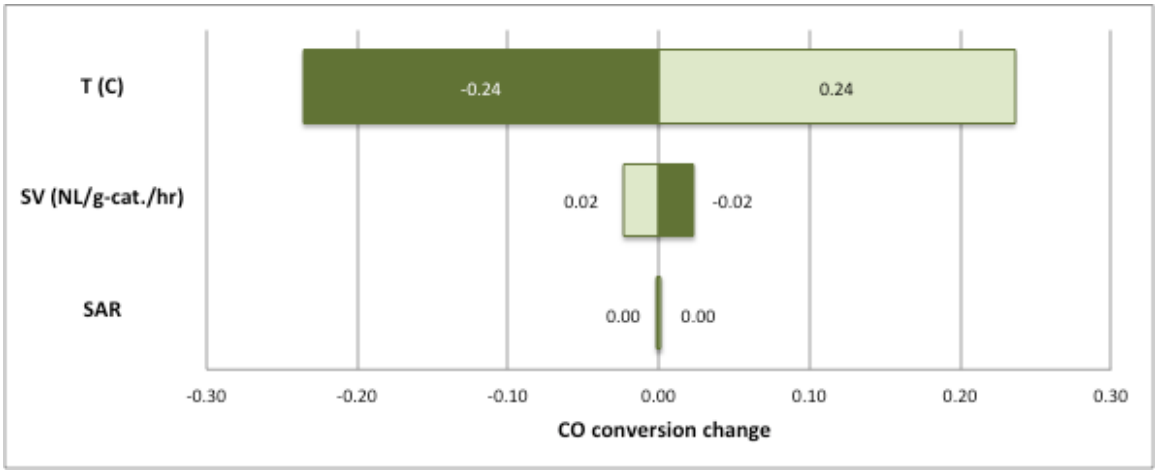

Figure 4.13 Sensitivity analysis result of CO conversion

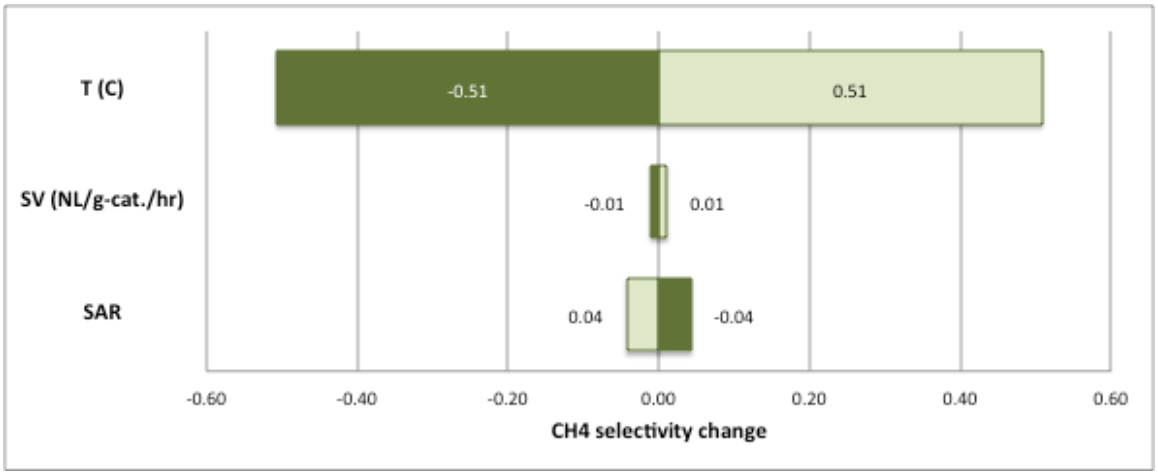

Figure 4.14 Sensitivity analysis result of CH_4 selectivity

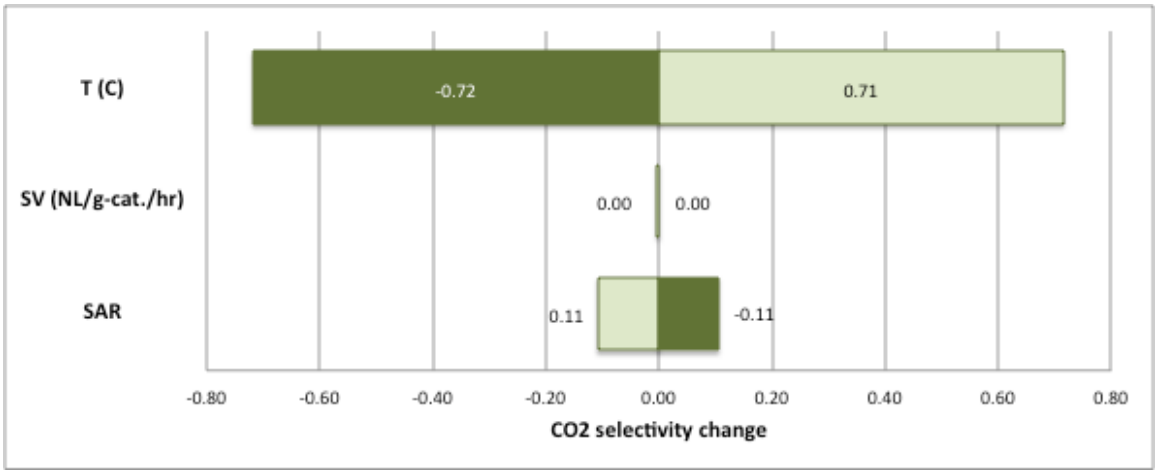

Figure 4.15 Sensitivity analysis result of CO_2 selectivity

4.3 Liquid Product Results and Discussion

4.3.1 GC Chromatogram

GC chromatogram of F-T liquid product is shown in figure 4.16. The picture on top is the product chromatogram from conventional F-T synthesis, and the one at the bottom is product chromatogram with zeolite-shell catalyst. In the chromatogram, each peak represents one kind of hydrocarbon compounds. Hydrocarbons with same carbon number are shown in one group, and the carbon number for a group of hydrocarbons is also shown in the figure. It is observed from the figure that carbon number distribution of conventional F-T liquids is over 20. For F-T liquids with zeolite shell catalysts, however, carbon number distribution is cut to 15. Also, in conventional F-T synthesis chromatogram, each carbon number only has one or two compounds. The high peaks are n-paraffin and the low peaks are olefin. Since hydrocarbon content has linear relationship with peak area, it can be found out from the figure that conventional F-T liquids are composed of high content of n-paraffin and small amount of olefin. However, in the chromatogram of liquid product with zeolite-shell F-T catalyst, more peaks are shown in every group. This indicates that other than n-paraffin and olefin, other hydrocarbons such as iso-paraffin and aromatics are produced. As a result, zeolite-shell catalyst can not only reduce liquid product distribution, but also promote formation of iso-paraffin and aromatics. The detailed analysis result is done using PIANO methods, where “P” is n-paraffin, “I” is iso-paraffin, “A” is aromatics, “N” is napthenes, and “O” is olefin. The PIANO analysis result will be discussed in section 4.3.2.

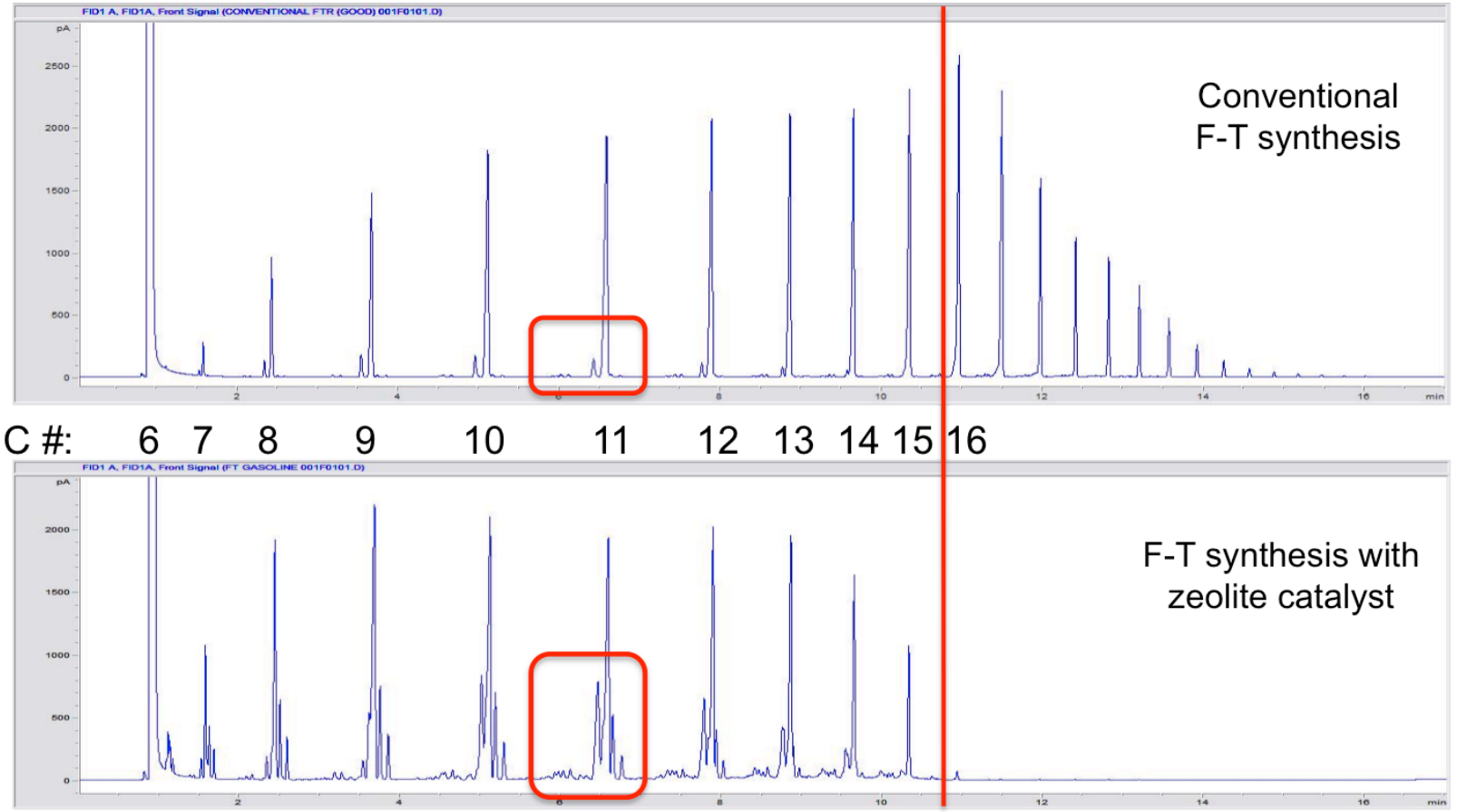

Figure 4.16 GC chromatogram of liquid product with conventional F-T catalyst and zeolite-shell catalyst

4.3.2 Fischer-Tropsch Synthesis Liquid Product Analysis

Carbon number distribution comparison of Fischer-Tropsch synthesis with conventional catalyst and zeolite-shell catalyst is shown in figure 4.17. The result with conventional F-T catalyst is from Aspen Plus simulation, and the result with zeolite-shell catalyst is obtained with SAR=80 catalyst at 250 ºC. It can be observed from the figure that Fischer-Tropsch synthesis product with the zeolite-shell catalyst doesn't follow the ASF distribution, which is mainly because of the hydrocracking and isomerization effect of the zeolite-shell catalyst. The cracking effect also causes an increase of methane selectivity.

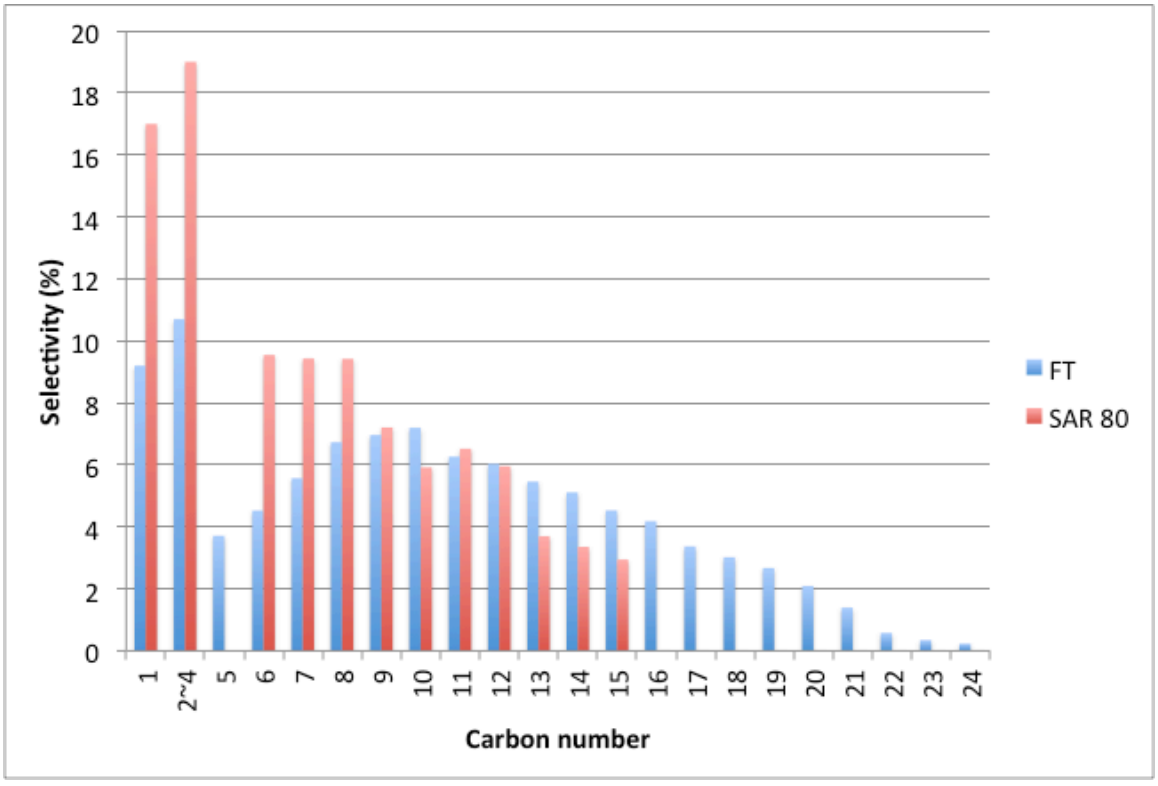

Figure 4.17 Comparison of Fischer-Tropsch synthesis product distribution

Fischer-Tropsch synthesis product distribution with gasoline-range, gaseous and heavy hydrocarbon is shown in figure 4.18. The four groups of bar chart in the figure represent distribution results from four different catalyst: conventional F-T catalyst, zeolite-shell catalyst with SAR of 80, 150, and 250, respectively. In each group, product distribution is evaluated at three temperatures of 220 ºC, 250 ºC, and 280 ºC, respectively. Note that distribution result of zeolite-shell catalyst is experiment result, while results of conventional F-T catalyst is obtained from Aspen Plus modeling. It is shown in the figure that at same reaction temperature, C12+ selectivity for conventional F-T catalyst is higher than that of all three zeolite-shell F-T catalysts. This is because zeolite-shell catalyst confines liquid product distribution, and push the distribution to lower carbon number range. Besides, it can be seen from the figure that for the same kind of catalyst, C1-C4 selectivity increases with temperature, but C12+ selectivity decreases with reaction temperature. However, temperature effect for gasoline range product is more complicated. For conventional F-T catalyst, gasoline range hydrocarbon selectivity increase with temperature. While the opposite trend is observed for SAR 150 catalyst. With temperature increase from 220 ºC to 280 ºC, gasoline range selectivity for SAR 150 catalyst decreases from 58% to 51%. It can also be found that compared with conventional F-T catalyst, gasoline range product for all three zeolite-shell catalysts has higher gasoline range selectivity.

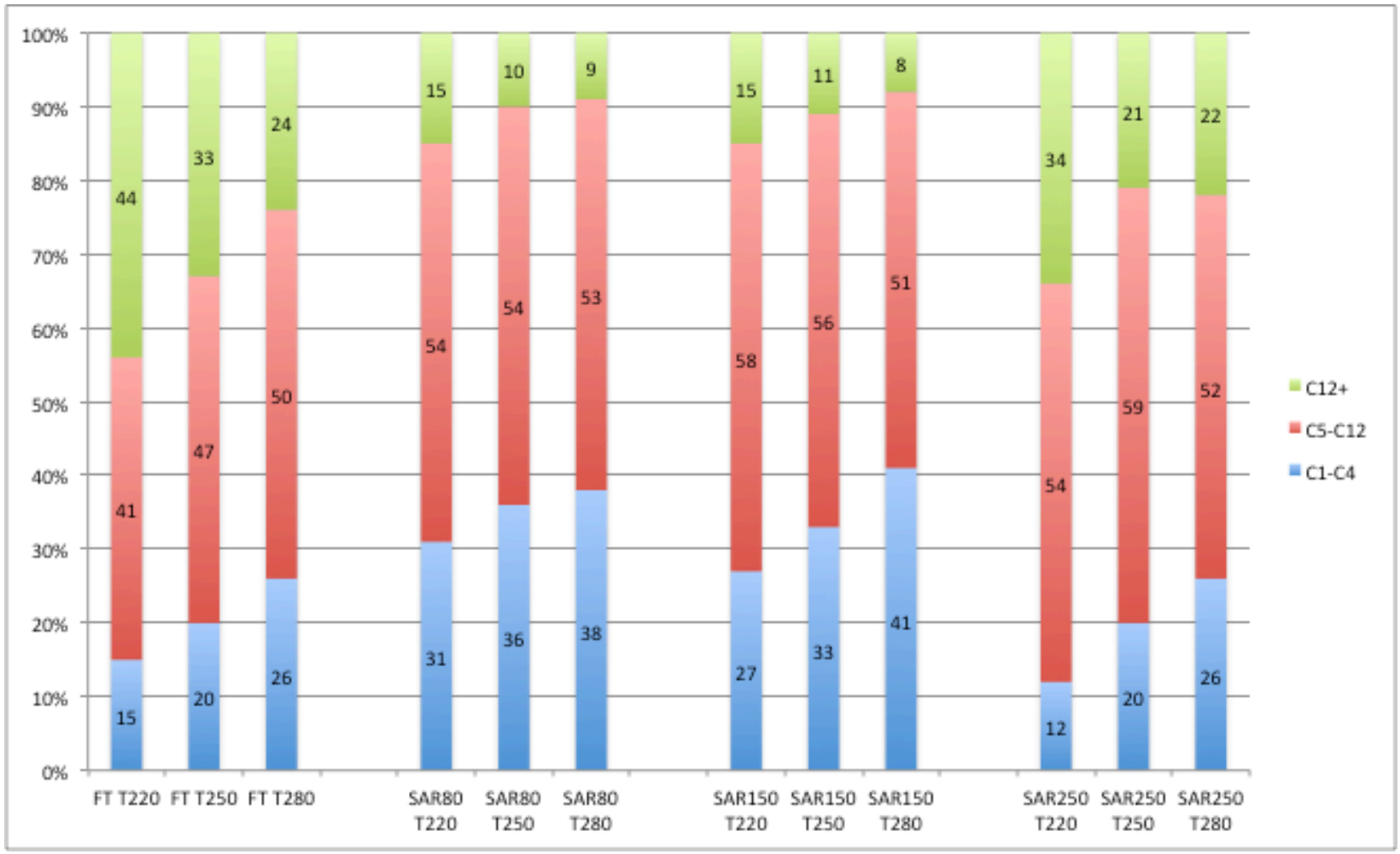

Figure 4.18 Gasoline-range, gaseous and heavy hydrocarbon distribution of F-T synthesis tests

PIANO test results of F-T gasoline product is presented in figure 4.19. PIANO stands for n-paraffin, iso-paraffin, aromatics, napthenes, and olefin, respectively. Among all five components, iso-paraffin, aromatics and olefin contributes to product octane value, hence high selectivity of these products are favorable. Liquid product selectivity is calculated in equation 4.4.

$$X\ selectivity = \frac{mass\ X\ produced}{total\ mass\ of\ gasolien\ range\ products} \times 100\% \qquad (4.4)$$

It is observed from the figure that, for each kind of catalyst, iso-paraffin selectivity is significantly promoted by increasing temperature. For SAR 250 zeolite-shell catalyst, iso-paraffin content is 0.6% at 220 ºC, but it is increased to 9.9% when temperature is at 280 ºC. As to SAR 80 catlayst, iso-paraffin content has 10% increase with temperature change from 220 ºC to 280 ºC. The maximum iso-paraffin selectivity obtained is 14.3% for SAR 80 zeolite-shell catalyst at 280 ºC and 180 psi. Selectivity of aromatics for SAR 150 catalyst increases with temperature, but no significant effect is observed for SAR 80 and 250 catalyst. At the same reaction temperature, olefin selectivity is enhanced with decreasing catalyst SAR. Reaction temperature does not significantly affect olefin selectivity.

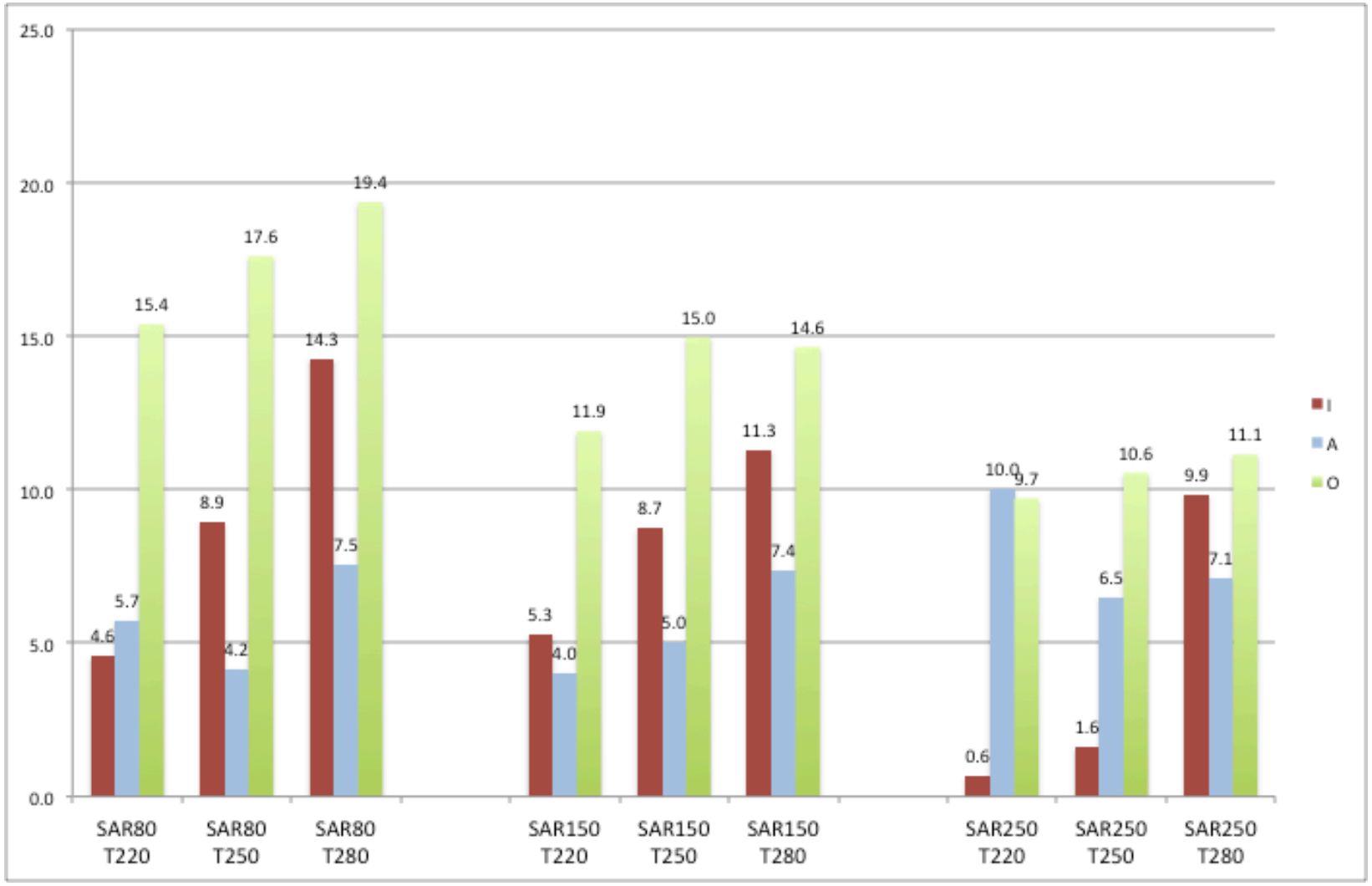

Figure 4.19 PIANO analysis result for gasoline range liquid products with zeolite-shell F-T catalyst

4.3.3 Sensitivity Analysis of F-T Liquid Product

The result of SAR and temperature effect on Fischer-Tropsch production distribution and iso-paraffin, olefin and aromatics selectivity are shown in figure 4.21 and 4.22. In the sensitivity analysis, the baseline is set at temperature of 250 ºC, and SAR of 160. The effect of changes is made by varying the input values with ±10% of baseline.

As shown in figure 4.20, C1-4 selectivity and C12+ selectivity are affected by SAR of zeolite-shell catalyst. With 10% increase of SAR, C1-4 selectivity decreases 5% and C12+ selectivity increases 9%. However, C5-12 selectivity is not influenced by SAR. This can be explained that, lowering SAR improves zeolite shell activity, which enhances cracking performance and shift product distribution to lower carbon number. On the other hand, increasing SAR inhibits zeolite activity, which suppresses cracking performance and shift product distribution to higher carbon number [119]. When more C5-12 product is cracked to C1-4 product, more C12+ is also cracked to C5-12 range, and vice versa. As a result, selectivity of C1-4 and C12+ product fluctuates with SAR, while C5-12 selectivity remains stable. In addition, selectivity of olefin and aromatics are not significantly affected by SAR, but iso-paraffin selectivity is promoted by decreasing zeolite SAR. This is also because of the enhancement of isomerization performance with lower SAR.

From figure 4.21 we can see that with 20% increase of reaction temperature, C1-4 selectivity has 17% increase while C12+ selectivity has 22% reduction. Besides, C5-12 selectivity is not significantly influenced by temperature. The reason is, zeolite activity is improved with increasing temperature, which promotes cracking performance and shift

product distribution to lower carbon number. While C5-12 range product is cracked to C1-4 products due to increasing temperature, more C5-12 range product is supplied by increasing cracking rate of C12+ products [120]. As a result, C5-12 selectivity is not significantly affected with changing temperature. In addition, it is found that aromatics selectivity does not have clear change with temperature. For iso-paraffin and olefin, with 10% increase of temperature, iso-paraffin selectivity has 49% increase while olefin content decreased 13%. This can be explained with hydroisomerization mechanism, which is shown in figure 4.20. While n-paraffin can be isomerized to iso-paraffin, it is realized in several steps. First, n-paraffin is dehydrogenized to form olefin, then straight chain olefin is skeletal isomerized to branched olefin. Finally, branched olefin is hydrogenated to iso-paraffin [121]. The hydroisomerization is promoted with temperature. At low temperature, isomerization reaction is suppressed, which cause high content of olefin. With increasing temperature, isomerization reaction is promoted and more olefin is converted to Isoparaffin, which cause decrease of olefin selectivity and increase of Isoparaffin selectivity.

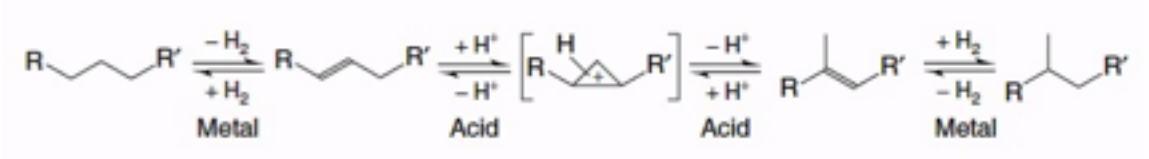

Figure 4.20 Hydroisomerization mechanism

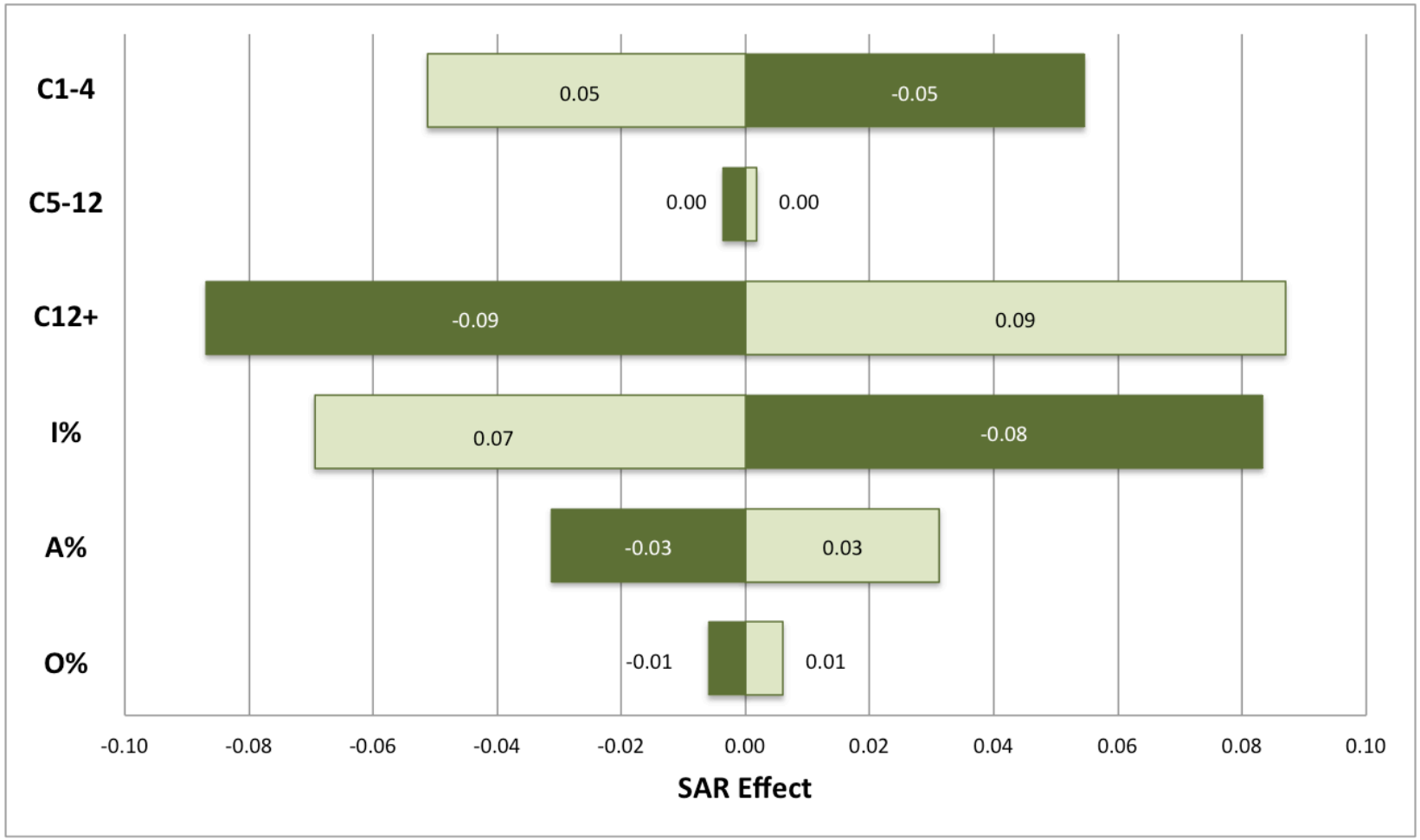

Figure 4.21 Sensitivity analysis of SAR effect

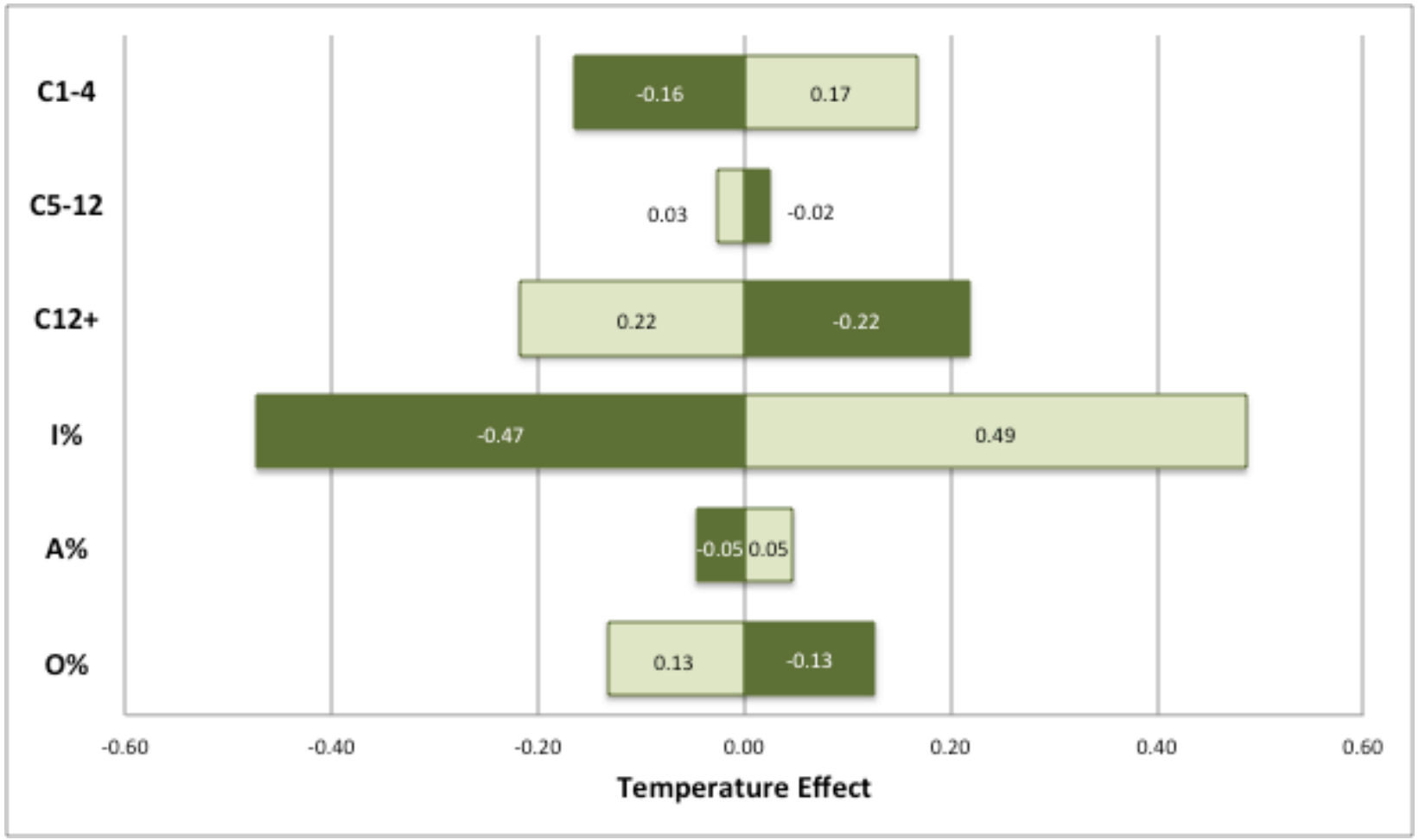

Figure 4.22 Sensitivity analysis of temperature effect

4.4 Catalyst Deactivation

4.4.1 Time Study of Catalyst Activity

Time study of catalyst activity is conducted for 430 hours using zeolite-shell F-T catalyst with SAR 150, and result is shown in figure 4.23. The reaction condition is temperature 250 ºC, pressure 180 psi, space velocity 1 NL/g-cat./hr. It is observed from the figure that CO conversion dropped about 10% in the first 150 hours, and decreased slowly by 3% in the following 280 hours. In addition, methane selectivity is increased about 2% in the first 150 hours, and stabilized during the following 280 hours. Both CO conversion decrease and methane selectivity increase shows catalyst deactivation. Catalyst deactivation with time on stream is generally ascribed to the decrease of metallic Co active sites. This can be explained with several deactivation mechanism, such as carbonaceous deposits on the catalyst active sites [122], and Co particle re-oxidation by water produced during F-T synthesis [123].

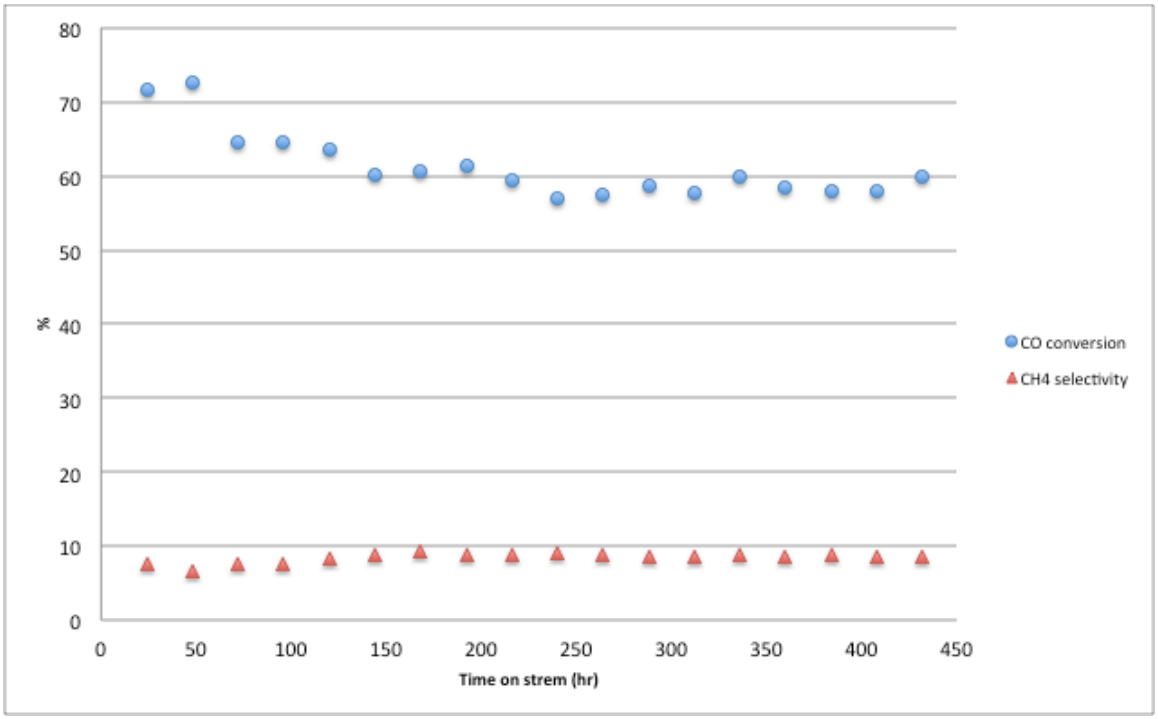

Figure 4.23 Time study of CO conversion and CH_4 selectivity

4.4.2 Catalyst Thermogravimetric Analysis

The thermal gravimetric analysis (TGA) result is shown in figure 4.24. Weight loss below 150 ºC is due to water evaporation, and weight loss over 200 ºC is due to carbonaceous deposits combustion. Thus TGA is used to evaluate catalyst deposits content. The catalysts tested are fresh conventional F-T catalyst, conventional F-T catalyst after 120 hours of F-T synthesis, and zeolite-shell F-T catalyst after 120 hours of test. The weight loss for fresh F-T catalyst is 6%. Compared with the weight loss curve of fresh F-T catalyst, it is clearly observed that the accumulation of heavy F-T synthesis wax and coke is serious for conventional F-T catalyst. However, weight loss for zeolite-shell catalyst with SAR 80 is decreased from 24% to 13%. Due to hydrocracking and

isomerization of heavy hydrocarbons by the zeolite shell [124], lower F-T synthesis wax and coke is accumulated on the zeolite-shell catalyst.

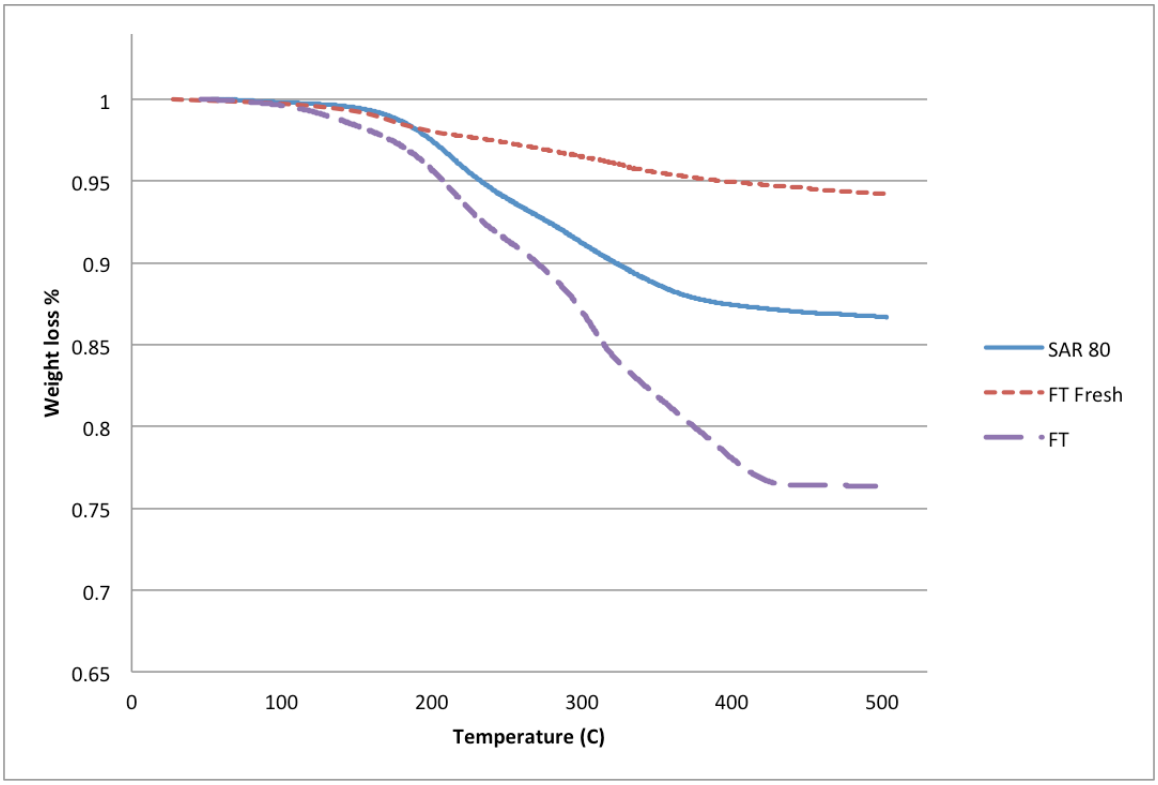

Figure 4.24 TGA study of catalyst after 120 hr. reaction

4.5 Conclusion

Performance of zeolite-shell F-T catalyst is tested under various conditions. The conclusions are summarized as follows.

1) CO conversion of Fischer-Tropsch synthesis is enhanced with increasing reaction temperature and decreasing space velocity. Zeolite silicon to aluminum ratio (SAR) does not have effect on CO conversion. CH_4 and CO_2 selectivity are promoted with increasing temperature and decreasing SAR. And they are not influenced by space velocity.
2) Compared with conventional F-T catalyst, zeolite-shell F-T catalyst confines product carbon number distribution to C1-C15, and improves gasoline range hydrocarbon selectivity. Gasoline range liquid product from zeolite-shell F-T catalyst also has higher iso-paraffin, aromatics and olefin selectivity.
3) Sensitivity analysis of F-T synthesis liquid product shows that iso-paraffin selectivity can be improved with increasing temperature and decreasing SAR. On the contrary, olefin selectivity is reduced with elevating temperature and reducing SAR.

4) Time on stream study and thermal gravimetric analysis is done to evaluate catalyst deactivation. Compared with conventional F-T catalyst, zeolite-shell F-T catalyst reduces coke and heavy F-T wax accumulation on catalyst activation sites, and slows down catalyst deactivation.

CHAPTER 5 Conclusion and Future Work

5.1 Conclusion

This thesis has investigated the direct production of gasoline range liquid hydrocarbons with high iso-paraffin content from syngas. It has provided a potential solution to efficiently produce renewable gasoline that can be used in gasoline engines directly. The main tasks completed in each chapter are concluded as follows:

1. In chapter 2, synthesis of H-ZSM-5 shell Co/Al_2O_3 Fischer-Tropsch catalyst is carried out, and various characterizations are performed. The conclusions are summarized as follows:
    1) H-ZSM-5 shell Co/Al_2O_3 Fischer-Tropsch catalyst with different silicon to aluminum ratio is successfully synthesized using secondary-growth hydrothermal synthesis method.
    2) The catalyst has good surface coverage, which is confirmed with SEM surface image result; SEM cross-sectional image shows a clear coating with thickness of 4.29 μm. EDX results show that the elemental composition of catalyst shell is similar to zeolite composition.

3) XRD analysis and confirms that H-ZSM-5 is successfully coated on Co F-T catalyst surface. Zeolite-shell F-T catalyst has higher surface area than conventional F-T catalyst, which indicate better reaction activity.

2. In chapter 3, two versions of lab-scale Fischer-Tropsch reactor system are designed and constructed. In addition, an automation system is also programmed for system control and data acquisition. The conclusions are summarized as follows:

    1) High-temperature high-pressure first generation lab-scale Fischer-Tropsch reactor system is designed and built. The reactor is compatible with both conventional F-T catalyst and new zeolite-shell F-T catalyst. It also has online gas and liquid sampling features to improve test efficiency and reduce total experiment time.

    2) Second generation lab-scale Fischer-Tropsch reactor system is designed and built with additional upgrades. Safety features are further improved with walk-in hood, emergency auto shut-off valve and pressure relief valve. In addition, the reactor structure is also simplified and total pipeline

length for the new reactor is also shortened to reduce product collection delay.

3) Automation system is created using LabVIEW program for data acquisition and recording. In addition, PID controllers with gain scheduling are used for heating control to achieve minimum temperature fluctuation. Finally, built-in alarm system can shut inlet gas flow automatically in case of emergency.

3. In chapter 4, performance of zeolite-shell F-T catalyst is tested at 180 psi, 220~280 ºC, and space velocity of 0.5~1.5 NL/g.-cat/hr. And silicon to aluminum ratio of zeolite-shell catalyst ranges from 80 to 250. The conclusions are summarized as follows.

   1) CO conversion of Fischer-Tropsch synthesis is enhanced with increasing reaction temperature and decreasing space velocity. The maximum CO conversion is 97.1% at 280 ºC with SAR=80 zeolite-shell catalyst. Zeolite silicon to aluminum ratio (SAR) does not have effect on CO conversion. CH_4 and CO_2 selectivity are promoted with increasing temperature and decreasing SAR. And they are not influenced by space velocity.

2) Compared with conventional F-T catalyst, zeolite-shell F-T catalyst confines product carbon number distribution to C1-C15, and improves gasoline range hydrocarbon selectivity. Gasoline range liquid product from zeolite-shell F-T catalyst also has higher iso-paraffin, aromatics and olefin selectivity. The highest gasoline-range iso-paraffin content is 14.3%, with 7.5% of aromatics and 19.4% of olefin, which is obtained at 280 ºC with SAR=80 zeolite-shell catalyst.

3) Sensitivity analysis of F-T synthesis liquid product shows that iso-paraffin selectivity can be improved with increasing temperature and decreasing SAR. On the contrary, olefin selectivity is reduced with elevating temperature and reducing SAR.

4) Compared with conventional F-T catalyst, zeolite-shell F-T catalyst reduces coke and heavy F-T wax accumulation on catalyst activation sites, which can reduce catalyst deactivation speed.

5.2 Future Work

1. Improve catalyst cracking and hydro-isomerization performance by lowering silicon to aluminum ratio and increasing zeolite shell thickness.
2. Test the effect of pressure on CO conversion, gasoline-range hydrocarbon selectivity and iso-paraffin content.
3. Scale-up Fischer-Tropsch synthesis reactor and connect the reactor to Steam Methane Reformer with PDU scale Steam Hydrogasification Reactor for biomass to gasoline production.
4. Perform economic analysis of the CE-CERT Fischer-Tropsch gasoline process and compare it with conventional Fischer-Tropsch synthesis process with product cracking and upgrading.

References

1. *Annual Energy Outlook 2011*, April, 2011, US Energy Information Administration: Washington.
2. Hirunlabh, J., *Overview of renewable energies for future development in Thailand.* Reric International Energy Journal, 1997. **19**(2): p. 89-101.
3. Kaygusuz, K. and S. Keles, *Use of Biomass as a Transitional Strategy to a Sustainable and Clean Energy System.* Energy Sources Part a-Recovery Utilization and Environmental Effects, 2009. **31**(1): p. 86-97.
4. Shen, L., et al., *Life cycle energy and GHG emissions of PET recycling: change-oriented effects.* International Journal of Life Cycle Assessment, 2011. **16**(6): p. 522-536.
5. Yasuhara, K., et al., *Effects of climate change on coastal disasters: new methodologies and recent results.* Sustainability Science, 2011. **6**(2): p. 219-232.
6. Lund, P.D., *The link between political decision-making and energy options: Assessing future role of renewable energy and energy efficiency in Finland.* Energy, 2007. **32**(12): p. 2271-2281.
7. Chum, H.L. and R.P. Overend, *Biomass and renewable fuels.* Fuel processing technology, 2001. **71**(1): p. 187-195.
8. Hoogwijk, M., et al., *Exploration of the ranges of the global potential of biomass for energy.* Biomass and Bioenergy, 2003. **25**(2): p. 119-133.
9. Demirbas, A., *Progress and recent trends in biofuels.* Progress in energy and combustion science, 2007. **33**(1): p. 1-18.
10. Yuan, J.S., et al., *Plants to power: bioenergy to fuel the future.* Trends in plant science, 2008. **13**(8): p. 421-429.
11. Zidansek, A., et al., *Climate changes, biofuels and the sustainable future.* International Journal of Hydrogen Energy, 2009. **34**(16): p. 6980-6983.
12. Dewulf, J. and H. Van Langenhove, *Renewables-based technology: sustainability assessment*. 2006: Wiley. com.
13. Pellegrini, L.F. and S. de Oliveira Junior, *Combined production of sugar, ethanol and electricity: thermoeconomic and environmental analysis and optimization.* Energy, 2011. **36**(6): p. 3704-3715.

14. Tyler, R.J., *Flash pyrolysis of coals. 1. Devolatilization of a Victorian brown coal in a small fluidized-bed reactor.* Fuel, 1979. **58**(9): p. 680-686.
15. Fukuda, H., A. Kondo, and H. Noda, *Biodiesel fuel production by transesterification of oils.* Journal of bioscience and bioengineering, 2001. **92**(5): p. 405-416.
16. Bothast, R. and M. Schlicher, *Biotechnological processes for conversion of corn into ethanol.* Applied Microbiology and Biotechnology, 2005. **67**(1): p. 19-25.
17. Raju, A.S.K., C.S. Park, and J.M. Norbeck, *Synthesis gas production using steam hydrogasification and steam reforming.* Fuel Processing Technology, 2009. **90**(2): p. 330-336.
18. Park, C.S. and J.M. Norbeck, *STEAM HYDROGASIFICATION OF COAL-WOOD MIXTURES IN A BATCH REACTOR.* 2008.
19. Jeon, S., et al., *Characteristics of steam hydrogasification of wood using a micro-batch reactor.* Fuel, 2007. **86**(17-18): p. 2817-2823.
20. Gray, D., *Increasing Security and Reducing Carbon Emissions of the US Transportation Sector: Transformational Role for Coal with Biomass*. 2010: DIANE Publishing.
21. Steynberg, A., *Introduction to fischer-tropsch technology.* Studies in surface science and catalysis, 2004. **152**: p. 1-63.
22. Schulz, H. and M. Claeys, *Kinetic modelling of Fischer-Tropsch product distributions.* Applied Catalysis A: General, 1999. **186**(1-2): p. 91-107.
23. Brady III, R.C. and R. Pettit, *Mechanism of the Fischer-Tropsch reaction. The chain propagation step.* Journal of the American Chemical Society, 1981. **103**(5): p. 1287-1289.
24. Hamelinck, C.N., et al., *Production of FT transportation fuels from biomass; technical options, process analysis and optimisation, and development potential.* Energy, 2004. **29**(11): p. 1743-1771.
25. Dry, M.E., *The Fischer-Tropsch synthesis, Catalysis: science and technology.* Springer, 1981: p. 160-253.
26. Steynberg, A., et al., *Fischer-Tropsch reactors.* Studies in surface science and catalysis, 2004. **152**: p. 64-195.
27. Sie, S. and R. Krishna, *Fundamentals and selection of advanced Fischer-Tropsch reactors.* Applied Catalysis A: General, 1999. **186**(1-2): p. 55-70.

28. Dry, M.E., *Practical and theoretical aspects of the catalytic Fischer-Tropsch process.* Applied Catalysis A: General, 1996. **138**(2): p. 319-344.
29. Davis, B.H., *FischerñTropsch synthesis: Overview of reactor development and future potentialities.* Topics in catalysis, 2005. **32**(3): p. 143-168.
30. Raje, A.P. and B.H. Davis, *Fischer-Tropsch synthesis over iron-based catalysts in a slurry reactor. Reaction rates, selectivities and implications for improving hydrocarbon productivity.* Catalysis Today, 1997. **36**(3): p. 335-345.
31. Davis, B.H., *Overview of reactors for liquid phase Fischer-Tropsch synthesis.* Catalysis Today, 2002. **71**(3-4): p. 249-300.
32. Jung, H., et al., *Investigation of Fischer-Tropsch synthesis performance and its intrinsic reaction behavior in a bench scale slurry bubble column reactor.* Fuel Processing Technology, 2010.
33. Woo, K.J., et al., *Performance of a slurry bubble column reactor for Fischer-Tropsch synthesis: Determination of optimum condition.* Fuel Processing Technology, 2010. **91**(4): p. 434-439.
34. Larachi, F., *Simulating the effects of liquid circulation in bubble columns with internals.* Chemical Engineering Science, 2006. **61**(13): p. 4195-4206.
35. Saxena, S., N. Rao, and P. Thimmapuram, *Gas phase holdup in slurry bubble columns for two-and three-phase systems.* The Chemical Engineering Journal, 1992. **49**(3): p. 151-159.
36. Rados, N., M.H. Al-Dahhan, and M.P. Dudukovic, *Modeling of the Fischer-Tropsch synthesis in slurry bubble column reactors.* Catalysis Today, 2003. **79**: p. 211-218.
37. Jager, B. and R. Espinoza, *Advances in low temperature Fischer-Tropsch synthesis.* Catalysis Today, 1995. **23**(1): p. 17-28.
38. Guettel, R. and T. Turek, *Assessment of micro-structured fixed-bed reactors for highly exothermic gas-phase reactions.* Chemical Engineering Science, 2010. **65**(5): p. 1644-1654.
39. Bianchi, C.L., C. Pirola, and V. Ragaini, *Choosing the best diluent for a fixed catalytic bed: The case of CO hydrogenation.* Catalysis Communications, 2006. **7**(9): p. 669-672.
40. Espinoza, R., et al., *Low temperature Fischer-Tropsch synthesis from a Sasol perspective.* Applied Catalysis A: General, 1999. **186**(1-2): p. 13-26.

41. Dry, M.E., *High quality diesel via the FischerñTropsch processña review.* Journal of Chemical Technology & Biotechnology, 2002. **77**(1): p. 43-50.
42. Iglesia, E., et al., *Bimetallic synergy in cobalt-ruthenium Fischer-Tropsch synthesis catalysts.* JOURNAL OF CATALYSIS-NEW YORK-, 1993. **143**: p. 345-345.
43. Steynberg, A.P., W.U. Nel, and M.A. Desmet, *Large scale production of high value hydrocarbons using Fischer-Tropsch technology.* Studies in surface science and catalysis, 2004. **147**: p. 37-42.
44. Jager, B., *Developments in Fischer-Tropsch technology.* Studies in surface science and catalysis, 1998. **119**: p. 25-34.
45. Dictor, R.A. and A.T. Bell, *Fischer-Tropsch synthesis over reduced and unreduced iron oxide catalysts.* Journal of Catalysis, 1986. **97**(1): p. 121-136.
46. Steynberg, A.P. and H.G. Nel, *Clean coal conversion options using Fischer-Tropsch technology.* Fuel, 2004. **83**(6): p. 765-770.
47. Ma, W.P., Y.J. Ding, and L.W. Lin, *Fischer-Tropsch synthesis over activated-carbon-supported cobalt catalysts: Effect of Co loading and promoters on catalyst performance.* Industrial & engineering chemistry research, 2004. **43**(10): p. 2391-2398.
48. Yates, I.C. and C.N. Satterfield, *Intrinsic kinetics of the Fischer-Tropsch synthesis on a cobalt catalyst.* Energy & fuels, 1991. **5**(1): p. 168-173.
49. Spath, P.L., *Preliminary screening-technical and economic assessment of synthesis gas to fuels and chemicals with emphasis on the potential for biomass-derived syngas*, 2003, DTIC Document.
50. Hilmen, A., et al., *Study of the effect of water on alumina supported cobalt Fischer-Tropsch catalysts.* Applied Catalysis A: General, 1999. **186**(1-2): p. 169-188.
51. Li, J., et al., *Fischer-Tropsch synthesis: effect of water on the deactivation of Pt promoted Co/Al2O3 catalysts.* Applied Catalysis A: General, 2002. **228**(1-2): p. 203-212.
52. Inderwildi, O.R., S.J. Jenkins, and D.A. King, *Fischer-Tropsch mechanism revisited: Alternative pathways for the production of higher hydrocarbons from synthesis gas.* The Journal of Physical Chemistry C, 2008. **112**(5): p. 1305-1307.

53. van Bekkum, H., E.M. Flanigen, and J. Jansen, *Introduction to zeolite science and practice*. 1991: Elsevier Science.
54. Haw, J.F., *Zeolite acid strength and reaction mechanisms in catalysis.* Phys. Chem. Chem. Phys., 2002. **4**(22): p. 5431-5441.
55. Den Hollander, M., et al., *Gasoline conversion: reactivity towards cracking with equilibrated FCC and ZSM-5 catalysts.* Applied Catalysis A: General, 2002. **223**(1-2): p. 85-102.
56. Buchanan, J., *Reactions of model compounds over steamed ZSM-5 at simulated FCC reaction conditions.* Applied catalysis, 1991. **74**(1): p. 83-94.
57. Corma, A., P. Miguel, and A. Orchillés, *Product selectivity effects during cracking of alkanes at very short and longer times on stream.* Applied Catalysis A: General, 1996. **138**(1): p. 57-73.
58. Grill, M., et al., *Preparation of zeolite Y and ZSM-5 coatings for cracking fuel in a cooling system for hypersonic vehicles.* Studies in surface science and catalysis, 2007. **170**: p. 258-266.
59. Guo, W., et al., *Coke and Its Precursor Formation During n-Dodecane and Toluene Supercritical Catalytic Cracking.* & Proceedings, 2008.
60. Zhao, G.-L., et al., *Catalytic cracking reactions of C< sub> 4</sub>-olefin over zeolites H-ZSM-5, H-mordenite and H-SAPO-34.* Studies in Surface Science and Catalysis, 2007. **170**: p. 1307-1312.
61. Mart √ ≠nez, A., et al., *Catalytic behavior of hybrid Co/SiO< sub> 2</sub>-(medium-pore) zeolite catalysts during the one-stage conversion of syngas to gasoline.* Applied Catalysis A: General, 2008. **346**(1): p. 117-125.
62. Mart √ ≠nez, A. and C. L √ ⩾pez, *The influence of ZSM-5 zeolite composition and crystal size on the in situ conversion of Fischer,ÄìTropsch products over hybrid catalysts.* Applied Catalysis A: General, 2005. **294**(2): p. 251-259.
63. Bessell, S., *Investigation of bifunctional zeolite supported cobalt Fischer-Tropsch catalysts.* Applied Catalysis A: General, 1995. **126**(2): p. 235-244.
64. Jong, S.J. and S. Cheng, *Reduction behavior and catalytic properties of cobalt containing ZSM-5 zeolites.* Applied Catalysis A: General, 1995. **126**(1): p. 51-66.
65. Tang, Q., et al., *Preparation of metallic cobalt inside NaY zeolite with high catalytic activity in Fischer-Tropsch synthesis.* Catalysis Communications, 2003. **4**(5): p. 253-258.

66. Espinosa, G., et al., *Catalytic behavior of Co/(Nano [beta]-Zeolite) bifunctional catalysts for Fischer-Tropsch reactions.* Catalysis Today, 2011.
67. Yang, G., et al., *Preparation, characterization and reaction performance of H-ZSM-5/cobalt/silica capsule catalysts with different sizes for direct synthesis of isoparaffins.* Applied Catalysis A: General, 2007. **329**: p. 99-105.
68. Li, X., et al., *One-step synthesis of H,ÄìŒ≤ zeolite-enwrapped Co/Al< sub> 2</sub> O< sub> 3</sub> Fischer,ÄìTropsch catalyst with high spatial selectivity.* Journal of Catalysis, 2009. **265**(1): p. 26-34.
69. Huang, X., et al., *CoZr/H-ZSM-5 hybrid catalysts for synthesis of gasoline-range isoparaffins from syngas.* Applied Catalysis A: General, 2011.
70. Street, J., et al., *Gasoline-range hydrocarbon production using biomass derived synthesis gas over Mo/H< sup>+</sup> ZSM-5.* Fuel, 2012.
71. Kibby, *Zeolite supported cobalt hybrid fischer-tropsch catalyst* 2011.
72. He, J., et al., *Designing a capsule catalyst and its application for direct synthesis of middle isoparaffins.* Langmuir, 2005. **21**(5): p. 1699-1702.
73. He, J., et al., *Multiple Functional Capsule Catalysts: A Tailor Made Confined Reaction Environment for the Direct Synthesis of Middle Isoparaffins from Syngas.* ChemistryñA European Journal, 2006. **12**(32): p. 8296-8304.
74. Li, X., et al., *One-step synthesis of H- zeolite-enwrapped Co/Al 2 O 3 FischerñTropsch catalyst with high spatial selectivity.* J. Catal, 2009. **265**: p. 26.
75. Belambe, A., R. Oukaci, and J. Goodwin Jr, *Effect of Pretreatment on the Activity of a Ru-Promoted Co/Al< sub> 2</sub> O< sub> 3</sub> Fischer–Tropsch Catalyst.* Journal of Catalysis, 1997. **166**(1): p. 8-15.
76. Hosseini, S., A. Taeb, and F. Feyzi, *Evaluation of Ru-promoted Co/γ-Al< sub> 2</sub> O< sub> 3</sub> catalysts in Fischer–Tropsch synthesis in a CSTR.* Catalysis Communications, 2005. **6**(3): p. 233-240.
77. Spivey, J.J., *Group communication with J.J. Spivey.* Oct. 2005.
78. Van'T Blik, H. and J. Niemantsverdriet, *Characterization of bimetallic FeRh/Sio< sub> 2</sub> catalysts by temperature programmed reduction, oxidation and Mössbauer spectroscopy.* Applied catalysis, 1984. **10**(2): p. 155-162.
79. Hurst, N.W., et al., *Temperature programmed reduction.* Catalysis Reviews Science and Engineering, 1982. **24**(2): p. 233-309.

80. Arnoldy, P. and J.A. Moulijn, *Temperature-programmed reduction of CoOAI2O3 catalysts.* Journal of Catalysis, 1985. **93**(1): p. 38-54.
81. Beck, J.S., R.M. Dessau, and D.H. Olson, *Method of preparation of ex situ selectivated zeolite catalysts for aromatic alkylation applications*, 1997, Google Patents.
82. Beck, J.S., S.B. McCullen, and D.H. Olson, *Multiple impregnation technique for the preparation of ex situ selectivated zeolite catalysts*, 1995, Google Patents.
83. Beck, J.S., D.H. Olson, and S.B. McCullen, *Method of preparation of ex situ selectivated zeolite catalysts for enhanced shape selective applications and method to increase the activity thereof*, 1995, Google Patents.
84. de Moor, P.-P.E., T.P. Beelen, and R.A. van Santen, *In situ observation of nucleation and crystal growth in zeolite synthesis. A small-angle X-ray scattering investigation on Si-TPA-MFI.* The Journal of Physical Chemistry B, 1999. **103**(10): p. 1639-1650.
85. Lawton, S.L., et al., *Zeolite MCM-49: a three-dimensional MCM-22 analogue synthesized by in situ crystallization.* The Journal of Physical Chemistry, 1996. **100**(9): p. 3788-3798.
86. Wang, Z. and Y. Yan, *Controlling crystal orientation in zeolite MFI thin films by direct in situ crystallization.* Chemistry of materials, 2001. **13**(3): p. 1101-1107.
87. Yan, Y., M.E. Davis, and G.R. Gavalas, *Preparation of Zeolite ZSM-5 Membranes by In-Situ Crystallization on Porous. alpha.-Al2O3.* Industrial & engineering chemistry research, 1995. **34**(5): p. 1652-1661.
88. Wang, Z. and Y. Yan, *Oriented zeolite MFI monolayer films on metal substrates by in situ crystallization.* Microporous and mesoporous materials, 2001. **48**(1): p. 229-238.
89. Gouzinis, A. and M. Tsapatsis, *On the preferred orientation and microstructural manipulation of molecular sieve films prepared by secondary growth.* Chemistry of materials, 1998. **10**(9): p. 2497-2504.
90. Xomeritakis, G., et al., *Growth, microstructure, and permeation properties of supported zeolite (MFI) films and membranes prepared by secondary growth.* Chemical engineering science, 1999. **54**(15): p. 3521-3531.

91. Lovallo, M.C., A. Gouzinis, and M. Tsapatsis, *Synthesis and characterization of oriented MFI membranes prepared by secondary growth.* AIChE journal, 1998. **44**(8): p. 1903-1913.
92. Lai, Z., M. Tsapatsis, and J.P. Nicolich, *Siliceous ZSM‐5 Membranes by Secondary Growth of b‐Oriented Seed Layers.* Advanced Functional Materials, 2004. **14**(7): p. 716-729.
93. Bernal, M.a.P., G. Xomeritakis, and M. Tsapatsis, *Tubular MFI zeolite membranes made by secondary (seeded) growth.* Catalysis today, 2001. **67**(1): p. 101-107.
94. Richter, H., et al., *Preparation of zeolite membranes on the inner surface of ceramic tubes and capillaries.* separation and Purification Technology, 2003. **32**(1): p. 133-138.
95. Wang, Z., J. Hedlund, and J. Sterte, *Synthesis of thin silicalite-1 films on steel supports using a seeding method.* Microporous and mesoporous materials, 2002. **52**(3): p. 191-197.
96. Persson, A., et al., *The synthesis of discrete colloidal particles of TPA-silicalite-1.* Zeolites, 1994. **14**(7): p. 557-567.
97. Zhao, J., et al., *Cracking of n-dodecane during supercritical state on HZSM-5 membranes.* Fuel Processing Technology, 2010. **91**(9): p. 1090-1097.
98. Huang, L., et al., *Fabrication of ordered porous structures by self-assembly of zeolite nanocrystals.* Journal of the American Chemical Society, 2000. **122**(14): p. 3530-3531.
99. Lai, R., Y. Yan, and G.R. Gavalas, *Growth of ZSM-5 films on alumina and other surfaces.* Microporous and mesoporous materials, 2000. **37**(1): p. 9-19.
100. Song, W., et al., *Synthesis, characterization, and adsorption properties of nanocrystalline ZSM-5.* Langmuir, 2004. **20**(19): p. 8301-8306.
101. Sano, T., et al., *Preparation and characterization of ZSM-5 zeolite film.* Zeolites, 1991. **11**(8): p. 842-845.
102. Hedlund, J., et al., *ZSM-5 membranes synthesized without organic templates using a seeding technique.* Journal of membrane science, 1999. **159**(1): p. 263-273.
103. Wu, E., et al., *ZSM-5-type materials. Factors affecting crystal symmetry.* Journal of Physical Chemistry, 1979. **83**(21): p. 2777-2781.

104. Marturano, P., et al., *Fe/ZSM-5 Prepared by Sublimation of FeCl< sub> 3</sub>: The Structure of the Fe Species as Determined by IR,< sup> 27</sup> Al MAS NMR, and EXAFS Spectroscopy.* Journal of Catalysis, 2000. **192**(1): p. 236-247.
105. Bjørgen, M., et al., *Methanol to gasoline over zeolite H-ZSM-5: Improved catalyst performance by treatment with NaOH.* Applied Catalysis A: General, 2008. **345**(1): p. 43-50.
106. Li, Y.-G., W.-H. Xie, and S. Yong, *The acidity and catalytic behavior of Mg-ZSM-5 prepared via a solid-state reaction.* Applied Catalysis A: General, 1997. **150**(2): p. 231-242.
107. Ison, A. and R.J. Gorte, *The adsorption of methanol and water on H-ZSM-5.* Journal of Catalysis, 1984. **89**(1): p. 150-158.
108. Van Koningsveld, H., H. Van Bekkum, and J. Jansen, *On the location and disorder of the tetrapropylammonium (TPA) ion in zeolite ZSM-5 with improved framework accuracy.* Acta Crystallographica Section B: Structural Science, 1987. **43**(2): p. 127-132.
109. Yang, Z., Y. Xia, and R. Mokaya, *Zeolite ZSM‐5 with Unique Supermicropores Synthesized Using Mesoporous Carbon as a Template.* Advanced Materials, 2004. **16**(8): p. 727-732.
110. Yao, M., et al., *An XRD and TEM investigation of the structure of alumina-supported ceria–zirconia.* Journal of Catalysis, 1997. **166**(1): p. 67-74.
111. Zhao, R., et al., *A highly efficient oxidation of cyclohexane over Au/ZSM-5 molecular sieve catalyst with oxygen as oxidant.* Chemical communications, 2004(7): p. 904-905.
112. Ogura, M., et al., *Formation of uniform mesopores in ZSM-5 zeolite through treatment in alkaline solution.* Chemistry Letters, 2000. **29**(8): p. 882-883.
113. Yan, Z., et al., *Fischer–Tropsch synthesis on a model Co/SiO< sub> 2</sub> catalyst.* Journal of Catalysis, 2009. **268**(2): p. 196-200.
114. Huang, X. and C.B. Roberts, *Selective Fischer–Tropsch synthesis over an Al< sub> 2</sub> O< sub> 3</sub> supported cobalt catalyst in supercritical hexane.* Fuel Processing Technology, 2003. **83**(1): p. 81-99.
115. Schulz, H., *Short history and present trends of Fischer–Tropsch synthesis.* Applied Catalysis A: General, 1999. **186**(1): p. 3-12.

116. Li, J., et al., *Fischer–Tropsch synthesis: effect of water on the catalytic properties of a ruthenium promoted Co/TiO< sub> 2</sub> catalyst.* Applied Catalysis A: General, 2002. **233**(1): p. 255-262.
117. Köseoglu, R.Ö. and C.R. Phillips, *Hydrocracking of Athabasca bitumen: Kinetics of formation of gases.* Fuel, 1988. **67**(4): p. 552-556.
118. Bunluesin, T., R. Gorte, and G. Graham, *Studies of the water-gas-shift reaction on ceria-supported Pt, Pd, and Rh: implications for oxygen-storage properties.* Applied Catalysis B: Environmental, 1998. **15**(1): p. 107-114.
119. Nawaz, Z., et al., *Effect of Si/Al ratio on performance of Pt–Sn-based catalyst supported on ZSM-5 zeolite for n-butane conversion to light olefins.* Journal of Industrial and Engineering Chemistry, 2010. **16**(1): p. 57-62.
120. Bezergianni, S., S. Voutetakis, and A. Kalogianni, *Catalytic hydrocracking of fresh and used cooking oil.* Industrial & Engineering Chemistry Research, 2009. **48**(18): p. 8402-8406.
121. Niwa, M., N. Katada, and K. Okumura, *Characterization and Design of Zeolite Catalysts: Solid Acidity, Shape Selectivity and Loading Properties*. Vol. 141. 2010: Springer.
122. Egiebor, N.O., W.C. Cooper, and B. Wojciechowski, *Synthesis of motor fuels from HY-zeolite supported Fischer-Tropsch iron catalysts.* Applied Catalysis, 1989. **55**(1): p. 47-64.
123. Van Berge, P., et al., *Oxidation of cobalt based Fischer–Tropsch catalysts as a deactivation mechanism.* Catalysis Today, 2000. **58**(4): p. 321-334.
124. Zhao, T.-S., et al., *Selective synthesis of middle isoparaffins via a two-stage Fischer-Tropsch reaction: Activity investigation for a hybrid catalyst.* Industrial & engineering chemistry research, 2005. **44**(4): p. 769-775.